DEVELOPMENT OF A COMPOSITE TISSUE-ENGINEERED INTERVERTEBRAL DISC: *IN VITRO* AND *IN VIVO* STRUCTURE AND FUNCTION

A Dissertation

Presented to the Faculty of the Graduate School

of Cornell University

In Partial Fulfillment of the Requirements for the Degree of

Doctor of Philosophy

by

Robert Daniel Bowles

May 2011

DEVELOPMENT OF A COMPOSITE TISSUE-ENGINEERED INTERVERTEBRAL DISC: *IN VITRO* AND *IN VIVO* STRUCTURE AND FUNCTION

Robert Daniel Bowles, Ph. D.

Cornell University 2011

Degenerative disc disease and its associated spinal disorders are a leading cause of disability in the United States and around the world. Currently a number of treatments exist, but they are mostly palliative in nature and fail to restore function to the spine. The field of tissue engineering provides the opportunity to create treatments that will replace the diseased tissue with new tissue and that can not only relieve the symptoms of the patient, but can also restore function. This dissertation focuses on the development of a composite tissue-engineered intervertebral disc (TE-IVD) that can be used to replace the diseased intervertebral disc (IVD) in the spine.

TE-IVDs were developed with circumferentially aligned collagen fibrils and cells in the annulus fibrosus (AF) region of the IVD by contracting cell-seeded collagen gels around a cell-seeded alginate gel nucleus pulposus (NP). Altering the original collagen concentration and cell seeding density was able to regulate the final AF composition and collagen alignment in the TE-IVD. Using the tunable AF region of the TE-IVD, the effects of altering the AF composition and architecture on TE-IVD tissue development were studied both *in vitro* and in the native disc space. It was determined that changes in the AF composition led to altered pressurization of the TE-IVD under load and this change in mechanics regulated the *in vivo* tissue development. These *in vivo* studies were the first to demonstrate that tissue-

engineered total disc replacement (TE-TDR) could produce an integrated and mechanically functional IVD-like tissue in the native disc space.

Despite the enthusiasm for TE-TDR, this is the first body of work that demonstrated a TE-IVD could replace and restore function to the spine when implanted into the disc space. Furthermore, the field has largely focused on the collagen organization of the AF in TE-IVD design, but this dissertation presents AF hydraulic permeability as a key design parameter due to its ability to regulate proper tissue development in the native disc space. Overall, this work represents a benchmark in TE-IVD research and pushes TE-TDR towards the clinic.

BIOGRAPHICAL SKETCH

Robby was born in Ft. Worth, TX into a military family. He would spend the next 18 years of his life moving around the country every few years. During this tenure, he would live in 6 states, 8 cities, 13 homes, and attend 7 schools. He graduated first in his class from Airline High School in 2000. Robby then attended the University of Pennsylvania where he graduated *magna cum laude* in 2005 with a B.S.E. in Biomedical Engineering and a minor in Mathematics. During his time at the University of Pennsylvania, Robby worked in the labs of Dr. Dawn Elliott from 2002-2003 and Dr. Steven Nicoll from 2004-2005. In these labs, Robby developed his interest in both the intervertebral disc and tissue engineering, which he would later combine for his dissertation research.

In 2005, Robby began pursuing his Ph.D. at Cornell University in the lab of Dr. Lawrence Bonassar. He passed up positions at higher ranked programs to pursue his interest in intervertebral disc tissue-engineering, a decision he would not regret. In addition to research, Robby would serve on the boards of the Biomedical Engineering Society and the Graduate and Professional Student Assembly. Robby also participated in the Graduate Student School Outreach Program and NSF GK-12 teaching outreach programs. It was a direct result of these programs that he discovered his interest in teaching.

Robby will be taking a postdoctoral position in the lab of Dr. Lori Setton at Duke University following the completion of his Ph.D. At Duke he will continue in his passion for spinal research as he investigates drug delivery therapies for treatment of radiculopathy. Following his postdoctoral work, he plans to begin a career in academia studying the treatment of spinal disorders using regenerative medicine. In addition, Robby has developed an interest in developing medical technologies, specifically in orthpaedic regenerative medicine, for the developing world.

Dedicated to my wonderfully supportive family and friends.

ACKNOWLEDGMENTS

I would first like to thank my wonderful wife. She supported me the last 5 years with unbelievable care and patience. She put up with the late nights, weekends in the lab, the trips to NYC, and my general mood after many hours working. We both came to Ithaca and grew together through the experience. Without her, this would not have been possible.

Special thanks to my special committee, Dr. Lawrence Bonassar, Dr. Warren Zipfel, and Dr. Ronald Minor for their guidance and encouragement as I worked toward the completion of this degree. In addition, I would like to extend a special thanks to Dr. Roger Härtl who has acted as the clinical advisor to this project. His help and input has been invaluable in making sure this work was clinically relevant.

I would like to specifically thank Judy Thoroughman and Belinda Floyd for their support and hard work, which enabled the whole process to run smoothly. I would like to thank all of my fellow lab members, the biomechanics group, and graduate students that provided encouragement and feedback throughout this process. And finally, I would like to extend a special thanks to all those that have encouraged me to pursue my dreams including my family, teachers, and friends.

Funding for this work was provided by AOSpine North America, the AO Research Fund, National Science Foundation GK-12, Cornell Center for Materials Research, Cornell Nanobiotechnology Center, and the Office of the Provost at Cornell University.

TABLE OF CONTENTS

LIST OF FIGURES

CHAPTER 1

CHAPTER 2

CHAPTER 3

CHAPTER 4

CHAPTER 5

CHAPTER 6

LIST OF TABLES

Chapter 1

LIST OF ABBREVIATIONS

AF	Annulus fibrosus
AI	Alignment index
ALD	Adjacent level disease
ANOVA	Analysis of variance
BSA	Bovine serum albumin
CT	Computed tomography
DICOM	Digital imaging and communications in medicine
DMMB	1,9 Dimethylmethylene blue
DNA	Deoxyribonucleic acid
ECM	Extracellular Matrix
EDTA	Ethylenediaminetetraacetic acid
ELF	Electroforce
EP	Endplate
FBS	Fetal bovine serum
FDA	Food and Drug Administration
FFT	Fast-fourier transform
GAG	Glycosaminoglycan
IACUC	Instiutional animal care and use committee
IHC	Immunohistochemistry
IVD	Intervertebral disc
LBP	Lower back pain
MRI	Magnetic resonance imaging

MSC	Mesenchymal stem cells
NB-TDR	Non-biological total disc replacement
NP	Nucleus Pulposus
NSF	National Science Foundation
PBS	Phosphate buffered saline
PGA	Polyglycolic acid
PLA	Polylactic acid
PLL	Posterior longitudinal ligament
PLLA	Poly-l-lactic acid
PMMA	Poly(methyl methacrylate)
PMT	Photomultiplier tube
SEM	Scanning electron microscopy
SIS	Small intestinal submucosa
SHG	Second harmonic generation
TE-IVD	Tissue-engineered intervertebral disc
TE-TDR	Tissue-engineered total disc replacement
TPEF	Two-photon excited fluorescence
VB	Vertebral body
W/V	Weight/volume

CHAPTER 1

INTRODUCTION

DEGENERATIVE DISC DISEASE

Intervertebral disc (IVD) degeneration is a leading cause of disability in the developed world, with approximately 65 million people in the United States alone suffering from prolonged back pain (1). Although, a direct connection between pain and IVD degeneration is not always evident, the vast majority of chronic spine ailments involve some amount of disc degeneration. Moreover, by age 50, more than 85% of the population will have some evidence of this disease.

Degenerative disc disease can lead to a number of pathological conditions that can cause pain and discomfort. Due to the proximity of the IVD to the nerve roots, protruding disc material can impinge the local nerve roots causing radiculopathy (2). In addition, peripheral sensitization and neoinnervation of the nerve fibers located in the outer lamellae of the annulus fibrosus (AF) and endplate can result in pain due to disc degeneration, and altered mechanical stimuli (3). Furthermore, disc degeneration and herniation are associated with inflammation and immune response that can lead to neuritis and increased sensitivity in the nerves (4). Finally, alterations in the AF and nucleus pulposus (NP) composition and structure lead to hypermobility in the spine that can result in greater inflammation and stimulation of the sensitized nerves. One of the difficulties of treating pain resulting from the IVD is the complex interactions between the inflammation, innervation, hypermobilitiy, and stenosis observed in IVD pathology. These interactions are currently an active area of investigation, as they are not fully understood to date.

The cost of treatment of degenerative disc diseases and its associated symptoms is estimated to be in excess of $50 billion per year in the United States. Due to the prominence of this disorder, a number of materials are currently being used for the treatment of degenerative disc disease (Table 1). Because the primary presentation of these disorders is pain, surgical treatments are primarily palliative, with less, if any, focus on restoring function to the diseased tissue.

Table 1 - Current Treatments for Degenerative Disc Disease							
Treatment	Physical Therapy	Partial Discectomy	Spinal Fusion	Total Disc Replacement	Dynamic Stabilization	IVD Transplant	Tissue Based Regeneration
Disease Severity	Mild - Moderate	Moderate - Severe	Severe	Severe	Moderate - Severe	Severe	Mild - Severe
Biomaterials	NA	NA	Autograft Bone, Allograft Bone, Synthetic Bone, Demineralized Bone Matrix, Growth Factors	Metal/ Polyethylene articulating joint	Metal/ Polyethylene screws, cords, spacers, flexible rods, flexible screws	Allograft IVD	Broad range of hydrogels, fibrous materials, and cells

Table 1.1 Current Treatments for Degenerative Disc Disease

CURRENT TREATMENTS

Spinal Fusion

One of the most common surgical treatments is partial or complete discectomy, in which the IVD is removed in an attempt to eliminate the source of the pain, whether the pain is caused by the impingement of the nerve root or discogenic in origin. In the case of complete discectomy, the spine must be stabilized through the fusion of the vertebral bodies. This allows the pain-inducing disc to be removed, but results in the loss of mobility at the operated motion segment. As a result, it is necessary for the remaining motion segments to provide the required flexibility to the spine. In addition, it is essential to maintain the anatomy of the spine to protect the integrity of the

integrated nervous system. This includes the disc space height that was originally maintained by the IVD.

This is accomplished by implanting autologous bone grafts, cadaveric allografts, or bone graft substitutes in the disc space in combination with rods, screws, plates, or cages. The hardware is designed to provide stabilization to the spine while the grafts are implanted to promote bone formation between the vertebral bodies during fusion. An optimal material used for spinal fusion will have an osteoconductive scaffold that promotes the ingrowth of bone, osteogenic capabilities that provide cells to the fusion site, and osteoinductive factors that promote the differentiation of progenitor cells into osteoblast cells. The materials currently used all have at least one of these properties and multiple materials are being combined to maximize these properties in many cases.

Bone Grafts

Bone grafts were the first material choice in promoting a fusion between the vertebral bodies (5). They provide the exact material that is desired in the disc space and in the case of autografts are osteogenic, osteoconductive, and osteoinductive. As a result, the material could be harvested from the patient and implanted in the disc space to promote fusion between the vertebral bodies while maintaining the disc space height formally maintained by the IVD. The two types of bone grafts available are autografts and allografts.

Autografts are obtained from the patient's own bone and are usually obtained from the iliac crest of the pelvis. Autografts provide the highest likelihood of fusion due to the presence of bone, osteoblasts, and bone morphogenetic proteins (BMPs). However, autografts can result in donor site morbidity and chronic pain at the harvest site (6, 7). In contrast, allografts are obtained from a human source other than the patient. This bone is acquired from tissue banks and circumvents the issues of donor

site pain and morbidity but introduce the possibility of disease transmission. When used alone, allografts tend to underperform autografts in producing a successful fusion (8-11). This is likely due to the lack of osetogenic cells and minimal osteoinductive factors contained in the allograft despite its osteoconductive scaffold. The allografts cells are purposefully removed during processing to reduce the likelihood of an immune response caused by the foreign cells. Recently, in an attempt to increase the likelihood of fusion, adult stem cells are being investigated as a possible way to overcome the lack of living cells in allografts (12).

Synthetic Bone Grafts

Autografts and allografts are both limited in supply since they require a donor and donor site. Synthetic bone grafts, on the other hand, could mimic the properties of bone and provide a material to promote fusion while circumventing the problems of autograft/allograft supply, donor site morbidity, donor site pain, and disease transmission. Bone has both an organic (collagen type I) and inorganic (hydroxyapatite) component. Synthetic bone grafts attempt to mimic the compositional content of the bone, usually the inorganic component, to provide a biodegradable osteoconductive scaffold to promote fusion. This involves producing calcium containing crystalline solids with porosity similar to that of bone that will promote bone ingrowth.

A number of synthetic materials designed to mimic the properties of bone, including various ceramics, are being investigated for use in fusion procedures. These materials are osteoconductive but, similar to allografts, do not contain cells. For this reason, they are often used in combination with autografts as bone graft extenders. The most commonly used materials are coralline hydroxyapatite, β-tricalcium phosphate, and calcium sulfate (13-15). The use of these materials as an extender allows for less

autograft material to be harvested, thus decreasing the risk of donor site morbidity and pain.

Demineralized Bone Matrix

While allografts and synthetic bone grafts provide an osteoconductive scaffold, they fail to provide substantial osteoinductive proteins to stimulate bone growth. The combination of both osteoconductive and osteoinductive properties similar to that found in autografts can further promote fusion beyond what an osteoconductive scaffold can produce alone.

Used as a bone graft extender, demineralized bone matrix is obtained by removing the mineralized component of allograft bone by acid extraction. The resulting matrix is predominantly type I collagen in addition to various growth factors including BMPs. As a result, demineralized bone matrix is both osteoconductive and osteoinductive. However, the mechanical stiffness of demineralized bone matrix are much lower than that of bone and must be used in combination with a material that can provide the necessary structural strength when implanted. For this reason, the material is used primarily as a bone graft extender to introduce the osteoconductive proteins into the disc space.

Growth Factors and Gene Therapy

Both autografts and demineralized bone matrix have osteoinductive proteins and demonstrate the ability of these proteins to stimulate bone growth. As a result, it is advantageous to develop techniques that allow these osteoconductive proteins to be utilized for spinal fusion in combination with techniques other than autografts and demineralized bone matrix. In addition, recombinant production of growth factors

enables greater control of the types and concentrations of growth factors delivered to the fusion site.

A number of growth factors including BMPs have been shown to be osteoinductive. As a result, the use of recombinant forms of these proteins has been combined with osteoconductive materials to be utilized in spinal fusion surgeries. Human trials have shown increased success over autografts when using either rhBMP-2 or rhBMP-7 in combination with a number of carrier matrices including collagen sponges, collagen type I powder, allograft bone, and ceramic granules (16-20). Overall, this provides a technique that is both osteoconductive and osteoinductive without requiring autograft harvesting.

One of the drawbacks of rhBMPs is their soluble nature and high doses need to be inserted in the carrier matrix to be effective over a sustained period of time. As a result, the associated cost of this type of procedure is quite high. One possible solution is to utilize gene therapy to introduce the osteoinductive BMPs to the fusion site. Such a technique allows sustained production of the BMPs at the fusion site without having to insert large amounts of rhBMP into the carrier. Currently, a number of animal studies are being performed to test the efficacy of such strategies and investigate the safety concerns related to gene therapy (21-23).

Motion Preservation

Despite the common use of spinal fusion for the treatment of various spinal complications, the procedure produces a number of deleterious consequences. First the fusion of the vertebral body results in a loss of motion at the fused site and often leads to adjacent level degeneration thought to be caused by the altered mechanical loading at the adjacent levels (24, 25). For this reason, a number of devices have been designed to preserve the motion of the IVD at the operated level.

Total Disc Replacement

Similar to what is performed in the knee and hip, the first attempts to preserve motion as an alternative to fusing the vertebral bodies were total disc replacement strategies. In this procedure the entire disc is removed and replaced by an artificial joint containing an articulating surface designed to provide motion to the joint segment. The devices reaching clinical trial have contained either two metal alloy endplates with an ultra high molecular weight polyethylene-articulating surface (Charité® and ProDisc®) or have a metal on metal design (Prestige®, Flexicore®, and Kineflex®). Currently, the Charité®, ProDisc®, and Prestige® have received FDA approval. Relatively short-term data indicates that these devices have been successful in reducing adjacent level degeneration (26, 27); however, it is unclear whether this will be true in the long term. Furthermore, it appears that these discs may suffer from polyethylene wear (28, 29), which could lead to osteolysis, dislodgement, and failure of the device. As a result, further investigation will need to be carried out to understand the long-term efficacy of the total disc replacement strategy.

Dynamic Stabilization

In addition to total disc replacement, a new class of devices is currently being investigated for treatment of spinal disorders. These devices are designed to provide controlled motion at the disc level without replacing the entire disc. The devices attach to the posterior elements of the spine and are composed of some combination of screws, cords, spacers, flexible rods, and flexible screws. One example of such a system is the Dyneses® system, which has received FDA approval as an adjunct to spinal fusion surgeries but is not approved as a stand-alone device, although clinical trials are underway. The Dyneses® system is made of pedical screws, surgical

polyurethane spacers, and polyethylene cords. This combination of parts is designed to maintain motion in a controlled manner that will decrease pain but allow motion similar to that of the healthy motion segment. Many similar devices can be imagined and quite a few are currently under investigation for the treatment of spinal disorders (30, 31).

IVD Transplantation

In addition to using hardware to maintain motion and stability in the diseased spine, a novel technique of transplanting cadaveric IVDs is being investigated. The hypothesis behind this procedure is that the transplanted healthy native tissue will most accurately restore the complex function of the IVD to the spine while relieving the pain and circumventing the issues associated with using traditional metal/polyethylene materials. In this method, segments of the boney vertebral bodies are left on either end of the IVD in order to promote integration of the transplanted disc into the motion segment. The low vascularity of the IVD reduces the risk of tissue rejection and allows the procedure to be performed without immunosuppressant drugs.

IVD transplantation was originally investigated in canine (32-34) and primate (35, 36) animal models and has now been tested in a small number of human patients (37). Animal models showed that the transplanted discs were able to successfully integrate with the native tissue by 6 months and form functional motion segments after an initial 2-4 months period of hypermobility. Despite forming functional motion segments, a loss of water and proteoglycans were observed in allografts from 6 to 24 months. In addition, nucleus cells had an irregular shape and mitochondrial swelling at 24 months compatible with degeneration. These findings indicate that the transplanted IVDs are capable of integrating and forming functional motion segments;

however, they show signs of degeneration over time after implantation. Immune response was localized to the boney interfaces (36). Human trials in five patients have been met with success as patients show no signs of significant pain at a 5-year follow-up (37). Radiologically, patients showed minimal disc height loss and a normal range of motion.

Overall, the animal models and early clinical results on IVD transplantation are promising. However, it will be important to carry out studies in a larger cohort of patients and investigate the long-term survival of the transplants. In addition, despite the apparent success of the procedure, IVD transplantation suffers from limited donor tissue, issues of size matching, and possible disease transmission. As a result, regenerative techniques are also being investigated for IVD tissue replacement.

Field Research Directions

Despite the development of total disc replacements and dynamic stabilization devices, it remains unclear what the long-term success these devices will have in reducing adjacent segment degeneration. While these devices are promising, it is likely that these devices will suffer from long-term failure modes (wear, fatigue, and loosening via osteolysis) similar to that of other traditional knee and hip polymer/metal implants (38). For these reasons, accelular and cellular tissue-based approaches that mimic the native IVD extracellular matrix (ECM) composition and architecture may be advantageous. The cellular component would allow the tissue to be remodeled and repaired over the life of the tissue while the ECM component could more accurately mimic the native intervertebral disc function than a metal-polymer implant. A tissue-based approach could create a treatment that could mimic this function, maintain mobility, and not suffer from the effects of wear, fatigue, and

osteolysis. For this reason, the investigation of tissue-based approaches for the treatment of spinal disorders is actively being pursued.

IVD STRUCTURE AND FUNCTION

In order to understand the material design criteria involved in IVD repair, one must first be familiar with the complex structure and function of the native IVD. Grossly, the IVD is a composite tissue containing an outer annulus fibrosus, an inner nucleus pulposus, and the cartilage endplates (39). Each of these regions is distinct in composition, as well as organization, and work in concert to provide the mechanical function of the IVD (Figure 1.1).

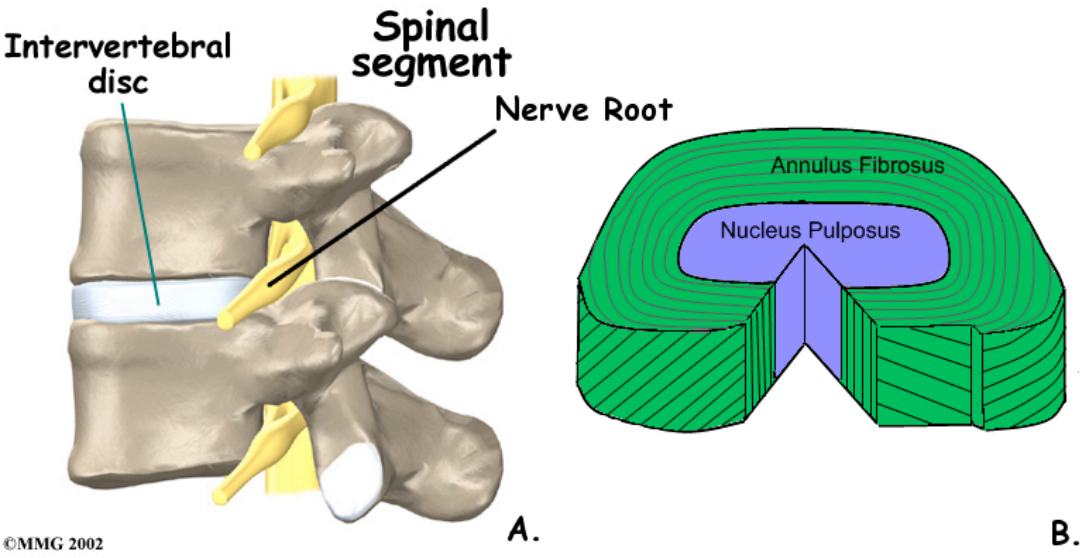

Figure 1.1 Intervertebral disc structure. (A.) IVD located in spine between vertebral bodies with the *cauda equina* (lumbar) or spinal cord (thoracic and cervical) running through the spinal canal. Nerve roots exit from the spinal canal through the intervertebral foramina. (B.) The IVD composed of the unorganized inner nucleus

pulposus and outer highly organized annulus fibrosus. The annulus fibrosus is composed of lamellae and alternating collagen fibril alignment (± 28°) between each adjacent lamella.

The nucleus pulposus is an isotropic, unstructured, gelatinous material that is enclosed by the highly structured annulus fibrosus fibrocartilage on the side and the hyaline cartilage endplates on the end of the vertebrae (Figure 1b). The encapsulation of the gelatinous nucleus pulposus by the annulus fibrosus allows the IVD to be both strong in compression while also withstanding complex tensile and shear forces in the annulus fibrosus. Upon compression, the nucleus pulposus is pressurized as the annulus fibrosus resists the radial expansion of the nucleus pulposus. It is this pressurization that gives the IVD its high compressive stiffness (40). In addition, during the bending and torsional movements of the spine, the complex collagen architecture of the AF bears the tensile loads (41). It is this elegant function that one hopes to restore when selecting materials for IVD repair, and for this reason, it is advantageous to understand the material components and architecture that accomplish this naturally.

Extracellular Matrix

Overall, the key components of the IVD are water, collagens, proteoglycans, elastin, and cells with varying amounts and types located in the distinct IVD regions (42-47). The IVD is extremely hydrated with the annulus fibrosus and nucleus pulposus having a water content of approximately 65% and 80% of wet weight respectively (46). In the annulus fibrosus collagens make up 70% of the dry weight with 84% of that being collagen type I and 14% collagen type II at the outer annulus fibrosus (42). In contrast, collagens only make up 20% of the dry weight of the NP

with 80% of that being collagen type II. Proteoglycans follow the opposite trend with the percentage starting low in the annulus fibrosus and increasing until reaching 50% of the dry weight in the nucleus pulposus (43).

Of these proteoglycans, the negatively charged large aggregating proteoglycans, aggrecan and versican are found in the intervertebral disc with members of the small leucine rich proteoglycan family (decorin, biglycan, lumican, and fibromodulin) also being present (48, 49). It is the negative charge of aggrecan that produces an affinity for water in the IVD via osmotic swelling and Donnan equilibrium. As a result, the high proteoglycan to collagen ratio produces the gelatinous nature of the nucleus pulposus and the high collagen content and structural organization of collagen gives rise to the fibrous nature of the AF.

Finally, elastin is found in both the nucleus pulposus and annulus fibrosus (47). The fibers are located predominately between the annulus fibrosus lamellae but are also found parallel to the collagen fibrils within the lamellae.

Organization

The degree of organization observed within the nucleus pulposus and annulus fibrosus is dramatically different. The NP has an unorganized collagen type II matrix dispersed within the proteoglycan rich tissue. This unorganized state leads to the isotropic nature of the NP and its capacity for significant swelling when liberated from the surrounding AF. In contrast, the AF has a very organized collagen type I fiber structure. The AF is macroscopically segmented into lamellae surrounding the NP core. In each lamella, the collagen fibrils are highly aligned at an angle of ± 28° to the transverse plane and this angle increases to 44° in the inner AF (50, 51), with the angle alternating in each successive lamella (Figure 1b). As a result, this organization leads to anisotropic mechanical properties and creates a tissue that is good at resisting the

tensile loads observed in torsion and bending as well as withstanding the hoop stresses that occur during compression. Overall, this tissue produces a unique set of mechanical properties in compression, extension-flexion, torsion, and bending that tissue based approaches of repair will need to recreate to restore function to the diseased or injured IVD.

IVD PRESERVATION, REPAIR, AND REGENERATION

By any measure, tissue based IVD repair and tissue engineering is a relatively new field. Extracting broad trends from published data is quite challenging even with the small number of studies to date (approximately 50 peer-reviewed manuscripts), since there is relatively little consistency in the cell types and materials used. The approaches can be broken down into NP, AF, and total disc repair.

Nuclear Replacement

The idea of nuclear replacement has received the most attention. This approach relies on the idea that replacing the herniated or diseased disc material will maintain or restore disc height and function to the spine. By replacing the NP, the disc height could be restored and the AF fibers are placed back into tension, similar to that of a healthy disc. This type of intervention requires a healthy AF and, as a result, would be a solution to an earlier stage of disease than used in spinal fusion and total disc replacement (52). Currently, clinically available products are material based but research is being conducted on creating tissue engineered material/cell solutions (Table 2).

Table 2 - Nuclear Replacement				
	Acellular		Cellular	
	Intradiscal Implants	*In Situ* Curable Polymers	Cell Only	Cell + Scaffold
Goal	Restore/Maintain Disc Height	Restore/Maintain Disc Height, Repressurize NP, Minimally Invasive	Restore/Maintain Disc Height, Repopulate Lost Cellularity To Produce *De Novo* Tissue	Restore/Maintain Disc Height, Repressurize NP, Repopulate Lost Cellularity To Produce *De Novo* Tissue
Materials	Springs and Hydrogels	Hydrogels, Polyurethane, Water/Oil Emulsion	Autologous Disc Cells, MSCs	Autologous Disc Cells, MSCs + Hydrogels, Type II collagen, Hyaluronan composite, calcium polyphosphate, chitosan

Table 1.2 – Nuclear replacement strategies

Acellular

Early attempts at nucleus replacement focused on acellular materials to restore disc height. The first attempt at nucleus replacement was conducted in 1955 by David Cleveland, in which he replaced the NP after discectomy with methylmethacrylate (53). Acceular strategies continue to be investigated today and are at various stages of clinical evaluation.

Cellular

Creating tissue-based strategies with a cellular component creates a tissue that can mature and repair over the life of the implant. As a result, this dramatically increases the theoretical limit for how long the treatment can be effective. The key to the successful development of a tissue based strategy is in the proper selection of the material, cell source, and signaling. The NP has been a prime target for this type of therapy due to the isotropic (unorganized) structure of the tissue, which eliminates the need to worry about complex tissue architecture during tissue development. Overall,

the goal is to produce a tissue that is gelatinous in nature with high proteoglycan content and unorganized type II collagen fibrils.

The choice of an animal source for IVD cells is challenging, as the time at which the cell population of the NP changes from notochordal to chondrocytic varies with species (54). Regardless of species chosen, it appears to be critical to ensure that cells are obtained from skeletally mature animals. To date, cells from 7 species have been investigated for use in IVD regeneration, including murine (55), lapine (56), porcine (57), ovine (58, 59), canine (60), bovine (60), and human (61). It is highly likely that human cell sources will be required for clinical use; however, obtaining cells from the human IVD tissue may be difficult due to the diseased state of the tissue. As a result, the use of mesenchymal stem cells (MSC) is being investigated. In fact, MSCs have been shown to take on a NP-like phenotype both in vitro and after being injected into NP tissue (62, 63) making them a suitable candidate for tissue based NP replacement.

Disc degeneration results in decreased cell density in the NP and reduced cellular activity. As a result, one of the proposed treatments for NP degeneration is to simply inject cells into the NP without scaffolding material to promote *de novo* tissue formation in the NP of the degenerated disc. NP cells (64), NP cells co-cultured with MSCs (65), MSCs (66), chondrocytes (67), and AF cells co-cultured with MSCs (68) have all been investigated for NP injection. In general, cells were able to produce proteoglycan rich matrix in the NP and delay degeneration in disc degeneration models. In a human trial, IVD cells were cultured and injected back into the NP after microdiscectomy surgery (69). Patients receiving the treatment showed decreased pain at 2 years compared to those receiving no injection of cells after microdiscectomy. These data indicate that injecting cells into the NP may be able to

delay degeneration in the IVD and be used as an adjunct to microdiscectomy to improve clinical outcomes.

While cell injection alone has shown potential to delay degeneration and promote *de novo* tissue formation, the use of a scaffolding material cells provides the additional ability to repressurize the NP by injecting the scaffold/cell material into the disc space. The isotropic gelatinous nature of the NP makes hydrogels a prime material candidate for NP tissue engineering. However, unlike acellular NP replacement, these materials must be deliverable in a noncytotoxic manner eliminating a number of hydrogels used in intradiscal implants. Wide ranges of scaffold materials have been used as substrates for cell culture. In general, NP cells have been cultured in hydrogels, with alginate (57-60) and gelatin (55) accounting for more than half of the studies published. Both materials appear to be well suited to maintaining NP cell phenotype and enabling proteoglycan synthesis, although significant accumulation of proteoglycan and collagen was not observed uniformly. Additional materials being utilized have been type II collagen (70), hyaluranon composites (71), calcium polyphosphate substrate (72), type I atelocollagen (66), and chitosan (73).

While a large portion of this work has been done *in vitro*, a number of studies are available investigating the effectiveness of cell/material nuclear replacement *in vivo*. These studies have been conducted in different animal models, lapine (64), canine (74), and murine (55). The results of these *in vivo* studies have been promising showing a delay in degeneration, restoration of disc height, and significant proteoglcyan rich ECM. In addition to the animal studies, interim results of a human randomized trial have been reported. In this study, autologous NP cells derived from therapeutic discectomy were cultured and delivered 12 weeks after discectomy in patients with chronic back pain (75). Their data suggests MR imaging improvement consistent with increased proteoglycan matrix within the NP and a reduction in low

back pain at 2 years when compared to controls. As a result, NP replacement may be a powerful adjunct to discectomy. However, it is important to note that this treatment must be conducted at an early enough stage that a functional AF is in place. Later stages of degeneration are unlikely to be treated by NP replacement alone.

Annular Repair

Due to the nature of disc herniation and the resulting disruption in the AF, it is necessary for the AF to be repaired to return proper mechanical function to the disc. In addition, the herniated region of the AF can allow the remaining NP or NP replacement to reherniate through the disruption. This can happen in up to 15% of patients after discectomy (76-78), and unfortunately, the AF has a limited healing capacity and will only produce a thin biomechanicaly inferior tissue without intervention (79). For this reason, it is a significant and relevant challenge to produce surgical treatments to repair the AF upon herniation.

Table 3 - Annular Repair		
	Acellular	Cellular
Goal	Provide Barrier To Reherniation	Produce Novel Tissue In Defect, Provide Barrier To Reherniation
Materials	Anchored Sutures, Meshes, Collagen PMMA Injections	Autologous Disc Cells, MSCs + Hydrogels, Electospun Nanofibrous Scaffolds, Chitosan, PGA/PLA, Collagen Sponges

Table 1.3. Annular repair strategies

Acellular

The earliest attempts to repair the disrupted AF involved suturing the AF to provide both a barrier to rehernation and to promote healing. Unfortunately, few studies have been performed to study the effectiveness of suturing. In one of the few studies available, no significant increase in healing strength was observed as a result of direct annular repair (80). In addition to suturing, a number of additional implants designed to close and act as barriers are being developed. These devices include sutures with anchors (81), meshes (82), and collagen PMMA injections (83). However, currently there are few data to determine the effectiveness of these devices and they continue to suffer from the poor intrinsic healing of the AF, as they do not directly promote healing. For this reason, tissue-based approaches are also being investigated to promote a functional healing in the defect in addition to simply closing it.

Cellular

The goal of introducing cells into an annular defect is to promote the production of a functional tissue in the defect to both inhibit NP reherniation, as well as restore the mechanical properties of the AF. The creation of a functional engineered AF tissue is more difficult to produce than the NP due to its highly organized architecture and anisotropic mechanical properties. The tissue must not only

contain the proper amounts of ECM, but they must also be organized properly to restore the mechanical function to the AF. The key organizational structures of importance are the high degree of alignment, the angle of alignment, and the alternating directions of alignment between lamellae. However, it must be noted that currently it is unknown to what degree this organization needs to be recreated to successfully reduce the number of cases of reherniation and slow the progression of the disease state.

Cell selection for AF repair requires the selection of a cell that can produce a highly organized type I collagen ECM. The most likely candidates for use in AF repair strategies are the AF cells themselves or MSCs. However, once again autologous AF cells suffer from the diseased state of the tissue and diseased state of the resulting cells (84). In addition, the availability of autologous AF cells varies greatly between patients and will likely require *in vitro* culture to expand to an adequate number of cells. These shortcomings may limit the effectiveness of these cells for clinical treatments. In comparison, MSC cells provide a more reliable cell source but are not without their own difficulties. Early work showed that MSCs differentiate into an NP-like phenotype and not an AF phenotype when cultured in hydrogels (63, 85). Nevertheless, the proper combination of scaffold and cell signaling may still be elucidated that promotes an AF phenotype from MSCs. In fact, more recent work has shown that when MSCs are placed on electrospun nano-fibrous scaffolds the cells take up a more AF like phenotype (86, 87). This may indicate scaffold selection as a key determiner of MSC phenotype and make proper material selection vital in producing a successful tissue based approach to AF repair.

A number of scaffolds with a wide range of properties have been investigated for AF tissue engineering. Early work used scaffolds seeded with AF cells that lacked the structure necessary to promote collagen alignment and organization. These

scaffolds included collagen type I/hyaluronan (71), type I atellocollagen (88), alginate (56), type I collagen/GAG (89), collagen sponges (90), collagen gels (90), fibrin gels (90), PGA/PLA (58), chitosan (91), and electrospun PLLA (87). These constructs in general allowed for significant production of proteoglycans and collagen but the ECM development was still substantially lower than native values of ECM. In addition, no collagen organization was observed in these scaffolds.

Recently, focus has turned to culturing cells on scaffolds that promote tissue organization and alignment in the hopes that an engineered AF tissue can be created that mimics the complex anisotropic function of the AF. This has been accomplished through the creation and use of aligned fibrous scaffolds. To date it has been achieved naturally with the use of small intestine submucosa (92), with the self assembly of contracted collagen gels (93), and with the aligned electrospinning of PCL (86). Each of these techniques has advantages and disadvantages for treating AF defects.

The small intestine submucosa (SIS) is obtained by processing small intestine to remove the mucosa layer. This results in a construct that contains oriented collagen fibers, proteoglycans, and trapped growth factors. This is ideal due to the similarity of the SIS ECM composition (aligned collagen and proteoglycans) and structure to the native AF. In addition, the trapped growth factors can be released and promote tissue development at the site of implantation. SIS has been investigated for the repair of a number of tissues previously, including blood vessels, bladder defects, rotator cuffs, knee ligaments, and meniscus. The use of SIS for annular repair is relatively new but has shown promise in a sheep model by repairing AF defects and returning partial function to the IVD (94).

Contracting collagen gels while controlling the boundary conditions has been shown to create aligned collagen fibrils and has been investigated for the repair of a number of tissues, including blood vessels, tendon, ligament, and cardiac tissue (95-

98). The advantages of the technique are the production of aligned collagen architecture and aligned cells that are seeded throughout the tissue. However, contracted collagen gel tissues have notoriously week mechanical properties in contrast to the native AF (95). At early time points after implantation it may be difficult for an implanted collagen gel to withstand the mechanical loading imposed upon the aligned collagen gel. Conversely, the collagen nature of the scaffold may promote earlier integration of the tissue with the native AF and the high permeability of the collagen gel may promote the transport of nutrients into the developing tissue. This increased transport in the developing tissue may be especially important in the low nutrient environment present in the IVD and allow the tissue to mature into an integrated mechanically functional tissue after implantation.

Electrospinning allows scaffolds to be produced that have fibers of similar size to that of the collagen fibrils found in the AF. In addition, electrospinning can incorporate fiber alignment into the scaffold and has been used to create engineered tissues that contain lamellae with alternating ±30° fiber orientation (86). These electrospun tissue structures developed tensile properties similar to that of native AF and showed promise for use in AF tissue engineering. However, the electrospinning process is not without its challenges. One of those challenges is the migration of cells into the electrospun scaffolds. Often, cells will fail to migrate to the center of the scaffold and will result in reduced tissue development at the center. Currently, a number of techniques are being studied to address these issues including the combination of composite electrospun materials that have differing degradation rates to encourage migration of cells into the scaffold (99). In addition, a big question is how these organized fibrils will integrate with the endplate and vertebral bodies once implanted. Without integration and anchoring of the fiber structure, the fiber architecture will not be engaged and will fail to provide the mechanical function they

are designed for. Further work is being conducted in the field to better understand how these electrospun scaffolds will integrate with the native tissue.

As can be seen, the amount of work done in the field of AF tissue engineering is limited and much of it has been *in vitro*. It will be important in the future direction of AF tissue engineering to understand how these strategies respond *in vivo* to the demands of AF defects. The major questions are centered on the ability of the repair strategies to confine the NP, the ability to restore pressurization capability to the IVD, and the ability to restore proper functioning to the AF in tension. Clearly, if these capabilities can be restored, it will have a profound effect on the clinical treatment of disc herniation.

Total Disc Replacement

A similarity exists between the IVD and an air filled tire, the tire being represented by the NP and the steel-belt reinforced rubber being represented by the AF. Furthermore, this similarity can be extended to the repair of the IVD as well. In certain situations, it will be advantageous to refill the air of the tire (nuclear replacement); in other situations, one may be able to patch a hole in the tire (AF repair); and finally, there are times when the entire tire must be replaced (total disc replacement). It is the final situation, in which the hernation or degeneration of the AF is so advanced that a sole NP or AF approach cannot be effective. For this reason that total disc replacement is currently being investigated.

Non-biological total disc replacement has been recently introduced into clinical practice in the US with the FDA approval of the previously discussed Charité device in 2004. The idea of a tissue-based composite disc, which is the focus of this disseration, was introduced with publication of the first tissue engineered composite disc around the same time (58). The idea that the entire IVD can be replaced by a

tissue-engineered structure is an ambitious one due to the complex structure of the IVD; however, the early studies showed promising ECM and mechanical properties with a PLA/PGA/alginate composite. There are four major design criteria in developing a tissue-engineered total disc replacement (TE-TDR): (1) to design a disc that can withstand the complex mechanical loading once implanted, (2) to recreate the mechanical function of the IVD, (3) to integrate with native tissues, and (4) to survive and develop in the nutrient deprived disc space. These design criteria are complex and are even competing. The development of a mechanically stiff disc designed to withstand the complex loading will likely have low permeability properties and may make it difficult to get sufficient nutrient transport throughout the disc in the low nutrient disc environment. Conversely, a highly permeable disc that can provide better nutrient transport will be less stiff and may have trouble withstanding the mechanical loads. Currently, it is unknown what the proper balance of these competing properties will be in a successful TE-TDR or even if a viable TE-TDR is possible in the native disc space.

Research Objective

In order to better understand the efficacy of TE-IVD at restoring function to the spine, this dissertation sought to develop a novel tissue engineered IVD and studied both the *in vitro* and *in vivo* development of these constructs. Overall, this body of work represents both a milestone in the reproduction of the native AF architecture in TE-IVD and is the first to study the development of TE-IVD in the native disc space. The overriding hypothesis is that TE-IVD can be implanted into the native disc space and develop an integrated cartilaginous tissue that reproduces mechanical function in the spine. In addition, it is hypothesized that the AF ECM architecture and composition will play a key role in the ECM development both *in*

vitro and *in vivo*. To address these hypotheses, the first aim focused on producing a TE-IVD with controllable AF composition in both collagen density and collagen architecture. The second aim developed an image-guided technique to produce TE-IVD in the proper size and shape for implantation into the native disc space. In order to study the efficacy of replacing the native disc with a TE-IVD, the third aim implanted TE-IVD in the native disc space of an athymic rat for 6 months and investigated the ECM development, integration, and mechanical properties of the motion segment. Finally, the fourth aim studied the effects of AF composition on *in vitro* and *in vivo* development by altering the AF composition and examining its effects *in vitro* and *in vivo* after 6 months of implantation.

Specific Aim 1 (Chapter 2)

Production of a novel TE-IVD with controllable AF composition in both collagen density and collagen architecture.

Effects of boundary conditions and original collagen density were studied in contracting collagen gels seeded with ovine AF cells. Resulting collagen and cellular architecture were observed using second harmonic generation microscopy (SHG) and two-photon excited fluorescence microscopy. Collagen gels with a collagen concentration of 1 mg/ml or 2.5 mg/ml were either contracted as annular gels around a polyethylene disk or contracted as an intact disk for 3 days. Data indicated that decreasing the collagen concentration led to increased contraction, as well as greater circumferential collagen alignment in the annular disk gels. Intact disk gels resulted in no alignment of the collagen fibrils after 3 days of contraction. Technique was used to produce TE-IVD with circumferentially aligned collagen fibrils by contracting annular collagen gels seeded with ovine AF cells around 3% (w/v) alginate seeded with ovine

NP cells for 2 weeks. Study demonstrated that a TE-IVD could be constructed and the AF composition and architecture controlled by altering the original collagen density.

Specific Aim 2 (Chapter 3)

Develop an image-guided technique to produce TE-IVD in the proper size and shape for implantation into the native disc space.

Geometric data of the athymic rat L4/L5 disc space was obtained using common imaging modalities MRI and μCT. T2 weighted MRI was used to obtain NP dimensions, while μCT was used to obtain the outer boundaries of the IVD. By combining this data, the native disc dimensions were obtained. NP dimensions were used to design injection mold of the NP and NP was created using 3% alginate and 25 x 10^6 cells/ml. TE-IVDs were fabricated by contracting 1 mg/ml collagen gel seeded with 1 x 10^6 cells/ml around alginate NP for 2 weeks. Data demonstrated technique produced accurate model from the imaging, and accurate TE-IVDs from the model. Five TE-IVDs were implanted in the L4/L5 disc space for 4 months to demonstrate implantation suitability. At 4 months the discs produced cartilaginous tissue in the disc space, while 3 of 5 discs fully or partially maintained disc space height. This data is the first to demonstrate that TE-IVD could be implanted and produce cartilaginous tissue in the disc space.

Specific Aim 3 (Chapter 4)

Study the efficacy of replacing the native disc with a TE-IVD by investigating the ECM development, integration, and mechanical properties of the motion segment after 6 months of implantation.

TE-IVDs were constructed for the athymic caudal 3/4 disc space using the image-guided fabrication method developed in aim 3. TE-IVD was implanted into the native disc space following removal of the native disc and maintained for either 6 weeks or 6 months. Engineered tissue development was analyzed using histological staining, quantitative biochemistry, 7T MRI, and axial mechanical testing of the motion segments. Data demonstrated that TE-IVD was able to maintain a majority of disc space height, integrate into the native disc space, produce native level ECM, and reproduce the axial mechanical function of the native motion segment after 6 months of implantation. This was the first study to demonstrate the feasibility of replacing a native disc with a TE-IVD in the native disc space by demonstrating the ability of the engineered tissue to closely mimic the properties of the native IVD after 6 months of implantation.

Specific Aim 4 (Chapter 5)

Study the effects of AF composition on *in vitro* and *in vivo* development by altering the AF composition and examining its effects *in vitro* and *in vivo* after 6 months of implantation.

Six groups of TE-IVDs were constructed by altering the original collagen concentration and cell seeding density of the AF during fabrication. AF composition and architecture were analyzed using SHG and TPEF imaging. *In vitro* mechanical function of TE-IVD groups was determined in unconfined compression by measuring the equilibrium modulus, instantaneous modulus, and hydraulic permeability. Two groups were selected for implantation into the native disc space and maintained for 6 months. Engineered tissue was studied with histological staining, quantitative biochemistry, and axial mechanical testing of the motion segments. *In vitro* data

indicated that changing the AF composition altered the pressurization of the TE-IVD under loading and was likely related to the changes in AF hydraulic permeability observed between groups. Furthermore, altering the AF composition pushed the TE-IVD towards a more IVD like phenotype in the disc space. In fact, tuning the AF produced an engineered tissue that had no statistically significant differences in proteoglycan and collagen in the AF or NP after 6 months of implantation.

CHAPTER 2

Specific Aim 1

Self-Assembly of Aligned Tissue Engineered Annulus Fibrosus and IVD Composite via Collagen Gel Contraction*

Abstract

Many cartilaginous tissues such as intervertebral (IVD) disc display heterogeneous collagen microstructure that results in mechanical anisotropy. These structures are responsible for mechanical function of the tissue and regulate cellular interactions and metabolic responses of cells embedded within these tissues. Using collagen gels seeded with ovine annulus fibrosus cells, constructs of varying structure and heterogeneity were created to mimic the circumferential alignment of the IVD. Alignment was induced within gels by contracting annular gels around an inner boundary using both a polyethylene center and alginate center to create a composite engineered IVD. Collagen alignment and heterogeneity were measured using second harmonic generation microscopy. Decreasing initial collagen density from 2.5 mg/ml to 1 mg/ml produced greater contraction of constructs, resulting in gels that were 55% and 6.2% of the original area after culture, respectively. As a result, more alignment occurred in annular shaped 1 mg/ml gels compared to 2.5 mg/ml gels ($p<.05$). This alignment was also produced in a composite engineered IVD with alginate nucleus pulposus. The resulting collagen alignment could promote further aligned collagen development necessary for the creation of a mechanically functional tissue engineered IVD.

---

* This chapter was recently published: Bowles, R.D., Williams, R.M., Zipfel, W.R., and Bonassar, L.J. Self-assembly of aligned tissue-engineered annulus fibrosus and intervertebral disc composite via collagen gel contraction. Tissue engineering 16, 1339, 2010.

Introduction

Lower back pain is one of the leading causes of disability in the United States with estimated indirect and direct annual costs ranging from $20 to $100 billion (100). Lower back pain (LBP) is frequently associated with diseased or injured intervertebral disc (IVD) (101-104). The IVD has two distinct regions, the annulus fibrosus (AF) and nucleus pulposus (NP) that are biochemically, mechanically, and cellularly distinct and work in concert to provide mechanical function (43, 105-107). The NP is primarily responsible for providing the IVD with its compressive properties while the AF provides the shear and tensile properties and containment of the NP (40). The NP extracellular matrix is unaligned and composed primarily of type II collagen and proteoglycans. In contrast, the AF is highly organized and predominantly composed of type I collagen and proteoglycans (42-45, 108-110). This highly organized aligned collagen fibril architecture provides the IVD with many of its complex anisotropic shear and tensile mechanical properties (111). It is the complex architecture of the IVD that is responsible for providing mobility to the spine while handling the hoop, torsional, and bending stresses imposed upon it during motion of the spine.

Current treatments for degenerative disc disease include spinal body fusions, partial discectomies, nucleus pulposus replacements, and total disc replacements (1). Spinal body fusions and partial discectomies focus on alleviating the symptoms of LBP but do not focus on maintaining function of the spine and the IVD. Furthermore, spinal body fusions often result in degeneration and damage to the adjacent disc levels due to the altered biomechanics (112). Replacing degenerated nuclear material holds promise for treating IVD disease, but can only be applied when the AF tissue is healthy.

Synthetic total disc replacements are used to completely replace the diseased IVD tissue and maintain the function of motion segments (113-116). However, the

long-term performance of these implants and their effects on the adjacent disc levels are unknown. Further, wear and fatigue that likely will occur in synthetic discs present additional complications for clinical use. As a result, recent efforts have focused on using tissue engineering strategies that can replace diseased IVD tissue to treat LBP.

Efforts to develop a tissue engineered IVD have focused largely on generating NP tissue, with fewer studies focusing on the AF (65, 67, 70, 117, 118). The NP is an ideal target for tissue engineering due to the isotropic nature and gel-like structure. However, because IVD disease and injury are often not limited to the NP, developing an implant that also focused on the AF is likely necessary for a variety of applications. A number of scaffolds have been suggested for AF tissue engineering including porous silk scaffolds (119), an alginate/chitosan hybrid (120), demineralized bone matrix (121), electrospun PCL fibers (122, 123), hyaluronic acid-nanofibrous scaffold (87), collagen/GAG scaffolds (124), and PGA mesh (58, 59). Mizuno et al. developed a composite structure of both the AF and NP (58, 59), but these structures had limited collagen organization in the AF. To date, few studies have attempted to address the aligned and anisotropic nature of the AF: the first used electrospun nanofibrous scaffolds with aligned PCL fibers (122, 123); while the second used a wet-spinning and lyophilization technique to create an aligned alginate/chitosan scaffold (120). In contrast, this work will attempt to create such collagen alignment using biological self-assembly that can be employed in an engineered composite IVD containing both AF and NP.

In efforts to engineer other types of tissue, aligned collagen fibril architectures have been generated by contracting collagen gels under a variety of boundary conditions (125-127). Costa et al. (128) used this technique to create circumferentially aligned fibrils by imposing an annular outer boundary on contracting collagen gels

seeded with human-dermal fibroblasts. The use of an inner mandrel has also been shown to produce aligned structures in tissue engineered blood vessels (98). The current study extends this work to create and regulate circumferential fibril alignment in tissue-engineered AF using cell-induced contraction of collagen gels around inner mandrels. While the native AF has a multilamellar cross-ply organization of the collagen fibrils, the larger circumferential organization is responsible for resisting the hoop stresses experienced during compression. For this reason this study has focused on creating circumferential alignment utilizing AF cells. The specific objectives of this study were to examine the influence of boundary geometry and construct composition on the development of collagen architecture induced by AF-cell driven gel contraction using second harmonic generation (SHG) and two-photon excited fluorescence (TPEF) microscopy (129-131) to image cell and collagen alignment. As a result, the purpose of this work was to demonstrate the feasibility of this technique and develop an understanding of the resulting collagen alignment that could be applied in future work to create mature engineered IVD.

Materials and Methods

Cell Preparation. The cell preparation techniques were based on previously described techniques (59). Sixteen IVDs were dissected out of the lumbar spine region of four adult skeletally mature (~14 month old) Finn/Dorset cross male sheep (Cornell University Sheep Program, Ithaca, NY) and washed in phosphate-buffered saline (PBS) solution (Dulbecco's Phosphate Buffered Saline, Gibco BRL, Grand Island, NY). The AF region of the discs was separated from the NP and dissected into small pieces that were digested in 200 ml of 0.3% w/v collagenase type II (Cappel Worthington Biochemicals, Malvern, PA) at 37° C for 9 hours. Digested tissue was filtered through a 100 μm nylon mesh (BD Biosciences, Bedford, MA) and

centrifuged at 936 x g for 7 minutes. The cells were washed 3 times in PBS, counted, and seeded at a density of 2500 cells/cm^2 in culture flasks with Ham's F-12 media (Gibco BRL, Grand Island, NY) containing 10% fetal bovine serum (Gemini Bio Products, Sacramento, CA), ascorbic acid (25 μg/ml), penicillin (100 IU/ml), streptomycin (100 μg/ml), and amphotericin B (250 ng/ml). Cells were cultured to confluence at 37° C , 5% CO_2 atmosphere, normoxia, pH of 7.2, and 300 mOsm. Following culture, cells were removed from T-150 flasks with 0.05% trypsin (Gibco). Cell viability and number were counted with a hemocytometer and trypan blue vital dye. Cells were then diluted to the appropriate concentrations and seeded in collagen gels.

Collagen Solution Preparation. Collagen type I was obtained from rat tails using established protocols (Pel-Freez Biologicals, Rogers, AZ) (132). Briefly, tendons were dissected from rat tails and transferred to a solution of dilute acetic acid (.1%) at a volume of 80 ml per gram of tendon at 4° C for 48 hours. The solution was centrifuged at 9000 rpm and the supernatant was transferred and centrifuged a second time to remove the unsolubilized collagen, blood, and muscle tissue. The solution was then subjected to the BCA assay (Pierce, Rockford, IL) to determine the collagen concentration of the resulting solution. The stock solution was stored at 4° C until needed.

Collagen Construct Fabrication. Prior to producing gels, tissue culture plates were incubated with a 2% BSA solution at 37° C for one hour to prevent construct adhesion to tissue culture plates upon gelation. The stock collagen solution was mixed with the appropriate volumes of 1 N NaOH, 1X PBS, and 10X PBS to return the pH to 7.0, maintain 300 mOsm, and produce the appropriate collagen concentrations for the

study (133). This solution was immediately mixed at a 1:1 ratio with the cell/media solution and pipetted into the appropriate tissue culture plate and allowed to gel for 30 minutes at 37° C. After the constructs had gelled, they were floated with 2 ml of the previously described media.

Collagen Disk and Annular Constructs. A total of 70 collagen disk constructs were created by pipetting 1 ml of collagen-cell solution into a 24 well tissue culture plate and allowing it to gel. Collagen annular constructs were created by pipetting 1 ml of the collagen-cell solution into a 12 well tissue culture plate with a 1 cm in diameter porous polyethylene disk at the center to yield an annular shaped collagen ring surrounding the polyethylene. Porous disk was selected to encourage gel to remain around disk when floated with media. Two groups were made for both constructs shapes with final collagen concentrations of 2.5 mg/ml and 1 mg/ml and a final cell concentration of 1×10^6 cells/ml. The discs were floated with 1 ml of media for the disk constructs and 2ml of media for annular constructs in each well to maintain similar degree of floating in wells during culture. Seven constructs per group were used for LIVE/DEAD cell viability assay (Invitrogen, Carlsbad, CA) immediately after construction. In addition, constructs were cultured for 3 days and allowed to contract freely with **7** constructs per group being harvested at 0, 1, 2, and 3 days. At each time point, constructs were digitally photographed to quantify construct area, then fixed with phosphate-buffered formalin for 48 hours, with sections of each sample being utilized for second harmonic generation microscopy analysis of collagen fibril orientation and histology.

Composite Discs. Alginate hydrogel NP was produced by mixing 3% (w/v) alginate seeded with 25×10^6 cells/ml with 2% $CaSO_4$ at 2:1 ratio and injected between glass

plates to produce 2 mm thick alginate sheet. 1.5 mm biopsy punch was shaped into NP shape dimensions obtained from rat lumbar discs and NP was punched out of sheet. Alginate NP was subsequently placed in center of 24 well plate and .405 ml of 2 mg/ml collagen solution was pipetted around alginate NP to produce 2 mm thick collagen ring surrounding 2 mm thick NP. A total of 21 composite discs were made and seven constructs were used for LIVE/DEAD cell viability assay (Invitrogen, Carlsbad, CA) immediately after construction. Gels were then floated with 1 ml of media and allowed to culture for zero and two weeks with **7** discs being harvested at each time point and processed in similar manner to annular and disk constructs.

Digital Imaging. All constructs were imaged with a digital camera (Canon Powershot G5) and quantitatively analyzed for surface area using the Image J software (NIH, Bethesda, MD) immediately following harvest on 0, 1, 2, and 3 days.

Second harmonic generation and two-photon excited fluorescence microscopy. Procedures of simultaneous second harmonic generation (SHG) microscopy of collagen type I fibrils and two-photon excited fluorescence (TPEF) microscopy of cells were based on those described previously (129, 131). SHG and TPEF images were obtained using a custom built multi-photon microscope with a Ti:Sapphire mode-locked laser providing 100 fs pulses at 80 MHz tuned to a wavelength of 780 nm. Images were acquired using a BioRad 1024 laser scanner coupled to an Olympus 1X-70 inverted microscope. Incident light was focused on the sample using either a 40x or 20x objective. Samples were loaded onto the microscope so that fibrils aligned in the circumferential direction of the constructs were in the 90° direction according to a specified coordinate system (Fig. 2.1). TPEF and back-propagating second harmonic signals were collected and separated by a dichroic filter into two

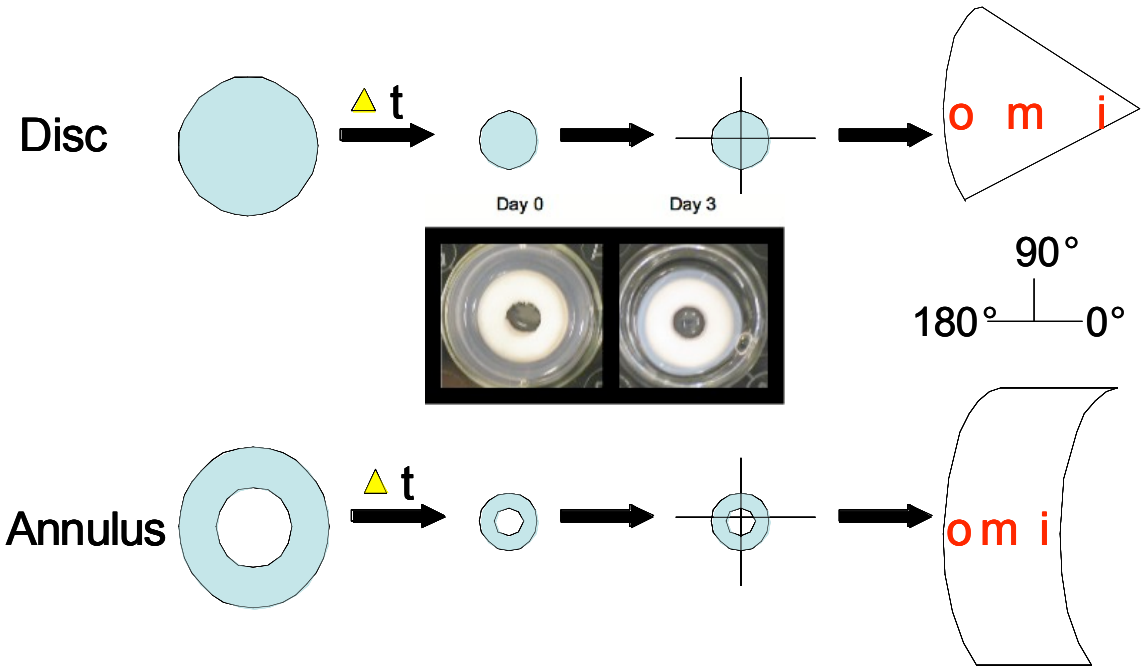

Figure 2.1. Overview of gel culture and imaging methods. Annulus and disk gels were contracted over three days before being segmented for imaging. Images were obtained from the outer(o), middle(m), and inner(i) regions of each gel, as defined here. Coordinates were defined in reference to the imaged gel segments.

photomultiplier tubes (PMTs). One PMT collected the epi-SHG at 360-410 nm produced by the collagen type I fibrils while the other PMT collected TPEF signal at 420-500 nm produced by the cells (primarily NADH). For both annular and disk constructs, SHG images were obtained to study the collagen fibril orientation throughout contraction. Z-series were collected with a 20x/0.7 NA water immersion objective to a depth of 80 μm (9 images at 10 μm intervals) at the outer, middle, and inner regions of the gels. The images were obtained for four samples for each time point and construct type. Images were also taken at higher resolution with an Olympus 40x/1.3 NA oil objective to observe fibril and cellular interactions.

Image Analysis. Collagen fibril orientation was calculated from SHG images with a custom MATLAB code based on a previously described technique (116). This technique has been applied to SEM, histological, and confocal images and is applied to SHG images in this paper (134-137). The algorithm relies on the fast fourier transform of the SHG images (Fig. 2.2a). The program summed the intensity of the FFT along lines at 5° increments from 0 - 180° (Fig. 2.2b) via the coordinate system described (Fig 2.1). The angular distribution of summed intensities was calculated, representing the relative orientation of the fibrils within the image (Fig. 2.2c). From this histogram, the mode was calculated, which represents the angle of maximum alignment, and using equation (1) an alignment index (AI) was calculated.

$$AI = \frac{\int_{\theta_m - 20^\circ}^{\theta_m + 20^\circ} I \partial\theta}{(40^\circ / 180^\circ) * \int_{0^\circ}^{180^\circ} I \partial\theta} \quad (1)$$

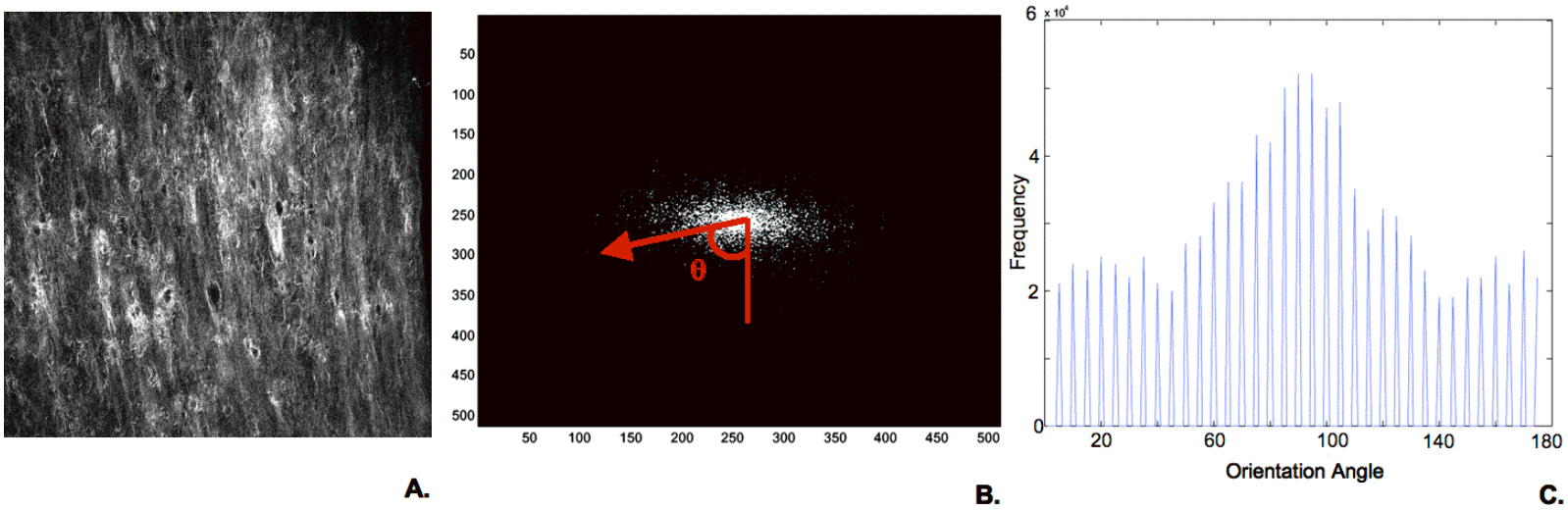

Figure 2.2. Collagen fiber alignment quantification. (A) SHG microscopy image. (B) Fourier transform of image (contrast adjusted). Fourier amplitude components (FFT image intensities) were summed up along angles at 5º increments from 0-180º and represented as an arrow and θ. (C) Summation of amplitudes resulted in a histogram of the image intensities along each 5º increment and from this histogram the mode was calculated and the alignment index was calculated according to equation 1.

AI ranges from 1 (unaligned) to 4.5 (complete alignment of fibers). Together the AI provides the degree of alignment observed while the mode angle provides the direction of alignment.

Histological Analysis. One sample at each time point was fixed for 24 hours with 10% phosphate-buffered formalin. The specimens were embedded within paraffin and serial sections of 5 μm were cut and stained with hematoxylin and eosin (H&E) for comparison to SHG and TPEF images.

Statistical Analysis. All statistical analysis was performed using three-factor ANOVA and Bonferroni post hoc test. The AI parameter was tested for the effect of time in culture (0, 1, 2, and 3 days), region of gel (outside, middle, and inside), and density of gel (1 mg/ml and 2.5 mg/ml).

Results

Contraction

Macro scale

The disk and annular constructs followed a similar contraction profile (Fig. 2.3). The 2.5 mg/ml disks contracted to 75±2.1 % of the original area by Day 3 compared to a contraction of 55±4.1 % of the original area for the 2.5 mg/ml annular gels on Day 3. The 1 mg/ml disks contracted to 15±1.1 % of original area while 1 mg/ml annular gels contracted to 6.2±1.4 % by Day 3. The 1 mg/ml gels contracted very quickly from Day 0 to Day 1 and approached steady state, compared to the slower and more steady

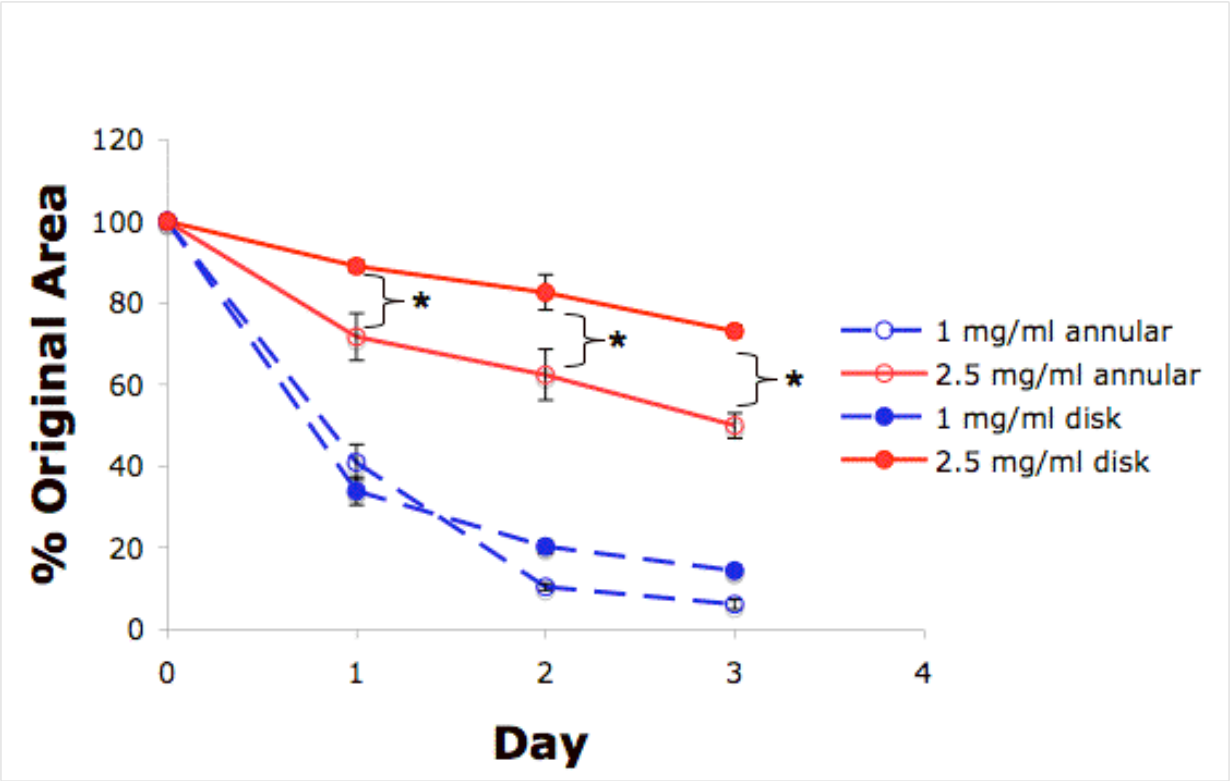

Figure 2.3. Contraction of disk and annular gels represented as a percent of the constructs original surface area. Data presented as means ± standard deviations for n = 7. (* = $p < .05$)

contraction seen in the 2.5 mg/ml gels over the 3 days. Neither the disks nor the annular constructs showed a change in thickness over the 3 days of contraction. In addition, constructs showed no difference ($p<.05$) between groups in viability after construction with a mean viability of all groups of 92±2%.

Micro scale

Collagen distribution inside the constructs changed markedly during the contraction process (Fig. 2.4a). At Day 0, collagen was distributed uniformly throughout the sample. Over the course of 3 days, the distribution became more heterogeneous in the disks, with more collagen evident in the pericellular region surrounding AF cells. This effect occurred at both concentrations, but was more pronounced in 1.0 mg/ml gels. Further, in regions where cells were in tight proximity, collagen fibers were rearranged to form larger bundles on lines between cells (Fig. 2.4b). On a larger length scale, this collagen rearrangement resulted in the development of circumferential collagen fibril and cellular alignment within the annular gels (Fig. 2.5)

Fibril Orientation

Collagen disks showed little change in fibril alignment over the 3 days of contraction for both the 1mg/ml and 2.5 mg/ml disks, as indicated by AI values that ranged from 1.2-1.3 over 3 days (data not shown). In contrast to the disk constructs, the annular constructs showed a large degree of fibril alignment in all regions of the constructs over the 3 days of contraction (Fig 2.6). The AI of the 1.0 mg/ml annular construct increased from <1.3 at Day 0 to 1.6 at Day 1, and remained at ~1.6 for Day 2 and 3. No significant differences were noticed between regions of the constructs on the same day when the data was analyzed based on region.

In 2.5 mg/ml gels AI increased slowly and more steadily over the 3 days of contraction, changing from ~1.3 on Day 1 to 1.4 by Day 3 ($p<.05$ compared to Day 0).

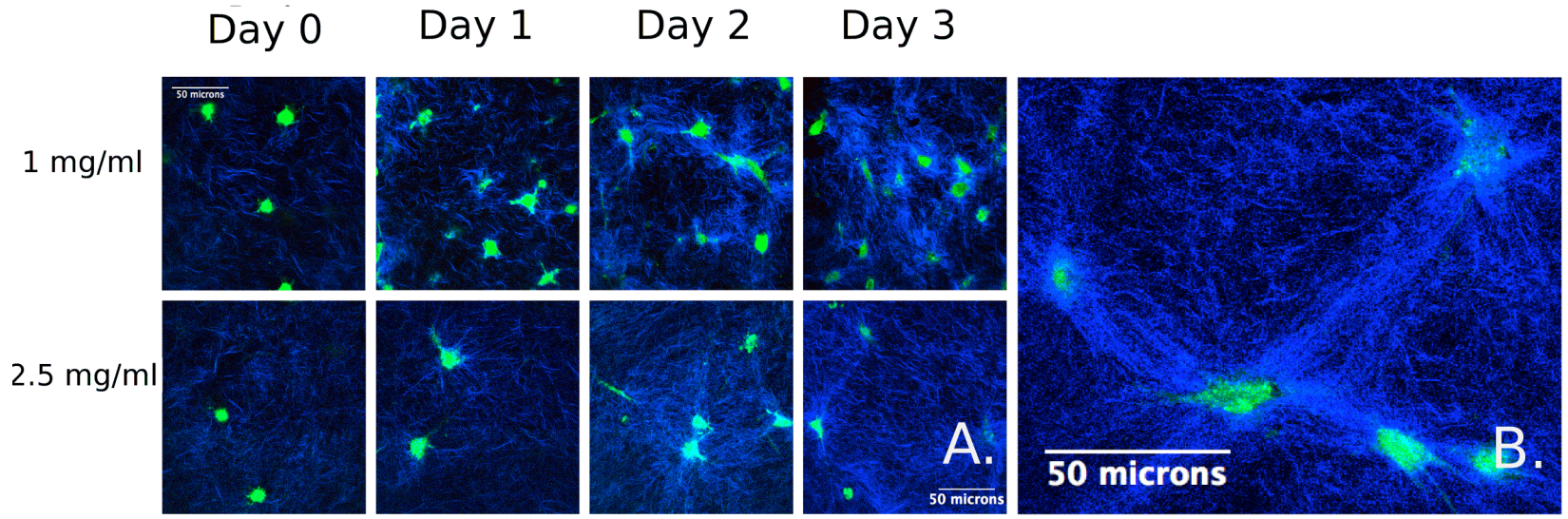

Figure 2.4. SHG-TPEF images (A.) from inside region during contraction of 1 mg/ml and 2.5 mg/ml collagen disk constructs over 3 days (B.) and magnified image showing aligned fibers between cells on Day 3 of contraction in 2.5 mg/ml collagen disks (blue - collagen, green - cell).

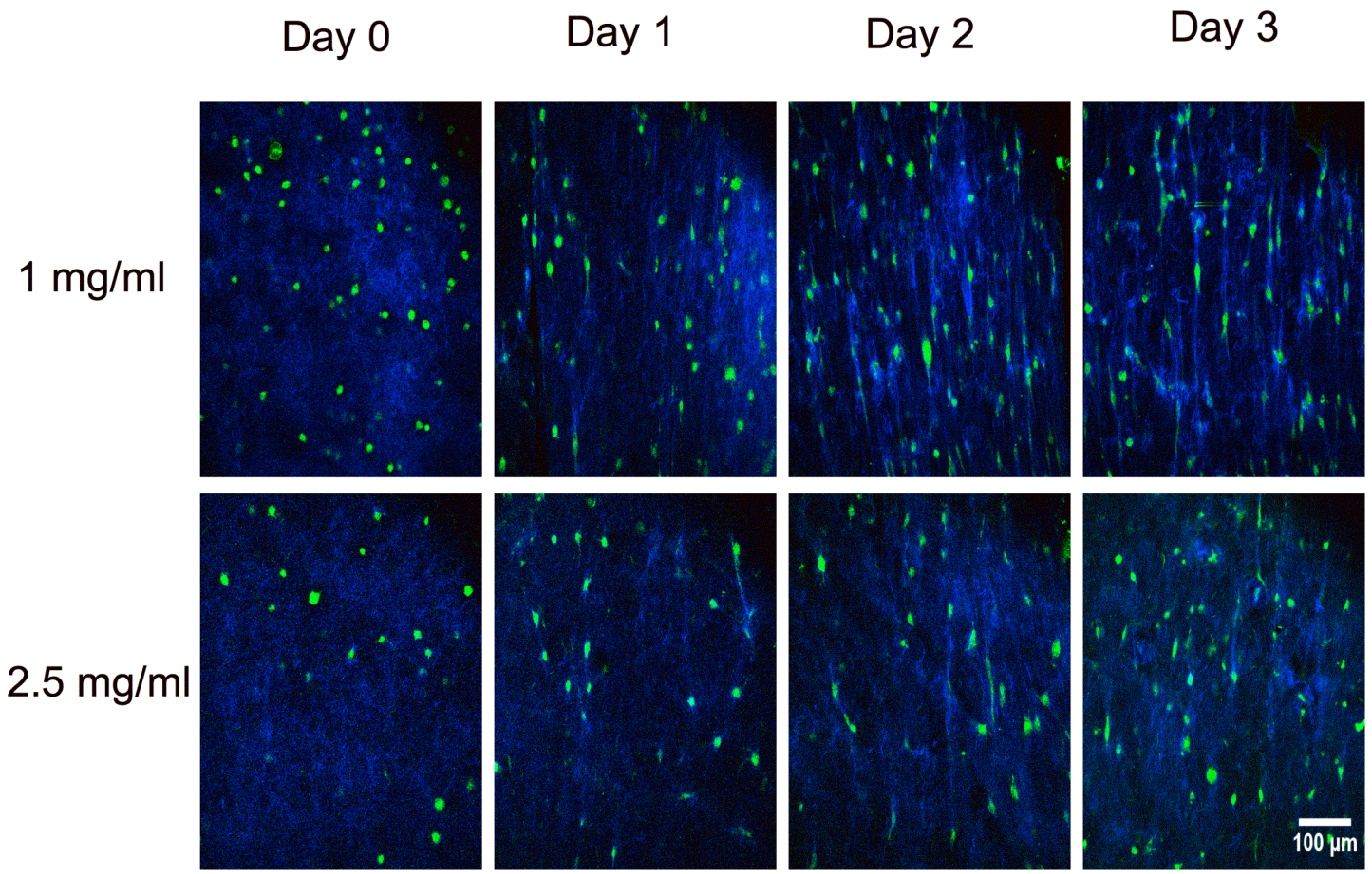

Figure 2.5. SHG-TPEF images from inside region during contraction of 1 mg/ml and 2.5 mg/ml collagen annular constructs over 3 days.

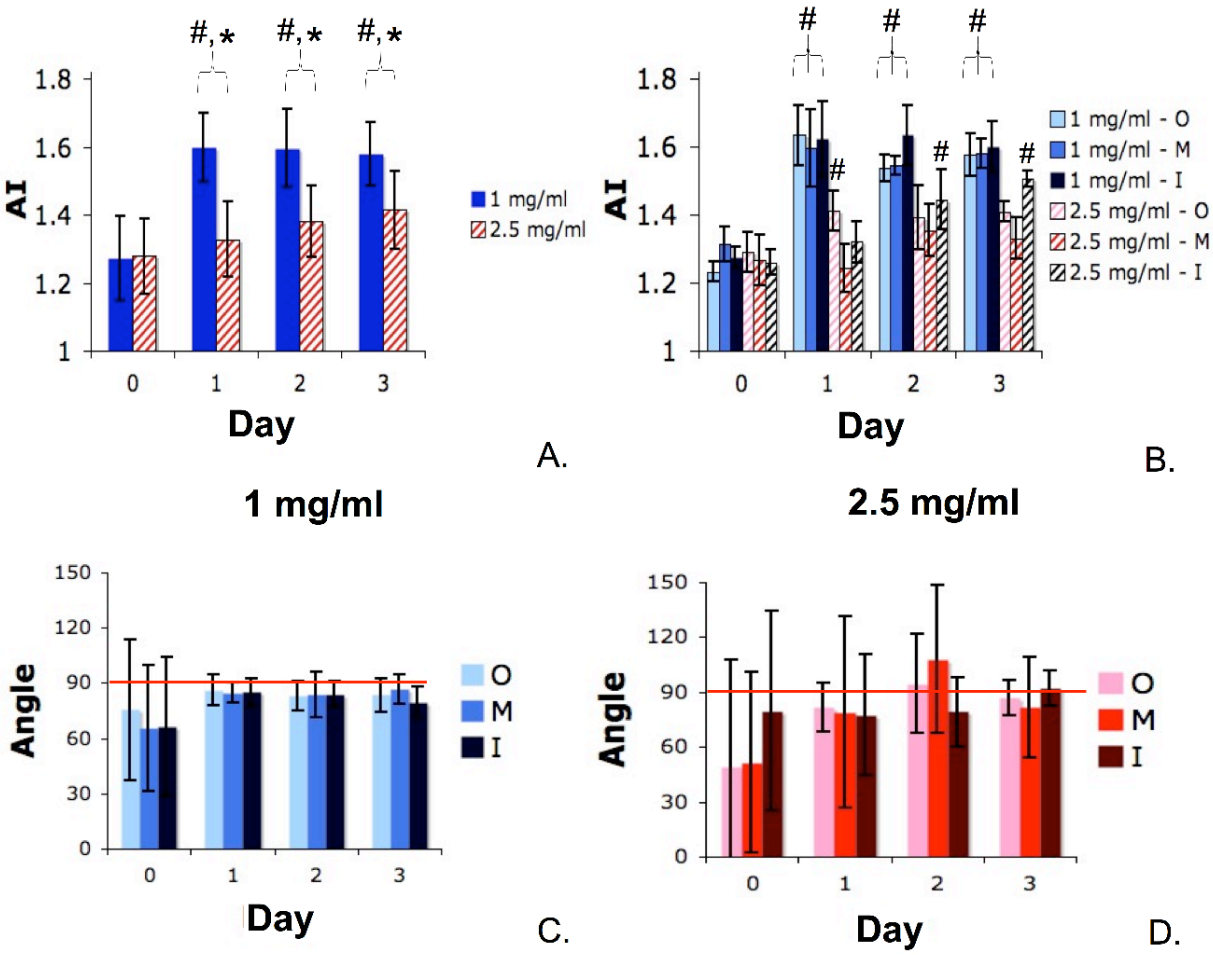

Figure 2.6. SHG alignment data for collagen annular gels with (A.) AI broken down by day and gel concentration (n = 21), (B.) AI further broken down by region of gel (n=7) (O - outside, M-middle, I - inside), and mode angle broken down by day, concentration, and region of gel for (C.) 1 mg/ml (n=4) and (D.) 2.5 mg/ml gels (n=7). Data presented as means and standard deviations. (# = $p < .05$ compared to day 0) (* = $p < .05$ for indicated groups)

In contrast to the 1 mg/ml annular gels, the 2.5 mg/ml gels showed regional heterogeneity, with the middle regions less aligned compared to the inner and outer regions over days 1, 2, and 3 (3 way ANOVA, $p<.05$). The 1 mg/ml gels showed significant increases ($p<.05$) in fibril alignment compared to the 2.5 mg/ml gels at Day 1, Day 2, and Day 3. With time, mode angles progressed toward 90° and distributions became narrower indicating a direction of alignment in the circumferential direction (Fig. 2.6 c,d). These trends were present for both 1.0 and 2.5 mg/ml gels, but were more pronounced for 1.0 mg/ml gels. Overall, the data indicates a circumferential alignment of collagen fibrils resulting from annular gel contraction around a polyethylene core.

Cellular Orientation

Disk gels showed no global alignment of cells over the 3 days of contraction despite showing some evidence of cellular elongation (Fig. 2.7). However, annular gels showed cellular elongation and circumferential alignment of the cells over the 3 days. The cells developed a spindle-shaped morphology elongated between and parallel to the collagen fibrils similar to the morphology and alignment observed in the IVD.

Composite Discs

Composite discs formed in size and shape of rat lumbar IVD. Collagen gel AF analogue seeded with AF cells contracted around alginate NP analogue seeded with NP cells. Collagen fibrils produced AI of 1.57 ± .06 in the circumferential direction (Fig. 2.8).

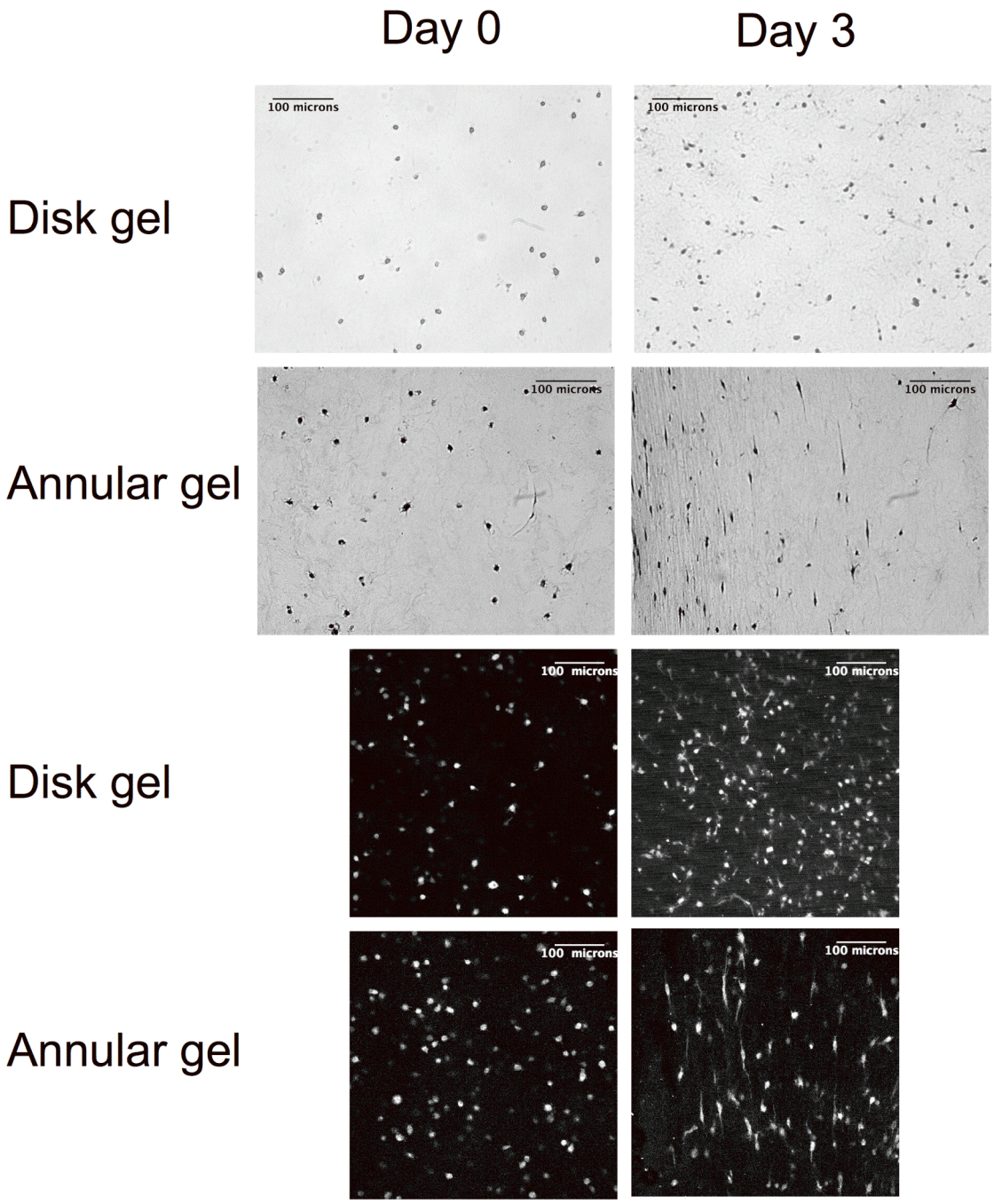

Figure 2.7. Hematoxylin and eosin staining and TPEF cellular imaging of 1 mg/ml disk gels and annular gels at Day 0 and 3 of contraction from inside region of gel.

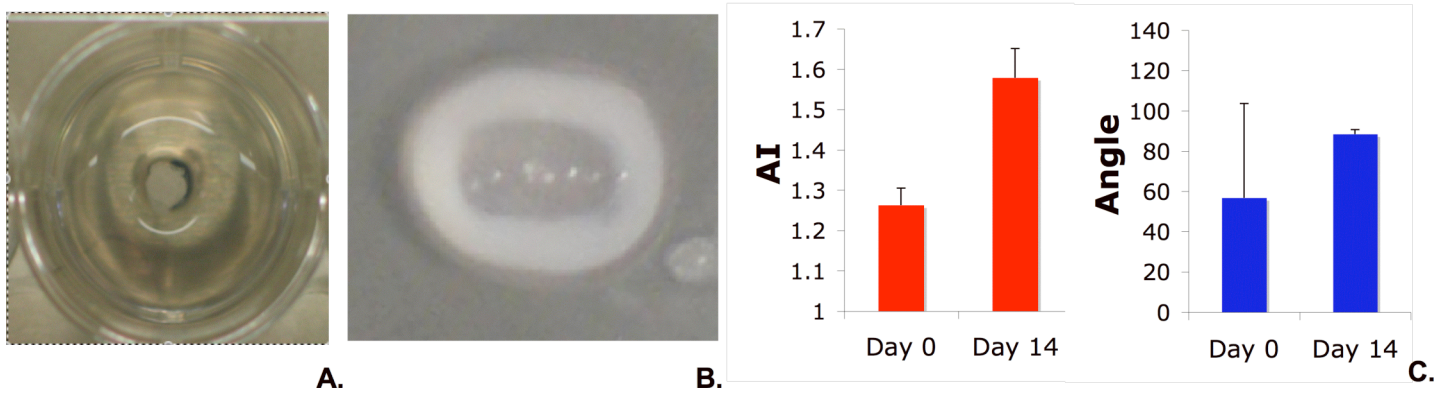

Figure 2.8. (A.) Composite disc before contraction with alginate NP in center of well and collagen solution poured around alginate NP. (B.) Composite disc after 2 weeks of culture with collagen gel contracted around alginate NP forming tissue engineered composite IVD. (C.) SHG alignment data measured across entirety of contracted collagen gel thickness indicating high degree of collagen alignment in circumferential direction at day 14.

Discussion

The broad goal of this work is to develop a method for self-assembly of an aligned IVD AF construct from seeded collagen gels that can be employed in an engineered IVD composite. This study focuses on remodeling of collagen gels by AF cells and the creation of annular constructs with circumferentially aligned fibrils. Previous efforts to make IVD tissue engineered constructs have focused mainly on developing the compressive properties of the tissue with less focus on the development of an aligned collagen fibril and cellular architecture in the AF region to provide the necessary tensile and shear properties. Some work has demonstrated the creation of aligned IVD cells in microgrooves (138) and created tissue engineered scaffolds with aligned nanoscale fiber orientation for use in AF tissue engineering applications (122, 123). However, to date none of these methods have yielded a composite IVD with aligned collagen fibrils and AF cells around an engineered NP.

In this study, the cellular and fibril architecture were controlled by the boundary conditions imposed on contracting collagen gels. This study demonstrates that over the 3 days of culture, a steady increase of circumferential alignment was observed in both the 2.5 mg/ml and 1 mg/ml gels (Fig. 2.7) with a fixed inner boundary. The increased alignment observed in the 1 mg/ml annular gel compared to the 2.5 mg/ml annular gel is likely due to the increased contraction observed in the 1 mg/ml annular gel (6.2±1.4 % of original area) compared to the 2.5 mg/ml annular gel (55±4.1 % of original area). The increase in alignment was consistent with the profile of the contraction curves of the two concentrations of gels in the annular gels. Furthermore, similar alignment was observed in a composite construct with a circumferentially aligned collagen AF contracted around an alginate NP (Fig. 2.8). In contrast to the annular gels and composite, minimal alignment was observed in the disk gels at 3 days. The ability to create an unaligned disk structure in combination

with the aligned annular gels may be useful in studying the effects of collagen architecture on tissue development in future studies. Overall, this technique enables control of the degree and heterogeniety of alignment through the original collagen concentrations of the gels and boundary conditions.

Similar techniques have been employed in other tissues to create aligned collagen fibril structures. Costa et. al. (128) used an analogous technique to create aligned collagen fibrils in engineered heart tissue, while Stegemann et al. (98) incorporated this technique in engineered blood vessels. Wagenseil et al. (139) showed that circumferential alignment developed by fibroblast populated gels resulted in mechanical anisotropy. Schneider et al. (140) demonstrated the ability of annulus fibrosus cells to contract collagen/GAG scaffolds. The results of the current study show the ability to use these techniques to create an annular construct with both circumferentially aligned collagen fibrils and aligned AF cells after 3 days of contraction.

While the main goal of this study was to create collagen alignment in the AF region, it is likely that the cell alignment and shape may be of great importance. In order to produce a mechanically functional tissue from a collagen gel, long-term culture is likely needed. Fibroblasts are known to increase collagen type I expression when maintained in an aligned spindle shape as compared to a randomly oriented structure and is further enhanced with the application of a tensile stimulation (141). The spindle shaped circumferential cellular alignment (Fig. 2.7) may be advantageous for the future development of the ECM in long-term culture, as well as for priming AF cells for mechanical stimulation.

The use of SHG-TPEF microscopy enabled the simultaneous study of collagen architecture and cell morphology. More collagen was observed in the pericellular region of the cells in the disk constructs over the three days of contraction and was

greater in the 1 mg/ml gels than in the 2.5 mg/ml gels. The increased concentration of collagen within these pericellular regions could result from newly synthesized collagen, as suggested by Torkian et al. (142), or from pulling of collagen fibrils into the pericellular region by cells. The observed similar profiles of the gel contraction and the development of the increased pericellular collagen between the two concentrations of gels along with the relatively short culture time suggest a contraction mechanism over a collagen production mechanism. The varying collagen architecture suggests that while tissue-scale variables, such as total collagen concentration, regulate mechanical properties, it is also important to characterize the microscale collagen architecture that may also yield insight into the process of tissue assembly.

The SHG-TPEF images also showed a cell-fibril-cell interaction. As the gels contracted, fibrils were aligned between adjacent cells in the disk and annular gels (Fig. 2.5). The alignment of collagen networks between two cellular islands seeded in collagen gels has been proposed in model and experimentally observed by Ohsumi et al. (143) but can be seen here in the SHG images occurring between individual cells. This provides a possible mechanism for the alignment of fibrils observed within the annular gels. Fibrils first become stretched between the cells and as the cells pull and contract around the fixed inner core the strained fibrils between cells will be predominately oriented in the circumferential direction due to the imposed physical boundary and circumferential tensile stresses. This would not result in aligned fibrils in unbounded disks as no boundaries have been applied and the cells will contract isotropically. Furthermore, this data suggests the possibility that cell patterning could be employed in collagen gels to further control the resulting collagen architecture of contracted collagen gels in the future.

Despite the advancements presented in this paper and observed in the field, the creation of a clinically applicable tissue engineered IVD faces a number of challenges.

One significant challenge is the creation of a disc with sufficient mechanical properties to replace the native IVD. Because mechanical properties are tied to the presence of adequate amounts of collagen and proteoglycan, this requires significant metabolic activity in an environment with low oxygen and high osmolarity (144, 145). In addition to mechanical concerns, an engineered IVD will need to integrate with the native tissue when implanted, and survive in the native disc space environment upon implantation. Despite these challenges the techniques described here for producing an aligned AF represent an important step toward making a functional composite IVD.

Furthermore, collagen alignment in the native AF is not only circumferential in direction, but also at an alternating angle of ±28° between adjacent lamellae and increasing to 44° at the inner AF (50, 51). Achieving this alternating pattern of alignment remains a persistent challenge in IVD tissue engineering with electrospinning being proposed as a possible solution (123). However, the current technique enables generation of the dominant circumferential alignment of the collagen fibrils/cells in a composite engineered IVD and provides techniques that in future work may provide this further complexity in structure. Furthermore, the ability to deposit successive layers of collagen gels may enable the generation of constructs with multiple lamellae. As a result, contracting collagen gels provides a powerful tool to create the complex structure of the AF and warrants further investigation.

CHAPTER 3

Specific Aim 2

Image-Based Tissue Engineering of a Total Intervertebral Disc Replacement for Restoration of Function to the Rat Lumbar Spine*

Abstract

Non-biological total disc replacement is currently being used for the treatment of intervertebral disc (IVD) disease and injury, but these implants are prone to mechanical wear, tear, and possible dislodgement. Recently, tissue engineered total disc replacement (TE-TDR) has been investigated as a possible alternative to more fully replicate the native IVD properties. However, the performance of TE-TDRs has not been studied in the native disc space. In this study, magnetic resonance imaging (MRI) and microcomputed tomography (μCT) imaging of the rat spine were used to design a collagen (annulus fibrosus)/alginate (nucleus pulposus) TE-TDR to a high degree of geometric accuracy with less than 10% difference between the TE-TDR and the native disc dimensions. Image-Based TE-TDR implants were then inserted into the athymic rats' (n=5) L4/L5 disc space and maintained for 16 weeks. Disc space was fully or partially maintained in three of five of the animals and proteoglycan and collagen histology staining was similar in composition to the native disc. In addition, good integration was observed between the TE-TDR and the vertebral bodies, as well as remnant native IVD tissue. Overall, this study provides evidence that TE-TDR strategies may yield a clinically viable treatment for diseased or injured IVD.

***** This chapter is currently in press: Bowles, R.D., Gebhard, H.G., Dyke, J.P., Ballon, D.J., Tomasino, A.T., Cunningham, M.E., Hartl, R., and Bonassar, L.J. Image-Based Tissue Engineering of a Total Intervertebral Disc Replacement for Restoration of Function to the Rat Lumbar Spine. *NMR in Biomedicine*, In Press.

Introduction

Back pain is one of the leading physical conditions for which patients see their doctors. One cause commonly associated with back pain is a diseased or injured intervertebral disc (IVD) (101-104). In patients who have failed non-operative treatment, surgery, including discectomy, spinal fusion, or total disc replacement, may be indicated. In 2004, discectomy procedures in the United States encompassed a total cost of $11.25 billion and spinal fusion surgeries a cost of $16.9 billion (146). Spinal fusion procedures are performed frequently and relieve pain; however, they often result in a loss of mobility and the possible development of adjacent level disease (ALD).

For this reason, non-biological total disc replacement (NB-TDR) technologies have emerged that are designed to retain mobility in the motion segment and reduce the occurrence of ALD. While there currently is a lack of long-term information from these studies, short-term data indicate that NB-TDR may be more successful in reducing the occurrence of ALD than fusion surgery (26, 27); however, NB-TDR is subject to mechanical failure, dislodgement, and polyethylene wear. Such wear debris may lead to osteolysis, as shown in several studies involving hip and knee replacements (28, 29). Consequently, tissue-engineered total disc replacement (TE-TDR) has been developed with the potential to restore function to the motion segment (58, 59, 87, 93). Despite the interest in TE-TDR, no work has been performed to understand how TE-TDR would perform in an actual *in vivo* disc space.

A major challenge in developing a TE-TDR is the complex composite structure of the IVD, which contains an inner nucleus pulposus (NP) and the surrounding lamellar annulus fibrosus (AF). The NP is an isotropic-gelatinous tissue predominantly made up of proteoglycans and collagen type II. In contrast, the AF is a highly anisotropic tissue primarily made up of collagen type I and proteoglycans (42,

44, 45, 108-110). The AF is macroscopically organized into concentric lamellae. The collagen fibrils within each lamellae are highly organized and aligned at an alternating ±28 ° angle in each adjacent concentric lamellae (50, 51). The IVD is integrated to the vertebral bodies by the cartilage endplate and directly by AF collagen bundles at the outer AF (39). This complex structure in the IVD is key to the mechanical functioning of the IVD (40) and creating this structure has been the focus in a number of IVD tissue engineering studies (58, 120, 121, 138, 147). However, much is assumed and little is understood about how these structures will develop, be maintained, and integrate *in vivo*. This type of information is vital in developing design criteria for the future construction of TE-TDRs.

A number of techniques and materials have been proposed in creating TE-TDRs including contracted collagen/alginate (147), electrospun PLLA/Hylauronic acid (87), and PLA/PGA/alginate (58, 59) composites. In addition, a number of studies have focused on strategies to engineer AF and NP that could be incorporated into a TE-TDR (67, 86, 118-121). The present work focuses on using the contracted collagen/alginate technique to produce a composite TE-TDR with a circumferentially aligned collagen AF and a cell-seeded alginate NP region (147). This technique combined with image-based construction of the molds and controlled contraction of the AF can produce an anatomically shaped TE-TDR that can be implanted *in vivo*.

One key to producing TE-TDRs that can be utilized clinically is the reproduction of the correct anatomical shape and size for each patient. Recently, MRI and μCT have been used for guiding the design of a tissue engineered meniscus and bone (148-152) and could be employed in designing a TE-TDR. CT and μCT can image the vertebral bodies and provide the outer boundary information of the IVD by examining the surface of the vertebral body (153), as well as provide information on the thickness of the disc space. In addition, a T_2 weighted MR image can provide

information on the NP shape and dimensions (154). Combining these imaging techniques can produce a model of the native IVD that can be used to create a TE-TDR. Such a technique would be applicable in the clinical setting and could produce TE-TDRs tailored to the patient.

Currently, many studies have focused largely on the *in vitro* evaluation of IVD tissue engineering strategies (58, 70, 86, 87, 118-121, 147) while a smaller subset have investigated the *in vivo* function of NP replacement strategies (65, 117). In addition, Mizuno *et al.* (58, 59) investigated the effects of subcutaneous implantation on an PGA/PLA/aglinate TE-TDR, which showed promising ECM (extraceullar matrix) and mechanical properties compared to native IVD levels. Despite this work, the behavior of TE-TDRs in the native disc space has not been investigated. The implanted disc will be subjected to mechanical loading (155), limited nutrient supply (156), and will need to integrate with the native tissue. As a result, a successful TE-TDR will need to be sufficiently stiff to withstand loading in the disc space, sufficiently permeable to allow nutrient transport to the developing tissue, and properly sized to fit into the disc space while sitting flush with the vertebral bodies to facilitate integration. However, currently it is unknown, beyond speculation, what range of stiffness and permeability are appropriate for a TE-TDR.

For this reason, the goal of this study was to determine the extent to which a composite collagen/alginate TE-TDR can maintain function of the rat lumbar spine. Specifically, the work produced an image-based collagen/alginate TE-TDR design tailored to the L4/L5 disc space of athymic rats and studied the performance of those discs *in vivo* for 16 weeks. The *in vivo* performance of composite TE-TDRs was assessed via x-ray to monitor disc height and histology to characterize the morphology of newly formed tissue and integration of the implant with surrounding tissues.

Materials and Methods

Magnetic Resonance Imaging. All MRI image data were acquired using a 3.0 Tesla Magnetic Resonance Imaging system (GE Medical Systems, Milwaukee WI) equipped with 50 mT/m gradients operating at 150 mT/m/ms. Athymic rats were anesthetized using 3%/2% isoflurane for induction and maintenance respectively. A sealed poly(methyl 2-methylpropenoate) box with intake and exhaust ports was used for imaging that also contained a warming gel pack to aid in maintaining core body temperature. A Hoult-Deslauriers transmit/receive radiofrequency resonator was designed in-house consisting of six inductively coupled, 19 mm diameter resonant loops arranged in a cylindrical geometry of length 35 mm with an inductively coupled drive loop placed at one end. The animal was placed prone in the solenoidal coil to promote a natural resting alignment of the lumbar spine thereby minimizing compressions on the disc space. The head and feet of the animal remained outside the coil while the lumbar region was aligned in the center of the imaging volume.

A 2D axial T_2-weighted fast spin echo (SE) sequence was used to visualize the NP region within the disc. Acquisition parameters included a 90 ms echo time, a 5500 ms repetition time, and an echo train length of 16 using an 8.0 cm x 6.4 cm field of view. A 320 x 256 acquisition matrix with a slice thickness of 1 mm provided 0.25 mm x 0.25 spatial resolution, and the data were zero-filled to a matrix of 512X512 for display.

μCT Rat spine from L3-S1 was imaged using an MS-8 Micro-CT Scanner (GE Healthcare, London, Ontario, Canada) at an isotropic resolution of 17μm. Scans were calibrated using an air, water, and mineral standard material (SB3, Gammex, RMI).

Disc Dimensions and Mold Design. μCT data were visualized in Microview (GE Healthcare Inc., Princeton, NJ) and converted to DICOM format. DICOM files were then imported into slicOmatic v4.3 (TomoVision, Montreal, Canada) where the bony surfaces of the vertebral bodies were manually segmented to obtain the overall shape and dimensions of the L4/L5 IVD (Figure 3.1). Segmentation resulted in point cloud images of the vertebral body bony surfaces, in which the dimensions contained in the μCT data were conserved. Point cloud images were then converted to surface and solid models of the outer boundary of the IVD in Studio 4.0 (Geomagic Inc., Research Triangle Park, NC) with dimensions conserved. In addition, the spacing between the vertebral bodies was obtained to determine the target thickness of the engineered IVD.

MRI data were imported in DICOM format and segmented manually using slicOmatic v4.3 to create point cloud images of the NP. Point cloud images were then converted to surface and solid models of the NP in Studio 4.0 (Geomagic Inc., Research Triangle Park, NC) (Figure 3.1). By segmenting and creating surface and solid models with the dimensions conserved for both the MRI generated NP data and the μCT generated total disc measurements, the data sets were in a compatible format and could be combined to provide the target shape and dimensions of the IVD and respective AF and NP. Data sets were combined in Studio 4.0 by placing the MRI generated NP model and the μCT generated total disc measurement model on the same plane and centering the NP model so that the AF had equal thickness on either side of the anterior-posterior plane and equal thickness on either side of the lateral plane.

In concordance with the collagen contraction method of creating engineered IVD (147), the shape and dimensions of the NP were used to create a single injectable mold of the NP region of the disc (149) that was used for all animals. Total disc

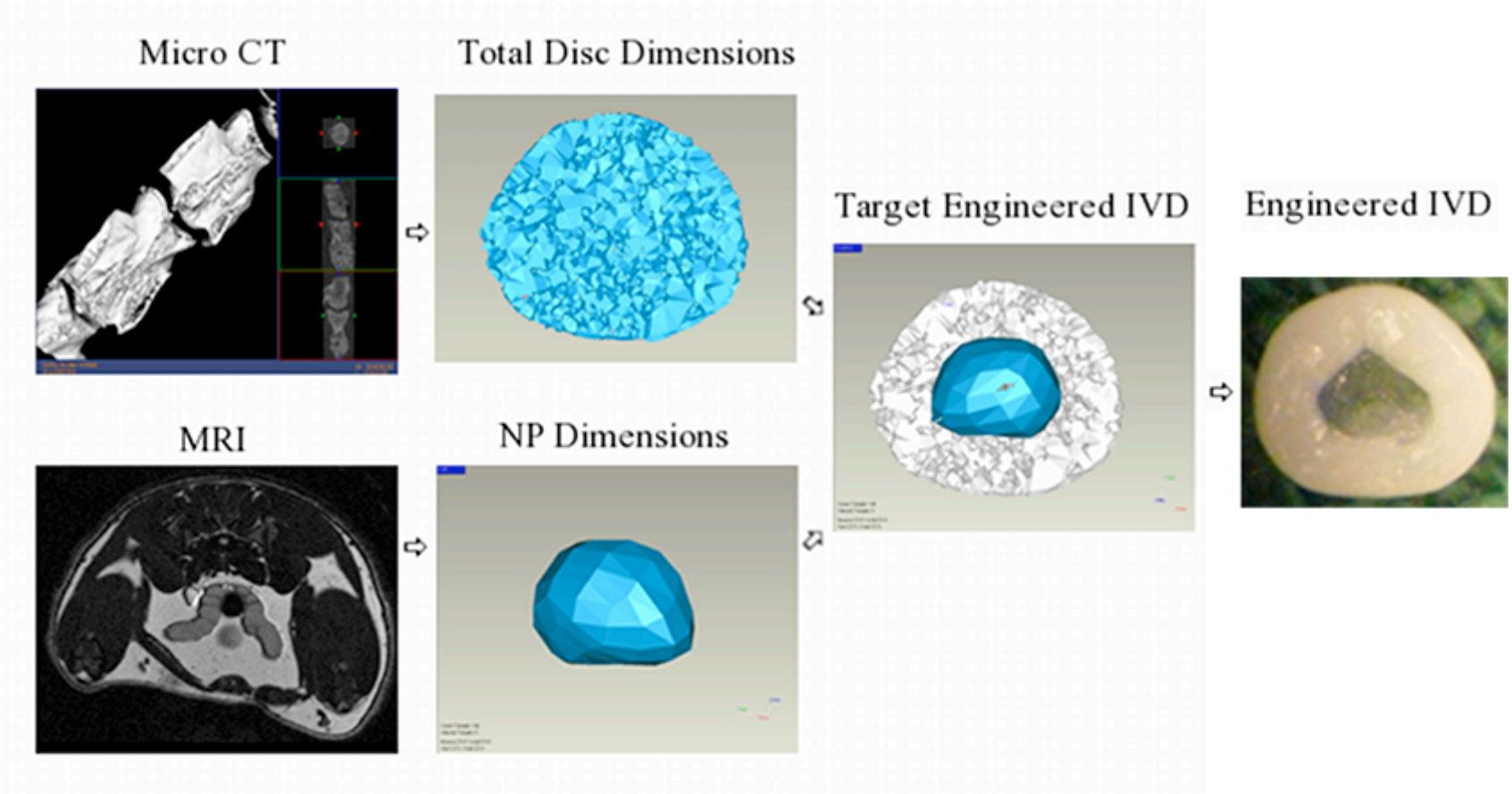

Figure 3.1 – The image-based model produced total disc dimensions from μCT using the vertebral body surface, and NP dimensions from T_2 weighted MRI images.

dimensions, NP dimensions, and AF dimensions were measured on the AP and lateral plane for the native disc, the image-based model, and the engineered discs.

Cell Preparation. Isolation and preparation of AF and NP cells were conducted as previously described (58, 59, 147). In brief, four IVDs were removed from the lumbar region of an adult skeletally mature Fin/Dorset cross male sheep (Cornell University Sheep Program, Ithaca, NY) and washed in phosphate buffered saline (PBS) solution (Dulbecco's Phosphate Buffered Saline, Gibco BRL, Grand Island, NY). The AF and NP were subsequently separated by inspection and dissected into small pieces that were digested in 0.3% collagenase type II (Cappel Worthington Biochemicals, Malvern, PA), with the NP digested for six hours and the AF for nine hours. Digested tissue was filtered using a 100 μm nylon mesh (BD Biosciences, Bedford, MA) and centrifuged at 936 x g for seven minutes. The cells were seeded at a density of 2500 cells/cm^2 in T150 flasks with Ham's F-12 media (Gibco BRL, Grand Island, NY) supplemented with 10% fetal bovine serum (Gemini Bio Products, Sacramento, CA), 25 μg/ml ascorbic acid, 100 IU/ml penicillin, 100 μg/ml streptomycin, and 250 ng/ml amphotericin B. Cells were cultured to confluence at 37°C, 5% CO_2 atmosphere, and normoxia. Following culture, cells were removed from T- 150 flasks with 0.05% trypsin (Gibco).

Engineered IVD Construction. 3% (w/v) alginate seeded with ovine nucleus pulposus cells (25 x 10^6 cells/ml) was injection molded (Figure 3.2) using mold derived from MRI and μCT images and alginate NP was placed in the center of a 24 well plate. Collagen type I gel solution (1 mg/ml) made from rat-tail tendon (132), seeded with ovine annulus fibrosus cells at a density of 1 x 10^6 cells/ml, was pipetted around the NP and allowed to gel at 37°C using established protocols (147). Constructs were

Figure 3.2 – Process of making TE-TDR implants. Image-based model used to produce injectable mold. Cell seeded alginate NP (3% w/v) created and placed in center of 24 well plate and cell seeded collagen gel (1 mg/ml) contracted around NP for 2 weeks.

floated with F12 media supplemented with 10% FBS, 100 IU/ml penicillin, 100 μg/ml streptomycin, and 25 μg/ml ascorbic acid. Media was changed every 3 days and constructs were cultured for 2 weeks allowing collagen gel region to contract around alginate NP to the dimensions derived from MRI and μCT data.

Implantation. After 2 weeks of *in vitro* culture, composite discs were implanted into the lumbar spine of athymic rats (n=5) (Figure 3.3). All animal procedures were performed in accordance with the guidelines of the IACUC of the Hospital for Special Surgery, New York, NY. Rats were anesthetized using ketamine ('Ketaset' -- 100 mg/ml) 80-90 mg/kg, and xylazine ('Rompun' -- 20 mg/ml) 5 mg/kg, which were mixed together and administered intraperitoneally. If necessary, anesthesia was prolonged by administration of isoflurane via nose cone. A modified anterior approach described by Rousseau *et. al.* was used to approach the lower lumbar spine (157). A method was for the first time established to remove the native disc and to prepare the disc space for implant insertion. The vertebral column was exposed and the native IVD (L4/L5) removed. Upon removal, the L4 and L5 vertebral bodies were minimally retracted to allow the insertion of the engineered disc into the disc space (Figure 3). The disc space was released to press-fit the implant in place and wound closure was performed in layers. An initial dose of 0.01-0.05 mg/kg buprenorphine ('Buprenex') was administered intraoperatively or immediately postoperatively prior to anesthetic recovery. Buprenorphine treatments were performed for two days postoperatively.

Upon implantation, rats were maintained for 16 weeks with lateral and anterior-posterior x-ray images taken of the implanted disc space immediately prior to surgery, immediately after surgery, and at 1, 4, 8, 12, and 16 weeks to monitor disc height. At 16 weeks, rats were sacrificed and the motion segments explanted.

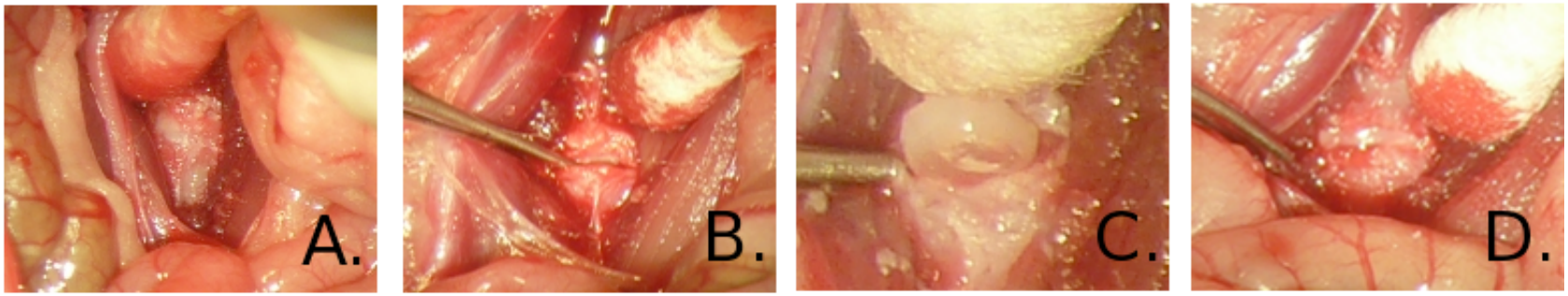

Figure 3.3 – Surgical implantation of a TE-TDR implant into the L4/5 disc space. (A.) L4/5 motion segment exposed. (B.) Native disc removed via scalpel. (C.) Vertebral bodies retracted and TE-TDR implanted into disc space. (D.) Vertebral bodies released resulting in successfully implanted TE-TDR specimen.

Histology. Spines and bone samples were cleaned of muscle and preserved in 10% phosphate buffered formalin or 4% paraformaldehyde in 0.05M cacodylate buffer, pH 7.4. Samples were fixed at room temperature for 2 days using a rotator or rocker plate to agitate samples during fixation. Following an overnight running water rinse, samples were decalcified in 10% EDTA in 0.05M Tris buffer, pH 7.4, until bone was soft and flexible. An overnight running water rinse was conducted in a VIP tissue processor to paraffin. Embedded samples were sectioned at 5 micron thickness and subsequently stained with safranin O for proteolycans, picrosirius red for collagen, and Hemotoxylin and eosin.

Immunohistochemistry. Paraffin sections were dewaxed in xylene and rehydrated to water by a decreasing concentration of ethyl alcohol baths. The sections were treated with 3% hydrogen peroxide in PBS to reduce endogenous peroxidase activity in the tissues. A protein block was added to reduce the non-specific binding between antibody and tissue components. The antibody for collagen type II (Santa Cruz Biotechnology, Santa Cruz, CA) was used at a concentration of 250 ug protein per ml of solution. To enhance the type II collagen localization, the sections were treated with 1% hyaluronidase in PBS, pH 5.5 for 30 minutes at 37° C, prior to adding the antibody. After an overnight incubation in primary antibody at 4° C in a humid chamber, the antibody was rinsed off with PBS, and treated with a biotinylated antimouse IgG followed by streptavidin reagents using the Vectastain ABC Kit (Vector Laboratories, Burlingame, CA) according to manufacturers instructions. The final reaction product was the brown deposit created by diaminobenzidine and hydrogen peroxide in the presence of the conjugated peroxidase.

Results

A model of the native IVD was obtained from μCT and MRI imaging and provided the target dimensions for an engineered IVD to be implanted in the L4/L5 disc space. μCT provided the outer boundary and thickness of the IVD (Figure 3.1a - e), which measured an anterior-posterior width of 3.23 mm, a lateral width of 3.8 mm, and a thickness of 0.99 mm, while MRI data provided the dimensions for the NP region of the disc (Figure 3.4), which measured an anterior posterior width of 1.50 mm and a lateral width of 1.93 mm. The combination of the NP (MRI) and total disc (μCT) data allowed for the dimensions of the AF to be determined with a measured AF width of 0.86 mm on the AP plane and 0.93 mm on the lateral plane. The dimensions of the image-derived model were within 10% of the manually measured dimensions of the native disc (Figure 3.4). In addition, the engineered constructs differed by less than 7% from those of the native disc. Finally, the process had a high degree of reproducibility with the standard deviations, represented by the error bars (Figure 3.4), ranging from 78 - 278 μm. These standard deviations were within 11.8% of the mean in all measurements.

Upon implantation, none of the rats showed any signs of neurological deficit due to the surgery and implantation. Radiographs indicated the disc space was fully or partially maintained in three of five animals at the implanted level (Figure 3.5) after 16 weeks. Two of the discs failed rapidly with a complete collapse of the disc space and interbody fusion occurring by 4 weeks with one disc losing disc space constantly over the 16 weeks to 50% of the original disc space. In the failed discs, posterior displacement of the vertebral bodies was observed (Figure 3.6, g3). In addition, a direct relationship was present between the maintenance of disc height and the presence of an intact posterior longitudinal ligament (PLL). In each of the animals with collapsed disc space the PLL had been removed during surgery but was left intact

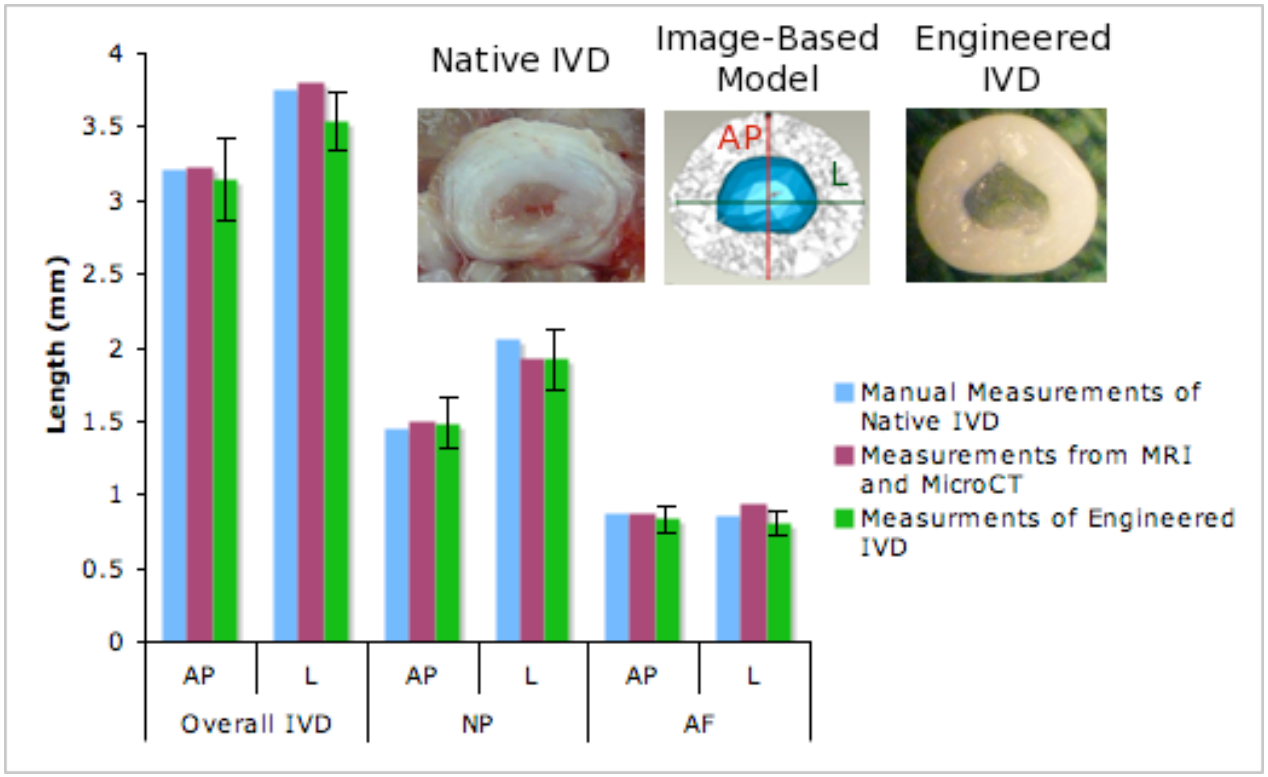

Figure 3.4. Comparison of disc dimensions between the native IVD, image-based model, and engineered IVD (n = 5). Data represented as means ± standard deviations for engineered IVD. Measurement planes indicated on picture of image-based model (red line represents anterior-posterior plane (AP) and green line represents lateral plane)

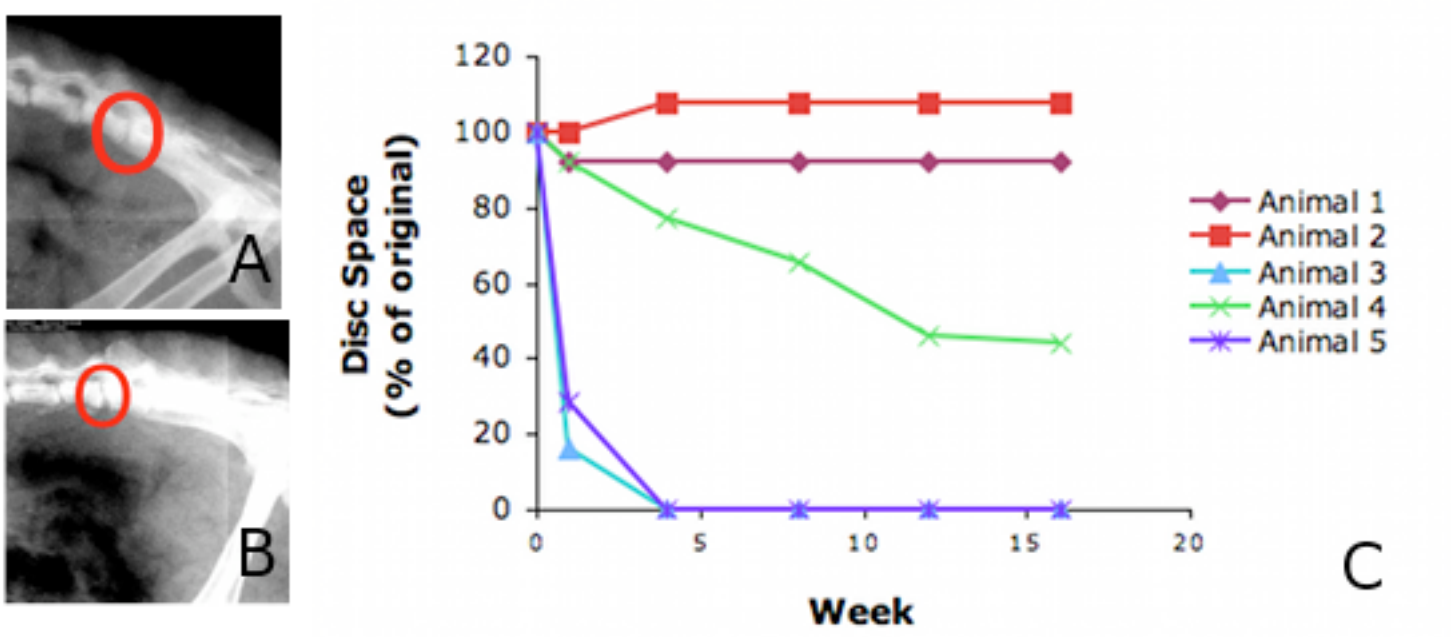

Figure 3.5 – X-ray image of disc space (A.) immediately following surgery and (B.) 16 weeks following implantation. (C.) Disc height measurements obtained over 16 weeks from 5 implanted animals.

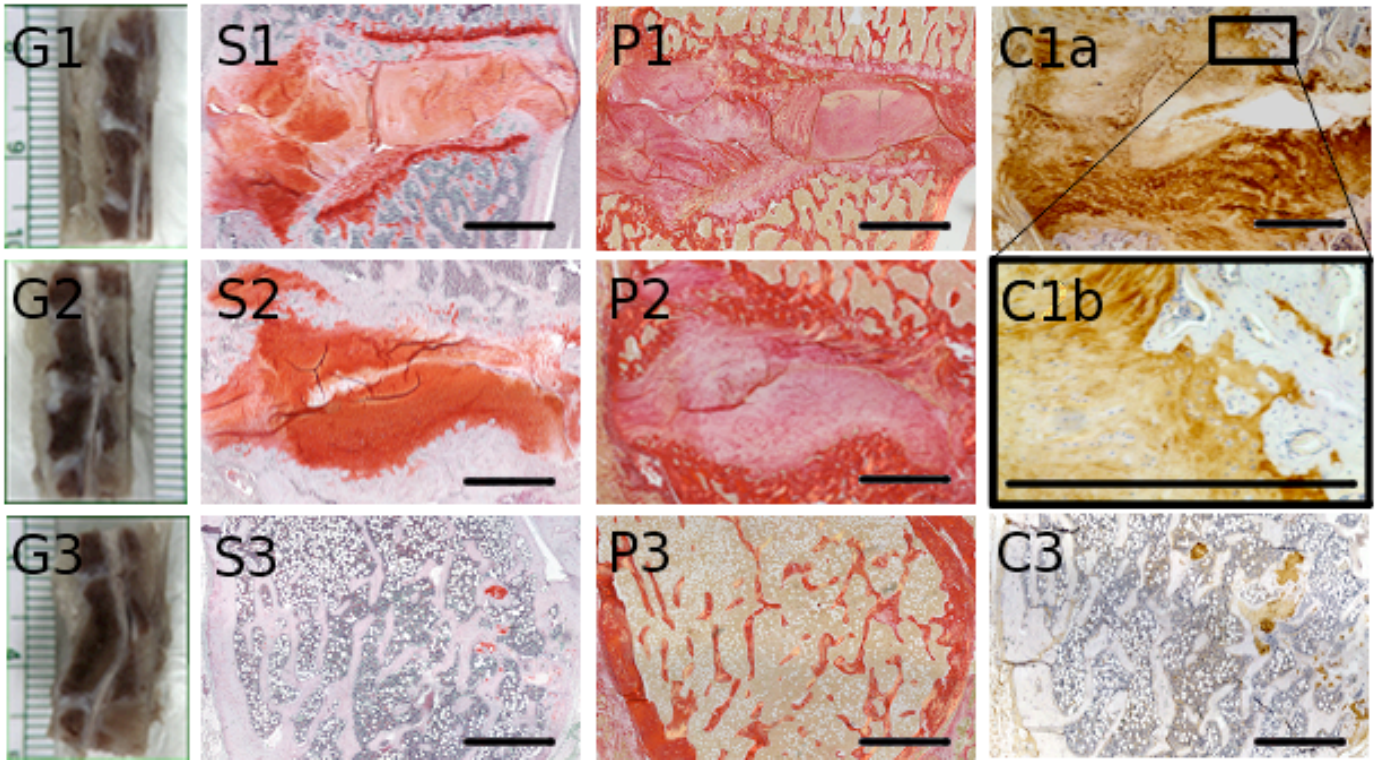

Figure 3.6 – Histology for animals one, two, and three. Gross sections (G1-3), Safranin-O (S1-3), and picrosirius red (P1-3) shown for all three animals. Collagen II IHC shown for animal one (C1a) and three (C3) with magnified vertebral bone implant interface (C1b) displayed for animal one, as well. G1-2, S1-2, P1-2, and C1a-b show tissue development in discs that maintained disc space. G3, S3, P3, and C3 show fused vertebral bodies at site of implanted disc. Scale bars = 1 mm.

in the animals that maintained disc space.

Histologically, the 3 samples that maintained disc height produced tissue with composition reminiscent of native IVD (Figure 3.6), while those that resulted in a collapsed disc space produced a fusion between the vertebral bodies. Implanted tissues were generally located anteriorly in the disc space with significant staining observed for both proteoglycans and collagen in the implanted discs at 16 weeks (Figure 3.6, s1-2, p1-2). Collagen II was seen distributed throughout the implanted disc at 16 weeks by immunohistochemistry. In addition, proper localization of proteogylcan and collagen was observed in one of the maintained disc spaces (Figure 3.7a, c). The NP region contained intense proteoglycan staining compared to the AF region of the implant while the AF region showed increased staining for collagen compared to the NP region. Good integration was observed between the AF and NP regions of the TE-TDR (Figure 3.7a, c) and between the TE-TDR and remnant native IVD (Figure 3.6s1, p1). Furthermore, picrosirius red staining and polarized light images indicated that the AF region contained collagen organization at 16 weeks (Figure 3.7a, b). Finally, in each of the animals that successfully maintained disc space, good integration was observed between the implanted disc and the vertebral bone (Figure 3.7d).

Discussion

The aim of this work was to use MRI and μCT to design a natively sized tissue-engineered IVD and study the performance of those implants in the rat lumbar spine. This research provides a method for using clinically relevant imaging data to design implants to a high degree of geometric accuracy. Initial characterization of these implants showed that the implanted TE-TDR was capable of maintaining disc height, integrating with the vertebral bodies, and developing in the native disc space.

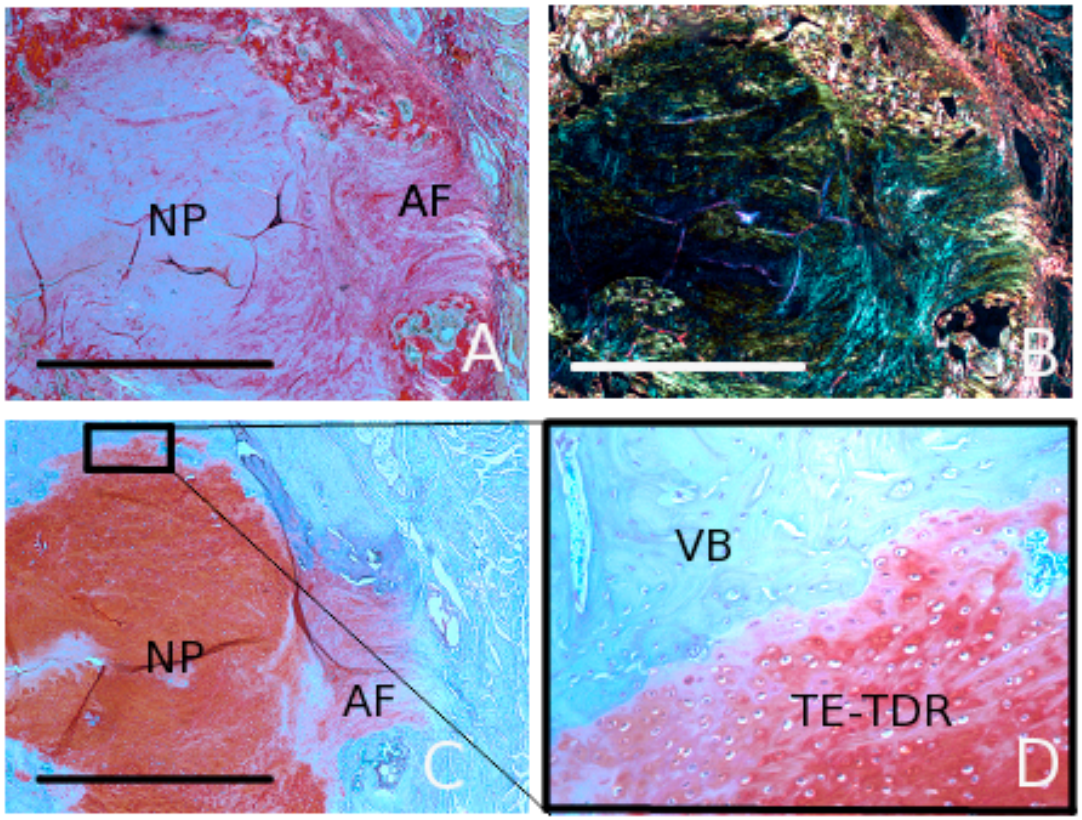

Figure 3.7 – (A.) Picrosirius staining and (B.) polarized light of showing collagen staining and organization in AF region of disc. (C.) Increased Safranin- O staining in NP region of disc. (D.) Integration between implanted TE-TDR and vertebral body (VB) bone. (Scale bars = 1mm)

Recently, a number of studies have focused on creating composite engineered IVD implants containing both an AF and NP (58, 59, 87, 147). However, little is known on how such total disc implants will be utilized clinically and how they will perform once implanted into the native disc space. A major concern is the production of a construct that is the correct size and shape for the targeted disc space. One possible solution is to make generalized measurements and have a number of sizes available during implantation to find the correct fit; however, this may not be practical in tissue engineering due to the cellular cost of producing multiple sized constructs. For this reason, the present work focused on using clinically applicable imaging modalities to determine the necessary disc dimensions for implantation.

Current work (149-152) has demonstrated the usefulness of μCT and MRI in providing shape and dimension information for bone and meniscal tissue engineering applications. These imaging modalities are also appropriate for the IVD with μCT imaging the bone-determined boundaries of the IVD/endplate and MRI imaging the NP. Utilizing these two techniques, a model of the desired IVD was successfully produced from the native rat disc (Figure 3.1). In addition, when comparing measurements obtained from the actual native disc and that obtained from imaging, the technique was shown to be quite accurate even for the relatively small rat discs (Figure 3.3) with the maximum deviations between measurements being 99 μm. While demonstrated here for the rat, this technique could be employed clinically to design tissue-engineered IVDs for larger animals or humans. It should be noted, however, one would not want to copy a degenerated NP in a tissue-engineered implant. A more likely clinical scenario would be to obtain the disc space boundaries using CT and design the NP within those overall boundaries using established values for the NP relative to the disc or obtain them from an adjacent healthy disc.

As in previous work, this study produced IVD composites using the collagen

contraction method, which resulted in an AF region with circumferentially aligned collagen fibrils and a cell-seeded alginate NP (147). By controlling the NP shape and dimensions through injection molding (Figure 3.2), an accurate alginate NP was created (Figure 3.4) compared to the native NP and image-based model; however, the thickness of the gel was purposely oversized. The degree of accuracy and repeatability is consistent with previous work by Hott *et al* when using alginate injection molding to produce tympanic membrane patches (158). The oversized implant was designed to be press fit into the disc space and combat slippage of the engineered disc from the disc space before integration. In addition, this allowed for the alginate and collagen material to be flush with the vertebral ends and promote integration between the native and engineered tissue. Once the NP was created, the collagen gel AF was contracted around the alginate NP to the AF dimensions provided by the image-based model. Upon completion, this technique resulted in engineered IVDs that were similar in dimension to that of the native IVD and image-based measurements (Figure 3.4).

Upon implantation into the rat L4/L5 disc space, three of five rats showed full or partial disc height maintenance at the implanted level (Figure 3.5). The failure of two of the discs to maintain disc height was seen in animals in which the posterior supporting tissue, including the PLL, had been more aggressively removed. In addition, posterior displacement of the vertebral bodies was observed in the failed animals (Figure 3.6, g3). It is known that posterior vertebral displacement is unlikely without posterior longitudinal ligament damage (159) and the presence of this failure mode indicates PLL involvement. For this reason, both the relationship between removal of the PLL and disc height collapse and the posterior displacement of the vertebral bodies upon failure indicate that removal of the posterior supporting tissue likely provided a mechanism for the destabilization of the spine and collapse of the

disc space. As a result, in future studies it will be important to avoid damaging the posterior ligaments during surgery. The maintenance of disc height in the remaining animals shows promise for this type of implant. This indicates that, under the proper conditions, a contracted collagen/alginate implant (147) can function in the basic capacity of maintaining disc height despite a relatively low stiffness of these discs when compared to the modulus of a native disc. Current work has focused on the replication of the native mechanical properties as a key outcome variable in *in vitro* IVD tissue engineering (59, 86). However, the data presented here indicates that it may not be necessary for clinically viable TE-TDR to fully replicate the native mechanical properties before implantation. As a result, this may allow for greater focus to be placed in the future on other properties of the TE-TDR, such as permeability, that would encourage nutrient transport and aid tissue formation and integration within the nutrient limited disc space.

In addition to the maintenance of disc height, the successful implants showed patterns of proteoglycan and collagen staining that were similar to native IVD (Figure 3.6). Significant proteoglycan and collagen staining was observed in the implanted tissue at 16 weeks (Figure 3.6, s1-2, p1-2, c1a-b) indicating a cartilaginous tissue being formed by the constructs within the disc space. Furthermore, in one of the successful constructs the NP region showed increased proteoglycan staining and lower collagen staining in comparison to the AF region (Figure 3.7a, c). And finally, polarized light indicated that the collagen organization in the AF was maintained after 16 weeks. These findings indicate that these constructs are quite capable of producing cartilaginous tissues in the disc space environment and promoting IVD like qualities in their development.

One event that is vital for total tissue-engineered discs to succeed in the disc space is the integration of the implant with the vertebral bodies. Without this

occurrence it is likely the disc will not remain in the disc space over time. This study observed very good integration between the implant and vertebral bodies (Figure 3.7d) and remnant IVD (Figure 3.6s1, p1) at 16 weeks. This is a promising aspect of collagen/alginate implants and demonstrates that, given the proper conditions, total tissue-engineered discs can integrate with their environment and create a mechanically functioning motion segment. Furthermore, not to be overlooked is the successful integration of the TE-TDR materials with the remnant native IVD. The integration indicates that these materials may be appropriate for use in annular repair following discectomy and may allow for new tissue to be developed in the annular defect and prevent reherniation following surgery. As a result, collagen and alginate should be investigated for annular repair of defects in future work.

While MRI and CT imaging modalities were used for the design of the engineered disc in this study, they could also be used to monitor engineered *in vivo* tissue maturation after implantation as well. This would provide a powerful technique to monitor tissue development in human patients when directly sampling the tissue is not an option. Specifically, $T_{1\rho}$-weighted MRI correlates to the proteoglycan content of cartilaginous tissues and has been used to monitor the degeneration of both articular cartilage and the intervertebral disc *in vivo* (160, 161). Furthermore, delayed gadolinium-enhanced MRI has been used to track the distribution of glycosaminoglycans, a proteoglycan component (162). So while these methods have traditionally been investigated to monitor the loss of proteoglycan in degenerating cartilaginous tissues, it follows that they could be used to monitor the development of proteoglycans in an implanted engineered tissue as well, thus allowing the production of a key IVD component to be tracked non-invasively during tissue development. Furthermore, the complex organization of the AF is known to influence the mechanical function of the IVD. Both quantitative T_2 imaging and diffusion tensor

MRI have been used to investigate the collagen fibril architecture in articular cartilage (163, 164). The use of similar techniques may allow the development of collagen organization in the AF region of engineered IVD to be monitored non-invasively. As can be seen, MRI can provide not only the desired dimensions for an engineered IVD but in future work could also be used to assess the *in vivo* development as well.

The potential exists for translating results from this study in the rat model to that of larger animal models. Increasing the size of the IVD may reduce partial volume effects by minimizing the contribution of adjacent tissue outside the disc in the slice direction. In addition, since larger animal models are studied in most cases on the same scanner platforms that are used clinically, translation of imaging techniques to humans is in principle straightforward.

Overall, this work provides both a method of creating anatomically shaped IVDs with clinically relevant imaging modalities, as well as providing the first insight into how engineered discs perform in the native disc space. Specifically, anatomically shaped engineered IVDs were seen maintaining disc height in a significant portion of cases, developing cartilaginous like tissue in the disc space, and integrating with the native bone. These results show promise that TE-TDRs can be developed in a manner that would be clinically applicable. In addition, a number of challenges were exposed including disc containment and early implant integrity. However, despite these challenges, total disc replacements show promise and further studies including larger animal group sizes, varying disc formulations, and augmentation techniques should be investigated in order to move total tissue-engineered discs closer towards potential clinical application.

CHAPTER 4

Specific Aim 3

Tissue-Engineered Intervertebral Disc Implants Restore Function to the Spine *In Vivo**

Abstracts

Degenerative disc disease is one of the leading physical conditions for which patients see their doctors in the US. The main target for this disease is the intervertebral disc (IVD), which frequently herniates, ruptures, or tears, often causing pain and limiting spinal mobility. To date approaches for replacement of diseased IVD have been confined to purely mechanics devices designed to either eliminate or enable flexibility of the diseased motion segment. Here we present the development of a living, tissue-engineered intervertebral disc composed of a gelatinous nucleus pulposus surrounded by an aligned collagenous annulus fibrosus. When implanted into the rat spine for times up to 6 months, tissue-engineered intervertebral discs maintained disc space height, produced organized extracellular matrix, and integrated into the spine, yielding an intact motion segment with dynamic mechanical properties similar to that of native IVD. These studies are the first to demonstrate the feasibility of engineering a functional spinal motion segment and represent a critical step in developing biological therapies for degenerative disc disease.

*This chapter is currently submitted for publication: Bowles, R.D., Gebhard, H.G., Hartl, R., and Bonassar, L.J. Tissue-Engineered Intervertebral Disc Implants Restore Function to the Spine In Vivo. Science Translational Medicine, In Review.

Introduction

Among the most common physical conditions for which patients see their doctors are back and neck pain, which carry an estimated annual cost to society up to $100 billion (100). Unfortunately, current conservative and operative treatment options are mostly palliative in nature and fail to restore function to the spine. The most common surgical target for treatment of back and neck pain is the intervertebral disc (IVD), as diseased or injured IVDs are commonly associated with back and neck pain (101-104). Such surgeries typically involve removing the affected IVD and replacing it with a mechanical device designed to either fuse the adjacent vertebrae or to preserve some motion. Regardless of which approach is used, motion segment mobility is altered, often precipitating degeneration in adjacent motion segments. (25). Non-biological total disc replacement implants were developed to avoid this loss of motion at the operated level, and as a result, reduce the incidence of adjacent segment disease. The efficacy of such implants is a matter of much debate (26, 165, 166); however, it is clear that non-biological total disc replacement implants suffer from failure modes commonly associated with traditional metal/polyethylene arthroplasty, such as mechanical failure, dislodgement, polyethylene wear, and associated osteolysis and implant loosening. More recently, increasing attention has been turned towards creating tissue-engineering strategies to repair and restore function to the diseased or injured IVD.

The intervertebral disc is composed of two distinct regions, the annulus fibrosus (AF) and the nucleus pulposus (NP). The NP is a gelatinous tissue with high proteoglycan content and type II collagen matrix that is surrounded by the AF, a highly organized fibrocartilage predominantly made of type I collagen and proteoglycans. A number of tissue engineering strategies have focused on creating either the AF or NP separately (167), but much interest has recently been focused on

creating a composite tissue-engineered total disc replacement (TE-TDR) implant that contains both the AF and NP region (58, 59, 87, 93, 168). The ultimate goal of such implants is to replace diseased IVDs with living tissue that would avoid the pitfalls of traditional metal/polyethylene arthroplasty. In addition, the TE-TDR implant could restore function to the spine by maintaining motion at the operated level and by reproducing the damping capabilities of the IVD. The successful replication of spinal motion and function in human IVD allograft transplantation (37) provides reason to believe that a TE-TDR implant could produce similar results.

Despite the promise of tissue engineering approaches for IVD replacement, the use of such an implant to restore the structure and function of a motion segment had yet to be demonstrated. Here we show that our previously documented approach to producing TE-TDR implants with circumferentially aligned collagen fibrils in the AF (93), combined with image-based design techniques to reproduce precise anatomy (148-152) yielded implants that integrated with the rat spine, reproduced appropriate tissue structure, and generated a mechanically functional motion segment in the rat spine.

Results

Engineered IVDs reproduce native shape and composite structure over 6 months of implantation.

To study the function of tissue-engineered IVD implants, we chose to replace healthy IVD in the rat caudal spine. The rat caudal spine was chosen for ease of surgical access, repeatability of the surgery, and the reasonable levels of stress and strain imposed on caudal discs (169-171). We constructed composite TE-TDR implants and inserted them into the caudal 3/4 disc space of athymic rats. Samples were harvested at 6 weeks and 6 months along with a separate control group

containing no implant (discectomy). In addition, we hypothesized that an explanted native disc would contain the properties of the "ideal" engineered disc. This idea is supported by the success of allograft IVD transplantation (172). As a result, an additional group was constructed in which the native disc had been removed and re-implanted into the disc space.

μCT and MRI images of the caudal 3/4 disc space were obtained and used to produce a TE-TDR implant with native dimensions (Figure 4.1a). μCT images allowed the outer boundaries of the IVD to be determined from the bony ends of the neighboring vertebrae and the NP dimensions from the MRI data. Using these clinically relevant imaging techniques to design the engineered disc and combining them with the collagen contracted-AF/alginate-NP engineered disc construction we have previously reported on (93), we constructed anatomically shaped discs (Figure 4.1d) that were surgically implanted into the native caudal 3/4 disc space (Figure 4.1c). The imaging and fabrication technique produced discs that mimicked the native morphology (Figure 4.1d (I., II.)). These anatomically shaped engineered discs were implanted into the native disc space and maintained composite structure immediately after implantation (Figure 4.1d (V.)). The postoperative MRI demonstrated increased hydration in the NP of the engineered disc compared to the AF, similar to the native disc. At 6 months, MRI demonstrated hydrated tissue in the disc space (Figure 4.1d (VI.)), which had a distinct cartilaginous appearance and IVD shape upon explantation (Figure 4.1d (III.)) indicating *de novo* tissue formation in the disc space

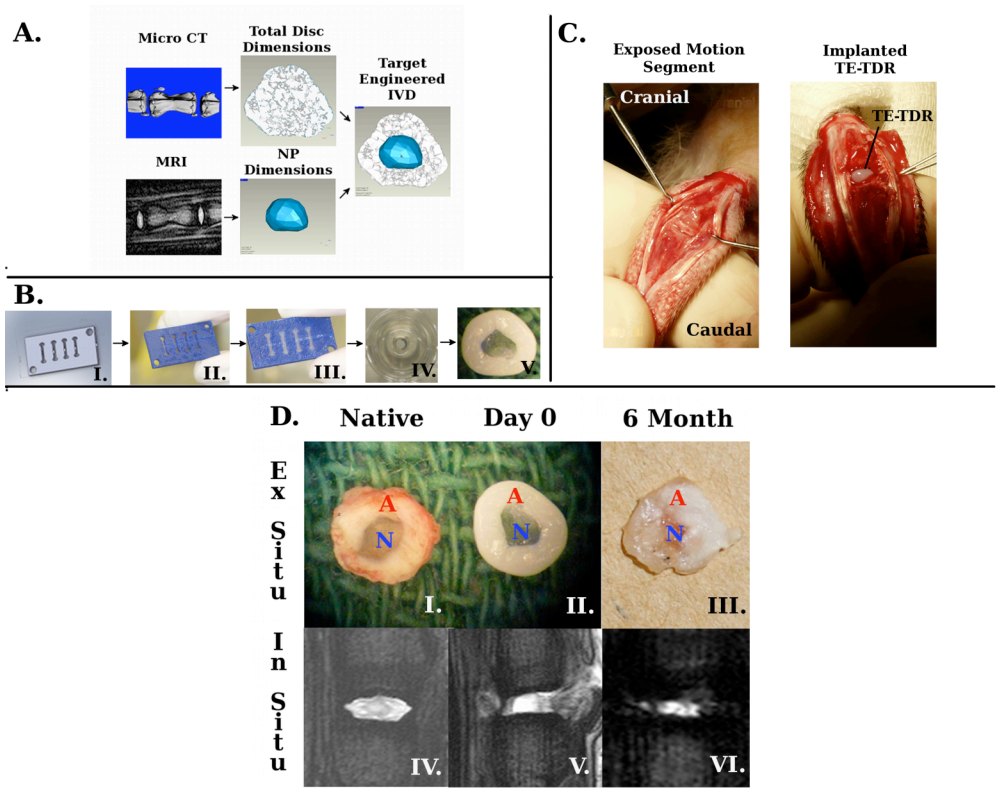

Fig. 4.1. Anatomical TE-TDR, designed from MRI and CT, survives in disc space for 6 months. **(A)** CT and MRI design procedure for obtaining TE-TDR dimensions. **(B.)** Fabrication of TE-TDR. (I.) NP dimensions used to design injection mold in CAD program. (II.) Injection mold 3D printed out of ABS plastic. (III.) Cell-seeded alginate was injected into mold. (IV.) Alginate NP was removed from mold and placed in center of 24 well plate, where cell seeded collagen was poured around alginate NP. (V.) After 2 weeks of culture, cell seeded collagen contracts around alginate NP to form composite TE-TDR. **(C)** Intra-operative images showing exposed caudal 3/4 disc space and implanted TE-TDR. **(D)** History of TE-TDR in native disc space. Intra-operative photo showing (I.) explanted native IVD sitting next to the (II.) TE-TDR that was implanted in its place. (III.) TE-TDR after being implanted into native disc space for 6 months. (AF region marked by red A and NP region marked by blue N) T2-weighted MRI of (IV.) native disc and (V.) TE-TDR immediately after implantation. (VI.) MRI of TE-TDR after 6 months of implantation.

Engineered IVD integrated well with neighboring vertebrae and produced an organized extracellular matrix with high levels of collagen and proteoglycan.

It was hypothesized that the engineered IVD would produce an ECM in the native disc space that was rich in collagen and proteoglycans, similar to the native IVD, and would integrate with the vertebral bodies. To test this, we performed histological staining for collagen and proteoglycans in the disc space, as well as quantitative biochemical analysis on the explanted tissue at 6 months for collagen, proteoglycan, and DNA (173-175). In the discectomy group, in which the native disc had been removed and nothing implanted in its place, the disc space collapsed with no production of collagen and proteoglycans (Figure 4.2c, d). In contrast, engineered discs contained abundant collagen and proteoglycan by 6 weeks and 6 months (Figure 4.2e, f, g, h, i). Collagen was dispersed throughout the disc tissue at both 6 weeks and 6 months as indicated by uniform staining by picrosirius red (Figure 4.2e, g). Collagen type I was distributed throughout the disc uniformly while type II collagen was localized to the NP region (Figure 4.S1). Proteoglycans were seen in both the AF and NP regions, with most abundant Alcian blue staining in the NP region, which was slightly smaller than the corresponding region in the native IVD (Figure 4.2b, f, h). Quantitative biochemical analysis confirmed the results seen in histology (Figure 4.2i). DNA content indicated that robust cell proliferation occurred within the disc space in both the engineered and re-implanted groups. The proteoglcyan content in the engineered disc after 6 months was not significantly different than the proteoglycan content of the AF, while the engineered NP attained ~70% ($p = 0.047$) of the proteoglycan content of the native NP (Figure 4.2i). The collagen content in the engineered disc space was not significantly different in the AF compared to the native but was significantly higher in the NP ($p = 0.010$). Despite this difference,

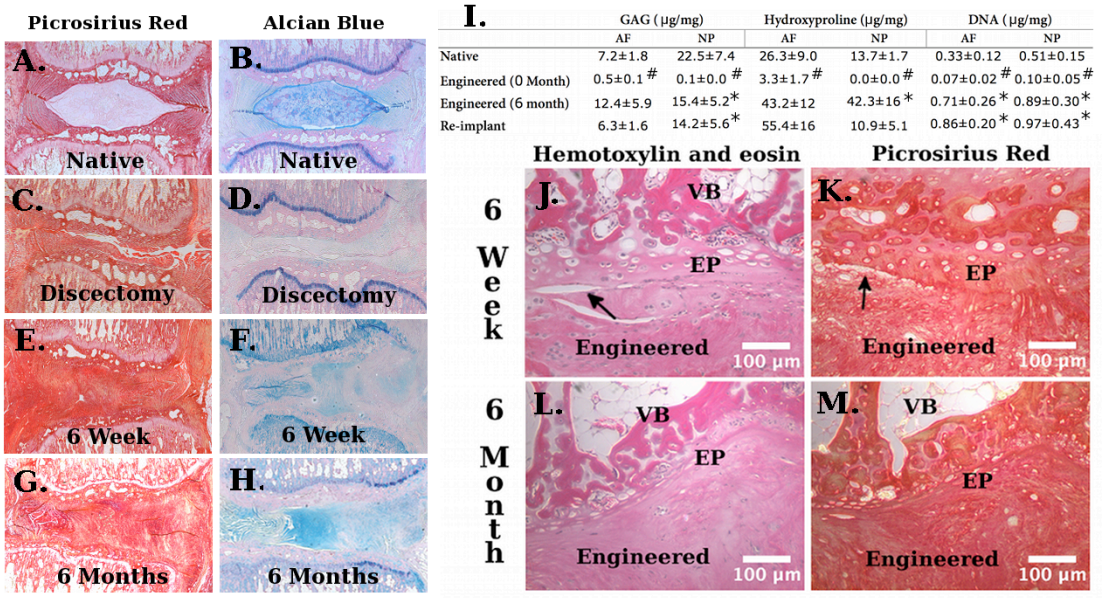

Fig. 4.2. TE-TDR produces integrated tissue with IVD-like collagen and proteoglycan content in the native disc space. Picrosirus red collagen staining for (A) native IVD, (C) discectomy group, (E) TE-TDR at 6 weeks, and (G) TE-TDR at 6 months. Alcian blue proteoglycan staining for (B) native IVD, (D) discectomy group, (F) TE-TDR at 6 weeks, and (H) TE-TDR at 6 months. (I) Biochemical analysis of GAG (proteoglycans), hydroxyproline (collagen), and DNA (cells) content at 6 months for both the native disc (n = 6) and engineered TE-TDR (n =6) and broken down by region of the disc (∗ = p<.05 compared to native; # = p<.05 compared to all groups). Histology of TE-TDR and native tissue interface (VB = vertebral bodies, EP = endplate) at (J, K) 6 weeks and (L, M) 6 months demonstrates progressive integration of TE-TDR with native tissue (arrows point to small disruptions of integration at 6 weeks, absent at 6 months).

collectively the analysis of the ECM produced by TE-TDR indicates phenotypically appropriate spatial deposition of collagen and proteoglycans. Furthermore, the engineered disc had similar levels of proteoglycans in the NP and collagen in the AF when compared to the re-implanted IVD after 6 months.

In addition to appropriate composition and arrangement of ECM, a critical requirement for a tissue engineered IVD is integration with neighboring vertebrae. Analysis of the implant-endplate interface by histology demonstrated progressive integration over 6 months of implantation. At 6 weeks, integration was apparent, but small discontinuities were observed at the endplate and engineered tissue boundaries (Figure 4.2j, k). At 6 months, the boundary was integrated completely with no large discontinuities observed at the endplate and engineered interface (Figure 4.2l, m). This integration suggests that the proteoglycan and collagen rich matrix produced by the engineered disc can function as a unit with the native spine.

Engineered IVD produced functional tissue that maintained disc height and had similar mechanical properties to native IVD.

To determine whether tissue engineered IVD implants generated a functional motion segment, we analyzed the disc height and the dynamic mechanical properties of the motion segments. Maintenance of vertebral spacing is a critical role of the IVD and is a primary clinical indicator of IVD health. As such, maintenance of disc height is a critical indicator of the performance of a tissue engineered IVD. Tissue engineered IVD implants maintained 88.9 ± 2.8 % of the disc height at 6 weeks and 75.0 ± 18 % at 6 months, while the discectomy group collapsed (37.3 ± 3.6 %) (Figure 4.3a). At 6 weeks and at 6 months the engineered disc was comparable to the re-implanted native disc at maintaining disc space (Figure 4.3a).

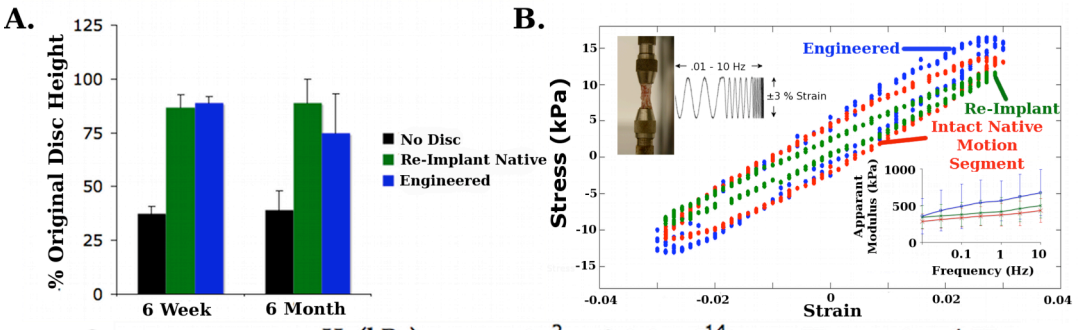

C.

	H_A (kPa)	K (m^2/Pa*s) (x 10^{-14})	% Hysteresis at 1 Hz
Native	238 ± 68	1.4 ± 0.3	41 ± 9
Engineered	196 ± 61	2.3 ± 0.6 *	46 ± 6
Re-implant	179 ± 51	1.5 ± 0.9	13 ± 6 *

Fig. 4.3. TE-TDR produces a mechanically functional tissue in the native disc space. (A) Percentage of disc space height maintained at 6 weeks and 6 months for disectomy group (n = 6), re-implant group (n=6), and TE-TDR group (n=12). (B) Dynamic compressive mechanical properties at 6 months for TE-TDR implanted motion segments (n = 6) and intact native motion segments (n = 6) showing representative stress strain curves at 1 Hz and apparent moduli over full range of frequencies. (C) Equilibrium modulus, hydraulic permeability, and % hysteresis (energy dissipation) for intact native motion segments (n = 6) and TE-TDR implanted motion segment (n = 6) (∗ = p<.05 compared to native).

The ability to properly sustain axial loads is a key function of the IVD (40). To investigate how the engineered discs restored this function of the spine, we analyzed the dynamic mechanical properties of the engineered discs 6 months after implantation. Intact motion segments were tested in order to assess effects of integration of the IVD tissue with the endplate and vertebrae, and the mechanical performance of tissue engineered IVD was compared to that of native motion segments and of spines that received re-implanted healthy discs (Figure 4.3b, c). The dynamic properties of the motion segments were assessed imposing sinusoidal strains of 3% amplitude over a physiologically relevant range of frequencies (.01 – 10 Hz). Similar viscoelastic stress strain curves were observed between the engineered, re-implanted, and intact native motion segments (Figure 4.3b). Motion segments with engineered tissue had a modulus ~30% higher than the native motion segment ($p = 0.020$) over the full range of frequencies tested. The capacity of the engineered IVD to dissipate mechanical energy, as indicated by the hysteresis in the stress-strain curve, was similar to that of the native motion segment (46% compared to 41%) (Figure 4.3c). The re-implanted disc showed no significant difference in apparent modulus compared to the native disc but dissipated significantly less energy than both the engineered and intact native motion segment. The ability to dissipate mechanical energy is a critical function of the IVD, and the lack of this function may contribute to adjacent segment disease seen after fusion or total disc arthroplasty. (165, 166). In this way, tissue engineered IVD may restore the energy damping capacity of the spine in a way that is not available with current treatment options.

In addition to dynamic mechanical testing, the motion segments were subjected to stress relaxation testing to determine the static compressive equilibrium modulus and the hydraulic permeability of the tissue. The equilibrium modulus of the engineered disc was not significantly different from the intact native disc (Figure 4.3c)

or re-implanted disc, while the hydraulic permeability was slightly lower ($p = 0.010$) in the native disc. Overall, both the dynamic and quasi-static compressive data indicates the engineered discs restored compressive mechanical function to the spine by producing a tissue with similar properties to the native IVD.

Discussion

The production of a tissue-engineered total disc replacement implant for use in the treatment of disc related back and neck disorders has been a recent area of scientific interest, but the successful creation of a functional engineered IVD in the native disc space had yet to be achieved (58, 59, 87, 93, 168). The ability to replace a diseased IVD with a living and mechanically functional engineered IVD provides great promise in the treatment of spinal disease. However, the implantation of a TE-TDR implant into the native disc space provides a number of challenges to the disc that had yet to be addressed due to the lack of *in vivo* studies.

The main challenges in developing and delivery of a tissue engineered IVD implant are thought to be: (1) generating functional tissue in the limited nutritional environment of the disc space (176), (b) securing the implants in the spine to ensure that they will integrate with the neighboring vertebrae (58, 59, 93, 168, 177), and (c) developing an implant that could withstand the complex mechanical loading of the disc space (178). Here we demonstrated that our tissue engineered IVD implants were able to meet all three of these challenges by producing a collagen and proteoglycan-rich, well-integrated, and mechanically functional tissue in the native disc space. This study provides the first evidence that a tissue engineered IVD implant can replace the native IVD in the spine, and be used to treat spinal pathology.

A critical piece of enabling technology involved the use of clinically relevant imaging modalities, MRI and CT, to design tissue engineered IVD. This technique

allowed the creation of a TE-TDR implant in the size and shape of the native IVD (Figure 4.1) and was integral to producing a disc that could be implanted and properly fit into the native disc space (Figure 4.1c). MRI and CT were used to design the disc because it is easily translatable to clinical practice and makes patient specific TE-TDR implant design possible. This is likely to be important for TE-TDR, as proper size matching was proven to be essential for IVD transplantation success (172). Once implanted, the TE-TDR implant maintained its composite nature and was properly fit for the disc space (Figure 4.1d (V.)). After 6 months of implantation, a hydrated tissue was produced within the disc space (Figure 4.1d (VI.)) that maintained the overall shape of the implanted TE-TDR implant and disc space (Figure 4.1d (III.)). Our study is the first to demonstrate the production of an anatomically shaped disc using clinically relevant design techniques, which could be successfully implanted into the native disc space and maintained for 6 months to produce an IVD-like mechanically functional tissue.

The production of proteoglycans and collagen in quantities similar to the native disc demonstrated that the cells not only survived in the nutrient depleted disc space but also successfully produced substantial *de novo* tissue. In previous TE-TDR work performed outside of the native disc space, a proteoglycan content of only ~25% was obtained *in vitro* for both AF and NP (168) while a proteoglycan content on the order of the native NP and ~33% of the AF was obtained in subcutaneous implantations (59). Production of collagen within these studies proved even more challenging with collagen being on the order of the NP but only ~5% of the native AF in the *in vitro* study and 52% of the AF and 15% of the NP in the subcutaneous implantation work. Overall, the previous literature demonstrated a trend indicating that other approaches to tissue engineering of IVD yielded tissue with collagen and proteoglycan contents far below that of native tissue. Our data demonstrates that robust collagen and

proteoglycan were produced within our TE-TDR construct in the disc space in both the AF and NP. Our study is the first to both produce a TE-TDR implant with robust ECM composition similar to the native IVD and to accomplish this in the native disc space.

There are likely a number of contributing factors to the success of this TE-TDR implant in producing a robust ECM in the disc space. These factors may include the increased cytokine signaling likely experienced in an *in vivo* environment and the anabolic effect that mechanical stimulation, which would be present in the native disc space, has been shown to have on IVD cells (179, 180). However, the disc space is known to have limited nutrient availability (i.e. glucose and oxygen) and poor waste product transport (e.g. lactate) out of the disc (156). The high permeability of the collagen/alginate TE-TDR construct at implantation may increase the availability of nutrients throughout the engineered IVD in the disc space and promote ECM production. At this time, it is unclear which of these effects, or others, are promoting such a robust ECM development, but it will be important in future work to further elucidate these mechanisms, as they will be important for the future design principles of TE-TDR implants.

In addition to the ECM production, the ability of the TE-TDR implant to integrate with the endplates of the neighboring vertebral bodies and produce a functional motion segment is a key finding of this work. This is the first study that demonstrates the ability of tissue engineered IVD to produce tissue that is integrated within the motion segment. Of key importance is that this integrated ECM produced by the TE-TDR implant is mechanically functional within the motion segment. This is particularly noteworthy, given the dynamic nature of the tests, which involve both tensile and compressive loading. The ability of the tissue-engineered motion segment to sustain tensile loads demonstrates that the new tissue generated by the implants is

well integrated with the vertebrae. This mechanical data is consistent with the histology that shows progressive integration of the implants into the spine over the course of 6 months.

In summary, our data is the first to demonstrate that a tissue-engineered IVD can be implanted into the spine, remain in place, withstand the mechanical loads, and survive and produce an integrated and mechanically functional ECM similar to the native IVD. These findings provide support for the development of tissue engineered IVD technologies and evidence that the challenges associated with nutritional deprivation and tissue integration can be overcome. Translating the success of studies in rats to larger animal models will be a key step in moving this technology closer to the clinical applications. Overall, our study demonstrates that the promising goal of implementation of a tissue engineered total disc replacement implant in the clinic may soon become a reality.

Materials and Methods

Cell Preparation. Cell preparation was based on previously described techniques (58, 93). IVDs were dissected out of lumbar region of skeletally mature (~14 months) Finn/Dorset cross male sheep (Cornell University Sheep Program, Ithaca, NY). Tissue was washed in phosphate-buffered saline (PBS) (Dulbecco's PBS; Gibco BRL, Grand Island, NY) and the separated into AF and NP region. Tissue was dissected into small pieces and digested in 200 mL of 0.3% w/v collagenase type II at 37°C for 9 hours for AF tissue and 6 hours for NP tissue. Digested tissue was filtered through 100 μm nylon mesh (BD Biosciences, Bedford, MA) and centrifuged at 936g for 7 minutes. Cells were counted and seeded at 2500 cells/cm^2 in culture flasks with Ham's F-12 media (Gibco BRL) that contained 10% fetal bovine serum, penicillin (Gemini Bio Products, Sacramento, CA), (100 IU/ml), streptomycin (100 μg/ml),

amphotericin B (250 ng/ml, and ascorbic acid (25 μg/ml). Cells were cultured at 37°C, 5% CO_2, and normoxia to confluence with media changes every 3 days. At confluence, cells were removed from flasks with 0.05% trypsin (Gibco BRL) and counted with a hemocytometer. Cells were then seeded into TE-TDRs.

IVD Fabrication. T2 weighted MRI images and μCT images were obtained of caudal 3/4 disc level (imaging specifics in imaging section). T2 weighted MRI images were imported in DICOM format to slicOmatic v4.3 (TomoVision, Montreal, Canada) and the NP was manually segmented and converted to point cloud images of the NP. Point cloud images were converted to surface and solid models in Studio 4.0 (Geomagic Inc., Research Triangle Park, NC). This resulted in a model containing the dimensions and shape of the NP (Figure 4.1a).

μCT images were converted to DICOM format and imported into slicOmatic v4.3 (TomoVision, Montreal, Canada) where the boney surfaces of the vertebral bodies were segmented to obtain the overall shape and dimensions of the caudal 3/4 disc space. The μCT derived dimensions of the disc space were then combined with the MRI derived NP model to obtain the target dimensions of the TE-TDR implant (Figure 1a).

TE-TDR implant of target dimensions was created using contracted collagen (AF)/alginate (NP) technique (93). MRI derived NP surface and solid model was transferred into solidworks to create injection mold of NP. Injection mold was 3D printed of ABS plastic on FDM 3000 machine (Stratasys, Eden Prairie, MN).

3% (w/v) alginate seeded with 25 x 10^6 NP cells/ml was injected into mold. Cell seeded alginate NP was then removed from molds and placed in the center of a well of a 24 well plate. 1 mg/ml collagen gel solution seeded with 1 x 10^6 AF cells/ml was subsequently poured and gelled around the alginate NP. Constructs were cultured

for 2 weeks in previously described media while collagen gel contracted around aliginate NP to the proper AF dimensions.

Surgery. After 2 weeks of *in vitro* culture, TE-TDR constructs were implanted into the caudal spine of athymic rats (n=18). All animal procedures were performed in accordance with the guidelines of the IACUC of the Hospital for Special Surgery, New York, NY. Rats were anesthetized using ketamine ('Ketaset' -- 100 mg/ml) 80-90 mg/kg, and xylazine ('Rompun' -- 20 mg/ml) 5 mg/kg, which were mixed together and administered intraperitoneally. If necessary, anesthesia was prolonged by administration of isoflurane via nose cone. A method was for the first time established to remove the native disc and to prepare the disc space for implant insertion in the tail. The vertebral column was exposed and the native IVD (caudal 3/4) removed. Upon removal, the caudal 3 and caudal 4 vertebral bodies were minimally retracted to allow the insertion of the engineered disc into the disc space. The disc space was released to press-fit the implant in place and wound closure was performed in layers. An initial dose of 0.01-0.05 mg/kg buprenorphine ('Buprenex') was administered intraoperatively or immediately postoperatively prior to anesthetic recovery. Buprenorphine treatments were performed for two days postoperatively.

In addition to TE-TDR implants, two control groups were studied. The discectomy group followed the above procedure and removed the native disc but implanted nothing back into the disc space (n=6). The re-implantation group followed the above procedure, removed the native IVD and then re-implanted that native IVD back into the disc space (n=6).

After implantation, rats were maintained up to 6 months. MRI images were taken of all available animals at 6 weeks and 6 months and analyzed for disc height. In the TE-TDR group, 12 animals were sacrificed at 6 months and analyzed for

histology, mechanics, and biochemistry. In addition, a smaller cohort of 6 animals was sacrificed at 6 weeks for histology. The two control groups were taken out to 6 months and analyzed for disc height.

Imaging. μCT images of rat caudal spine were obtained from caudal 3 to caudal 5 vertebrae on a Scanco μCT 35 system (Scanco Medical, Bassersdorf, Switzerland) with an isotropic resolution of 30 μm.

MRI images were obtained on a 7.0 Tesla Bruker 70/30 Magnetic Resonance Imaging (Bruker Biospin, Billerica, MA) system. Rats were anesthetized with 1.5% Isoflurane during imaging procedures. A high-resolution T1-weighted flash sequence (resolution: 78.1 um x 58.6 um x 1mm) was obtained for disc space measurements at 6 weeks and 6 months and a T2-weighted sequence (resolution: 104.2 um x 78.1 um x 1mm) was obtained for implant design and at 6 weeks and 6 months post implantation.

Histology. Spines and bone samples were cleaned of muscle and preserved in 10% phosphate buffered formalin and were fixed at room temperature for 2 days. Following an overnight running water rinse, samples were decalcified in 10% EDTA in 0.05M Tris buffer, pH 7.4, until bone was soft and flexible. An overnight running water rinse was conducted in a VIP tissue processor to paraffin. Embedded samples were sectioned at 5 micron thickness and subsequently stained with alcian blue for proteoglycans, picrosirius red for collagen, and Hemotoxylin and eosin.

Biomechanics. TE-TDR motion segments and intact native motion segments were both cleaned of surrounding tissue to result in bone-disc-bone motion segments after euthanizing the animals at 6 months. Prepared motion segments were mounted on ELF 3200 mechanical testing frame (EnduraTech; Minnetonka, MN) using modified

microvices (McMaster-Carr, Atlanta, Ga) (169). Unconfined stress-relaxation tests were performed at 5% strain incremental steps to a total of 20% strain. Equilibrium modulus and permeability were calculated by fitting resulting stresses to a poroelastic model (181). In addition, motion segments were subjected to a sinusoidal dynamic frequency sweep from 0.01 – 10 Hz at ±3% strain around zero strain. Apparent modulus and percent hysteresis were calculated from dynamic data. All data analysis was performed using Matlab software.

Biochemistry. Native IVD and TE-TDR tissue were both dissected out of disc space using scalpel. For the native IVD, NP and AF tissue were separated and tested individually. For the TE-TDR tissue, representative NP region at center of tissue was removed using 2 mm biopsy punch and tested as NP and surrounding AF region was tested as AF. Tissues were analyzed for GAG content using a modiefied DMMB assay (173), total collagen using the hydroxyproline assay (175), and DNA using the Hoechst dye assay (174). All data were normalized to wet weight.

Statistical Analysis. All statistical analysis was performed using two-factor ANOVA and Tukey post hoc test. Data represented as mean ± standard deviation. P values <.05 considered statistically significant.

Supllemental Material

Fig. 4.S1. Immunohistochemistry of engineered IVD tissue after 6 months.

Fig. 4.S2. Polarized light microscopy of collagen network in engineered IVD.

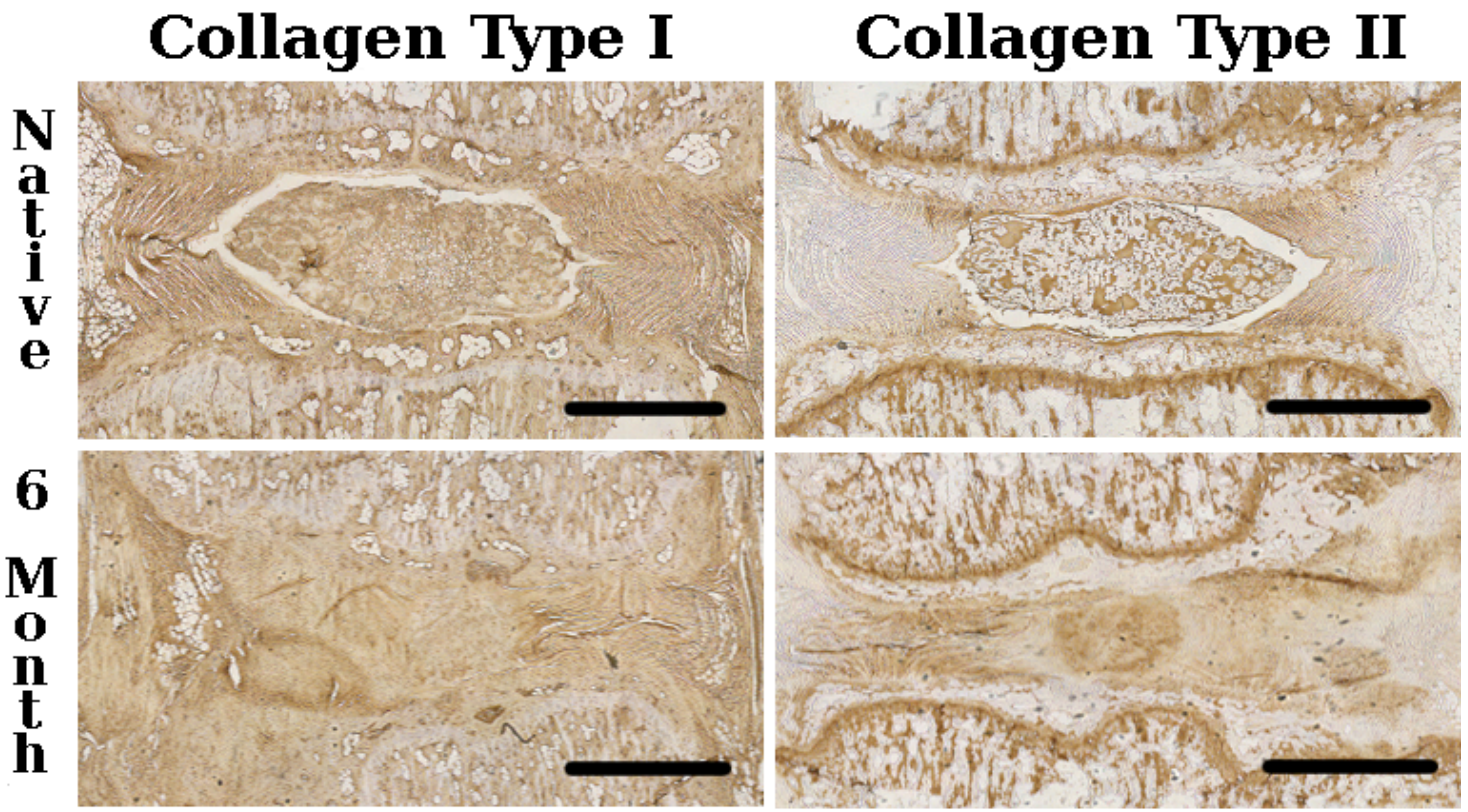

Fig. 4.S1. Immunohistochemistry of engineered IVD tissue after 6 months. Immunohistochemistry indicates that collagen type I was distributed uniformly throughout the disc space at 6 months while collagen type II was localized to the NP region of the engineered tissue. Similar trends were observed in the native disc space, as well. (scale bars = 1 mm)

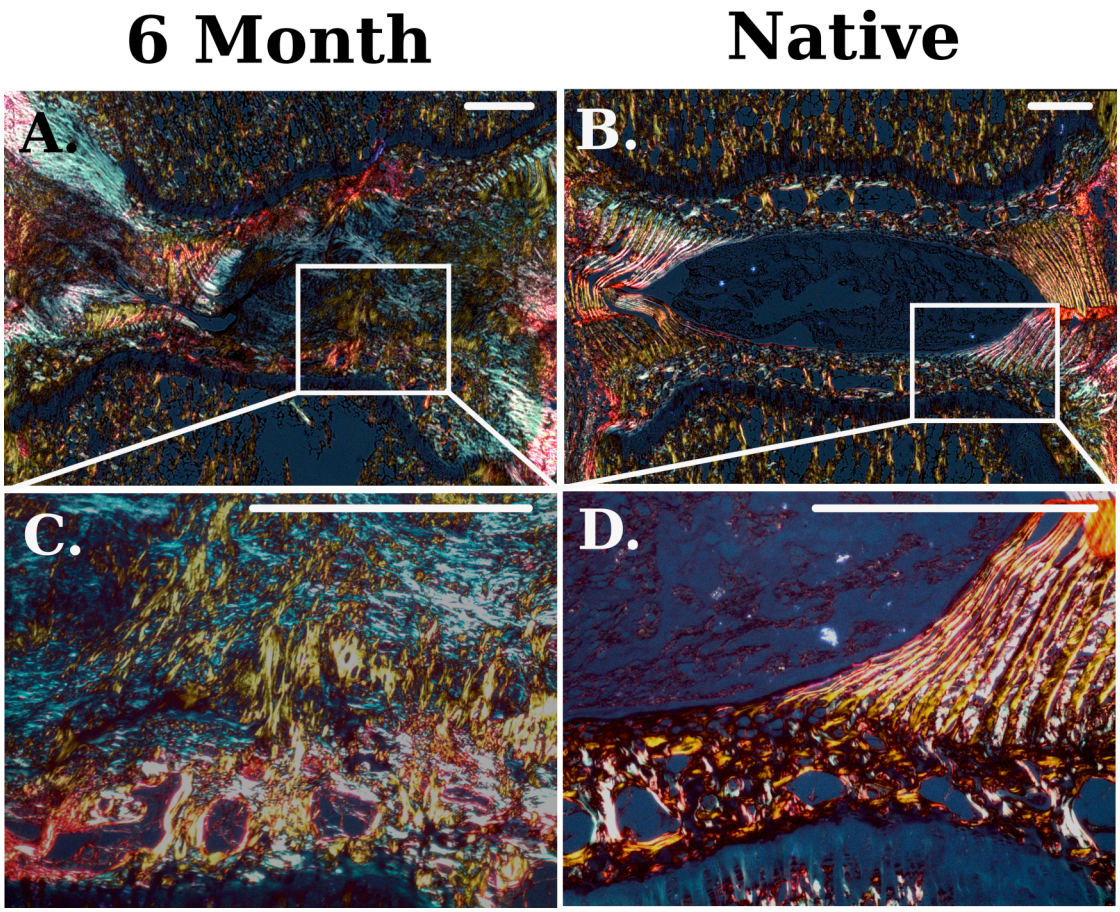

Fig. 4.S2. Polarized light microscopy of collagen network in engineered IVD. Polarized light microscopy image (40x) of (A.) engineered IVD after 6 months of implantation and (B.) native disc. Polarized light in engineered disc indicates organized collagen network present in *de novo* tissue. Increased polarized light in AF compared to NP region of disc indicates greater collagen organization is present in AF than NP in engineered IVD, a pattern consistent with native IVD. Increased magnification polarized light microscopy images (100x) of (A.) engineered IVD and (B.) native IVD at vertebral body interface demonstrates both contain a continuous collagen network that has collagen fibers that integrate into the vertebral body. While the integration in the engineered tissue is not identical to the native IVD, this integration of collagen fibrils allows the engineered tissue to produce a stable motion segment with similar axial mechanical properties to native tissue.

CHAPTER 5

Specific Aim 4

Annulus Fibrosus Composition Regulates ECM Development in Tissue Engineered Total Disc Replacement*

Abstract

Many novel tissue engineering therapies, including tissue-engineered total disc replacement (TE-TDR), are currently being investigated to treat orthopaedic spinal disorders. However, much of the promising work in tissue engineered total disc replacement has been performed *in vitro*. This paper studied the effects of annulus fibrosus composition on tissue-engineered IVD (TE-IVD) in the native disc space. 6 groups of TE-IVDs with varying AF compositions were subjected to mechanical testing *in vitro*. *In vitro* testing indicated that altered AF composition modified the hydraulic permeability of the AF and the subsequent pressurization of the TE-IVD under load. Based on the *in vitro* testing, 2 groups were selected and implanted into the athymic rat caudal disc space for 6 months. TE-IVD with lower AF hydraulic permeability and increased tendency to pressurize under load developed ECM that better mimicked the AF and NP phenotypes in the native disc space than the TE-IVD with higher AF hydraulic permeability and decreased tendency to pressurize. Both tissues produced mechanically functional tissues after 6 months. By regulating *in vivo* tissue development, AF hydraulic permeability proved to be a key design factor in TE-IVD. Overall, this study provides continued evidence of the promise of TE-TDR.

*This chapter will soon be submitted for publication: Bowles, R.D., Gebhard, H.G., Hartl, R., and Bonassar, L.J. Annulus Fibrosus Composition Regulates ECM Development in Tissue Engineered Total Disc Replacement. Biomaterials. In Preperation

Introduction

Degenerative disc disease and the associated spinal disorders are a major concern in healthcare. Surgical treatments of these disorders including spinal fusion, discectomy, and total disc replacement have reached a total cost of $28.6 billion/year in the United States alone (182, 183). Despite these efforts, many of these treatments are palliative in nature, fall short of providing long-term and functional relief of the debilitating symptoms, and have significant shortcomings. Specifically, spinal fusion results in a loss of mobility and is believed to lead to adjacent segment level disease (25), discectomy can suffer from re-herniation (184), and total disc replacement is prone to traditional wear and failure modes associated with metal/polymer implants (29). These shortcomings result in a need for novel intervertebral disc (IVD) degeneration treatments, and as a result, interest in developing tissue-engineering strategies for the treatment of degenerative disc disease has become prevalent.

Much of the focus in IVD tissue engineering has been on either replacement of the nucleus pulposus or repair of the annulus fibrosus tissue (65, 67, 70, 86, 117-121, 167). However, disc degeneration is often a disease of both the AF and NP, and as a result, a number of groups have been investigating the creation of composite tissue-engineered IVDs (TE-IVD) that contain both the AF and NP for use in tissue engineered total disc replacment (TE-TDR) (58, 59, 87, 93, 168). This has the advantage of removing both the diseased AF and NP and replacing it with a new tissue. Recent data from cadeveric allograft IVD transplantation indicates that replacing the entire IVD with a healthy IVD can be effective at treating spinal disorders related to the IVD (37). Despite these promising results, transplantation surgeries often lack sufficient quantities of donor tissue to meet demand. Tissue engineering hopes to get around this by creating TE-IVD that can be implanted without the need of cadeveric tissue.

Despite the interest in TE-IVDs and the effort to increase the complexity of the scaffolds, little work has been done to understand how these implants will develop in the native disc space. Recently, we presented preliminary data on the first implantations of TE-IVD into the native disc space by implanting our contracted collagen gel (AF)/ alginate gel (NP) TE-IVD into both the lumbar 4/5 and caudal 3/4 disc space of athymic rats (Chapter 3 and 4). This work demonstrated that TE-IVD could be implanted into the native disc space, produce an integrated cartilaginous tissue, and restore axial mechanical function to the spine. Even with these encouraging results, little is known on how altering the composition of the TE-IVD will affect its development in the disc space. This is particularly true for the AF, where several approaches have been presented for scaffold composition and organization (58, 59, 87, 93, 168).

We hypothesized that changes in the composition of the AF would have significant effects on the development of the TE-IVD *in vivo* by altering the mechanical function of the TE-IVD. For this reason, this study altered the AF composition of the TE-IVD by changing the original collagen and cell seeding density of the AF and investigated the mechanical and structural effects of these changes on the TE-IVD *in vitro*. Based on *in vitro* studies the two most promising AF compositions were chosen for implantation. The *in vivo* TE-IVD development was studied in the caudal athymic rat model for 6 months and the results interpreted in light of the *in vitro* data. Overall, this work aimed to provide an understanding of how AF composition affected *in vivo* development of TE-IVD in the hopes that the field could use this information to improve the design of TE-IVD for implantation into the native disc space.

Materials and Methods

Cell Preparation. Based on previously described techniques(58), 20 lumbar IVDs were dissected out of skeletally mature (~14 months) Finn/Dorset cross male sheep (Cornell University Sheep Program, Ithaca, NY). Tissue was separated into nucleus pulposus and annulus fibrosus tissue and was dissected in to small pieces that were digested in 0.3% w/v collagenase for 6 hours (NP) or 9 hours (AF). After digestion was complete, AF and NP cells were seeded at a density of 2500 cells/cm^2 in culture flasks and expanded to confluence at 37 °C in Ham's F-12 media (Gibco BRL) containing 10% fetal bovine serum (Gemini Bio Products, Sacramento, CA), ascorbic acid (25 μg/mL), penicillin (100 IU/mL), streptomycin (100 μg/mL), and amphotericin B (250 ng/mL).

Tissue Engineered IVD Fabrication. Six groups of tissue engineered IVD with varying AF formulations were fabricated (Fig. 5.1). Injection molds of the NP were designed from MRI scans of rat-tail IVD, as previously described (Fig. 5.1a) (Chapter 3) (185). Ovine NP cells were seeded at 25 x 10^6 cells/mL in 3% (w/v) alginate and injection molded into NP molds (Fig. 5.1b). After gelation, alginate NPs were placed in the center of a 24 well plate and cell seeded (1 x 10^6 cells/mL or 10 x 10^6 cells/mL) collagen solution (1, 2, or 3.5 mg/ml) made from rat-tail tendon (132) was pipetted around the alginate NP and gelled at 37°C using established protocols (Fig. 5.1 c, d) (93). Constructs were then floated with 1 mL of previously described culture media and cultured for 2 weeks with media changed every 3 days. This allowed the collagen gel to contract around the alginate NP over the 2 weeks of culture.

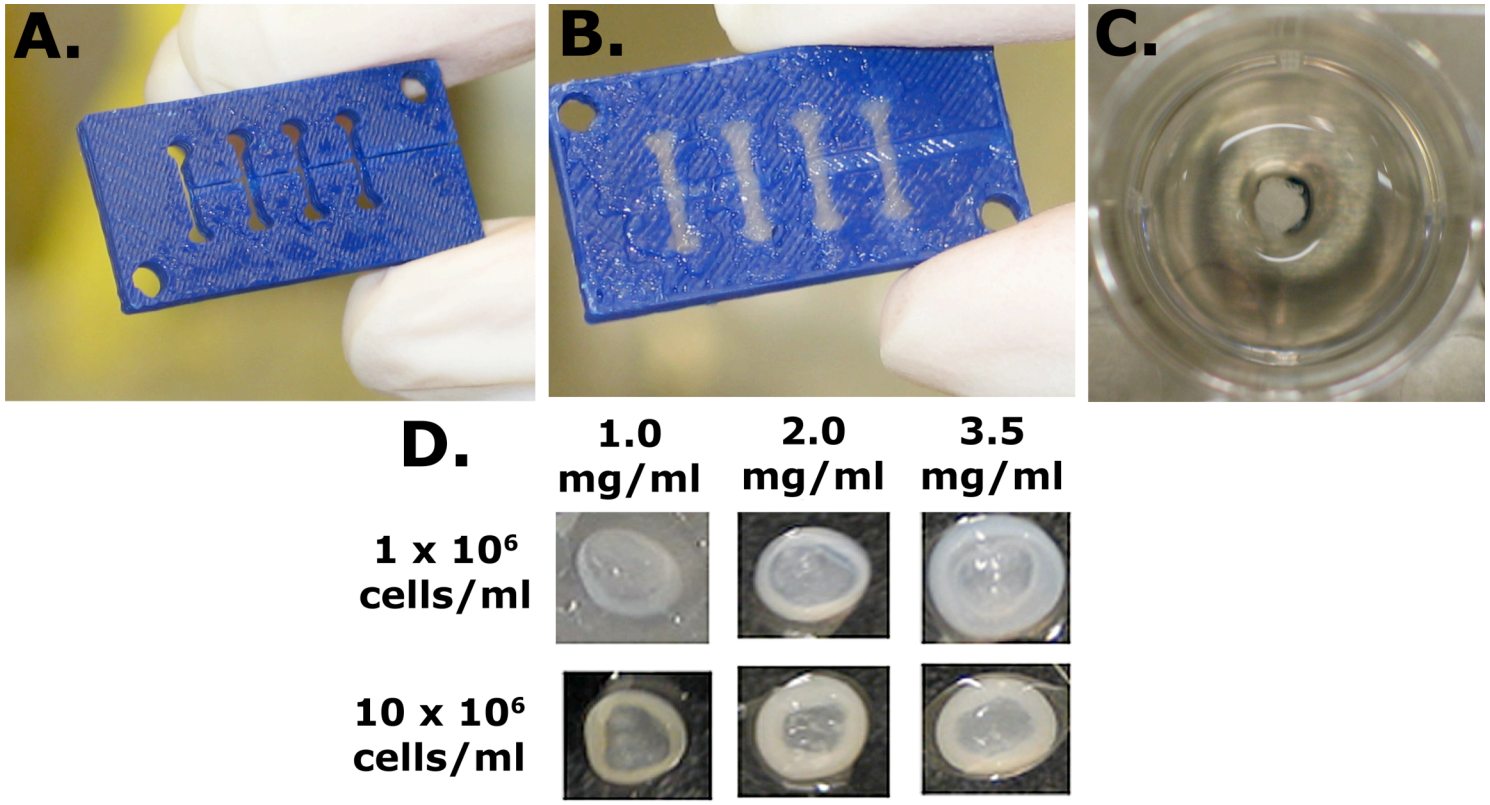

Figure 5.1 – Fabrication of TE-IVD. (A.) Injection mold of eight NPs is (B.) injection molded with cell seeded 3% alginate gel. (C.) Alginate NP is placed at center of 24 well plate well and cell seeded collagen solution is pipetted around and cultured for 2 weeks while AF contracts around NP. (D.) 6 different groups of TE-IVDs were constructed with varying collagen (1.0, 2.0, or 3.5 mg/ml) and cell seeding density ($1x10^6$ cells/ml or $10x10^6$ cells/ml)

IN VITRO

Mechanical Testing. After two weeks of contraction, 6 samples from each group were subjected to mechanical testing. Stress relaxation tests (EnduraTech; Electroforce (ELF) 3200 System, Minnetonka, MN) were performed in unconfined compression by applying 2.5% incremental strain steps up to a total of 70% strain. The tissue engineered IVDs were designed to be implanted into the rat tail and were purposefully oversized axially to press fit them into place. Upon being press fit in the native disc space, the discs were likely to be subjected to high strains (~50%). For this reason, the high total strain of 70% was selected. Stress relaxation load data were fit to a poroelastic model and the equilibrium modulus, instantaneous modulus, and hydraulic permeability were calculated for each group (181).

SHG and TPEF Imaging. In addition to mechanical testing, 6 samples from each group were imaged using simultaneous second harmonic generation and two-photon excited fluorescence microscopy (129, 131) to image the collagen fibrils (SHG) and cells (TPEF). 10 images were taken of the AF region of each group. Collagen fibril images from SHG were run through a custom Matlab code, which has been previously described (Chapter 2) (93), to produce an alignment index for the AF region. Briefly, the code takes the fast fourier transform of the image and produces a histogram of fibril orientation. From this histogram, the alignment index is calculated according to Equation 1.

(1)
$$AI = \frac{\int_{\theta_m - 20^\circ}^{\theta_m + 20^\circ} I \partial\theta}{(40^\circ / 180^\circ) * \int_{0^\circ}^{180^\circ} I \partial\theta}$$

As a result, AI will range from 1 (unaligned) to 4.5 (complete alignment of fibrils). AI was calculated for all 6 groups. For comparison, method produces an AI of ~1.67 for native AF. TPEF imaging was used to observe the shape and orientation of the AF cells.

IN VIVO

The 1 mg/ml and 2 mg/ml AF groups, seeded with 1 x 10^6 cells/ml, were implanted into the caudal spine of athymic rats due to their appropriate size, the collagen alignment observed in the AF, and distinct mechanical properties between the two groups.

Surgery. After 2 weeks of culture, constructs were implanted (n =12/group) into the caudal 3/4 disc space using previously described protocol (Chapter 4). All animal procedures were performed in accordance with the guidelines of the IACUC of the Hospital for Special Surgery, New York, NY. Briefly, rats were anesthetized using ketamine ('Ketaset' -- 100 mg/ml) 80-90 mg/kg, and xylazine ('Rompun' -- 20 mg/ml) 5 mg/kg, which were mixed together and administered intraperitoneally. If necessary, anesthesia was prolonged by administration of isoflurane via nose cone. The caudal 3/4 disc space was exposed and the native disc was removed with a scalpel. Upon native IVD removal, the vertebral bodies were minimally retracted and the tissue engineered IVD was implanted in its place. After inserting the disc, the vertebral bodies were released and allowed to press fit the disc into the disc space. Wound

closure was performed in layers. An initial dose of 0.01-0.05 mg/kg buprenorphine ('Buprenex') was administered intraoperatively or immediately postoperatively prior to anesthetic recovery. Buprenorphine treatments were performed for two days postoperatively. Rats were maintained for 6 months, at which time the caudal 3/4 motion segments were explanted and used for either histology (n=6) or mechanical testing and quantitative biochemistry (n=6).

Mechanical Testing. Motion segments were tested intact (vertebral body - IVD - vertebral body) according to previously described protocols (Chapter 4) and subjected to both a compressive stress-relaxation test and a dynamic frequency sweep. Motion segments were mounted on ELF 3200 mechanical testing frame (EnduraTech; Minnetonka, MN) using modified microvices (McMaster-Carr, Atlanta, Ga) (Fig. 5.6a) (169). Compressive stress relaxation tests were performed with incremental strain steps of 5% up to a total of 20% strain. Resultant load data were fit to a poroelastic model, and the equilibrium modulus and effective hydraulic permeability were calculated. Sinusoidal dynamic frequency sweep was performed over 0.01 – 10 Hz frequency range with amplitude of ± 3% strain around zero strain. Apparent modulus was calculated at each frequency. In addition to implant groups, intact native motion segments (n=6) were subjected to identical mechanical testing protocol for comparison.

Quantitative Biochemistry. Engineered IVD tissue (n=6) and native IVD (n=6) for comparison were explanted from motion segments and separated into AF and NP region. Tissue was assayed for collagen content using the hydroxyproline assay (175), GAG content using modified DMMB assay (173), and DNA content using the Hoechst dye assay (174). All data were normalized to wet weight.

Histology. Spines and bone samples were cleaned of muscle and preserved in 10% phosphate buffered formalin and were fixed at room temperature for 2 days. Following an overnight running water rinse, samples were decalcified in 10% EDTA in 0.05M Tris buffer, pH 7.4, until bone was soft and flexible. An overnight running water rinse was conducted in a VIP tissue processor to paraffin. Embedded samples were sectioned at 5 micron thickness and subsequently stained with alcian blue for proteoglycans and picrosirius red for collagen.

Results

In Vitro

Varying the collagen concentration and cellular density in the AF region of tissue engineered IVD during fabrication led to changes in the size of the AF and the architecture of the collagen fibril network (Fig. 5.1, 5.2, and 5.3). Over 2 weeks of culture, contraction of the AF region followed the expected trend of increased contraction for lower concentration gels; however, increasing the cellular concentration from $1x10^6$ cells/ml to $10x10^6$ cells/ml only showed a significant increase in contraction in the 3.5 mg/ml groups (Fig. 5.2). Second harmonic generation imaging of the collagen fibril network after contraction demonstrated a significant increase ($p < 0.05$) in circumferential alignment as the collagen concentration decreased in the $1x10^6$ cells/ml seeded group (Fig. 5.3), which is consistent with our previous findings (Chapter 2) (93). However, this trend was not present in the 10×10^6 cells/ml groups, as the collagen architecture was unaligned for the 1, 2, and 3.5 mg/ml groups (Fig. 5.3). In addition, the cellular morphology followed the same trends as collagen architecture, as indicated by the TPEF microscopy images. In the $1x10^6$ cells/ml groups, cells were generally spindle shaped and circumferentially aligned with the collagen fibrils (Fig.

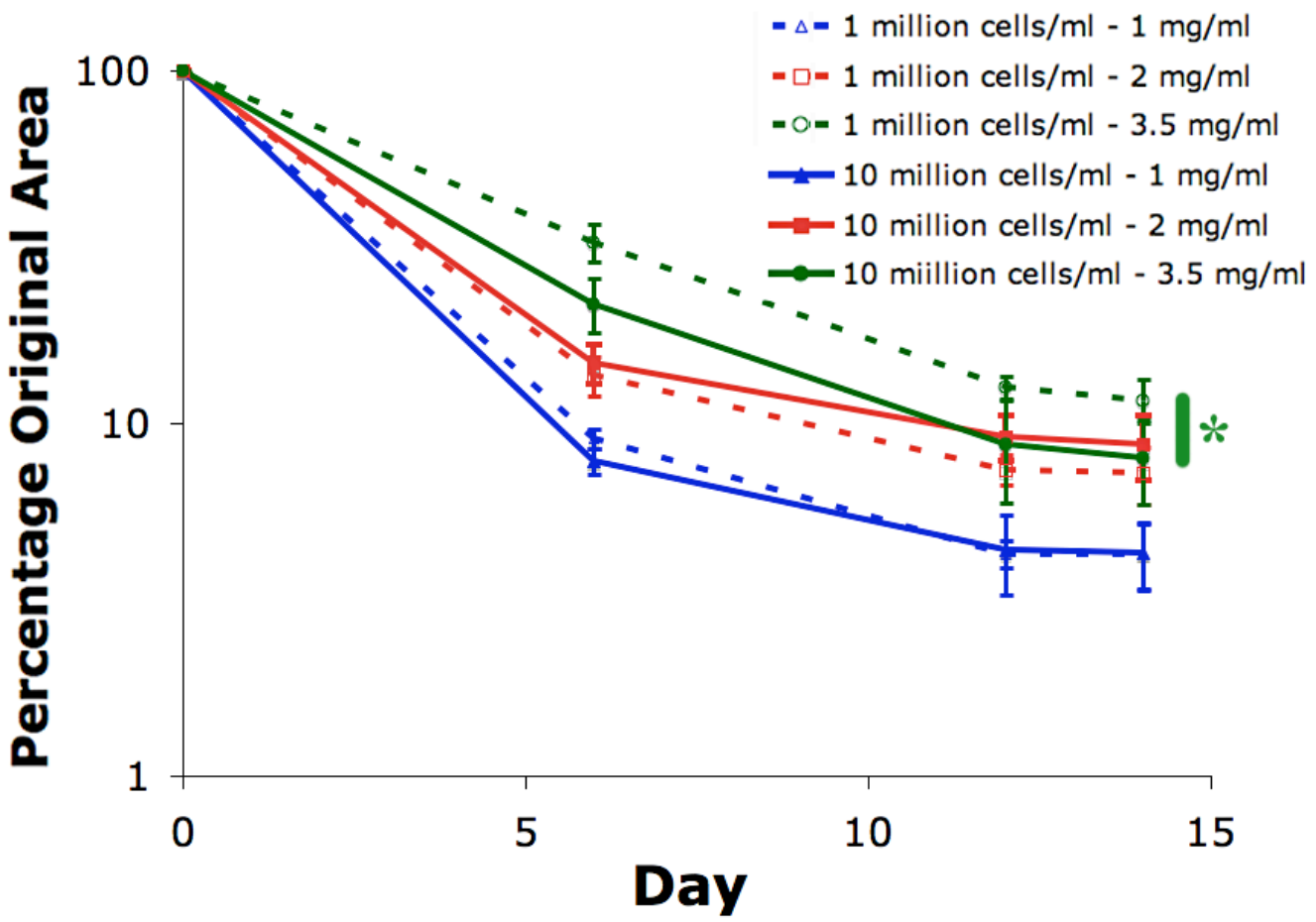

Figure 5.2 – Contraction of the TE-IVD AF region over 2 weeks of culture for all 6 groups. (Data presented as mean ± standard deviations, * = $p<0.05$, n =6)

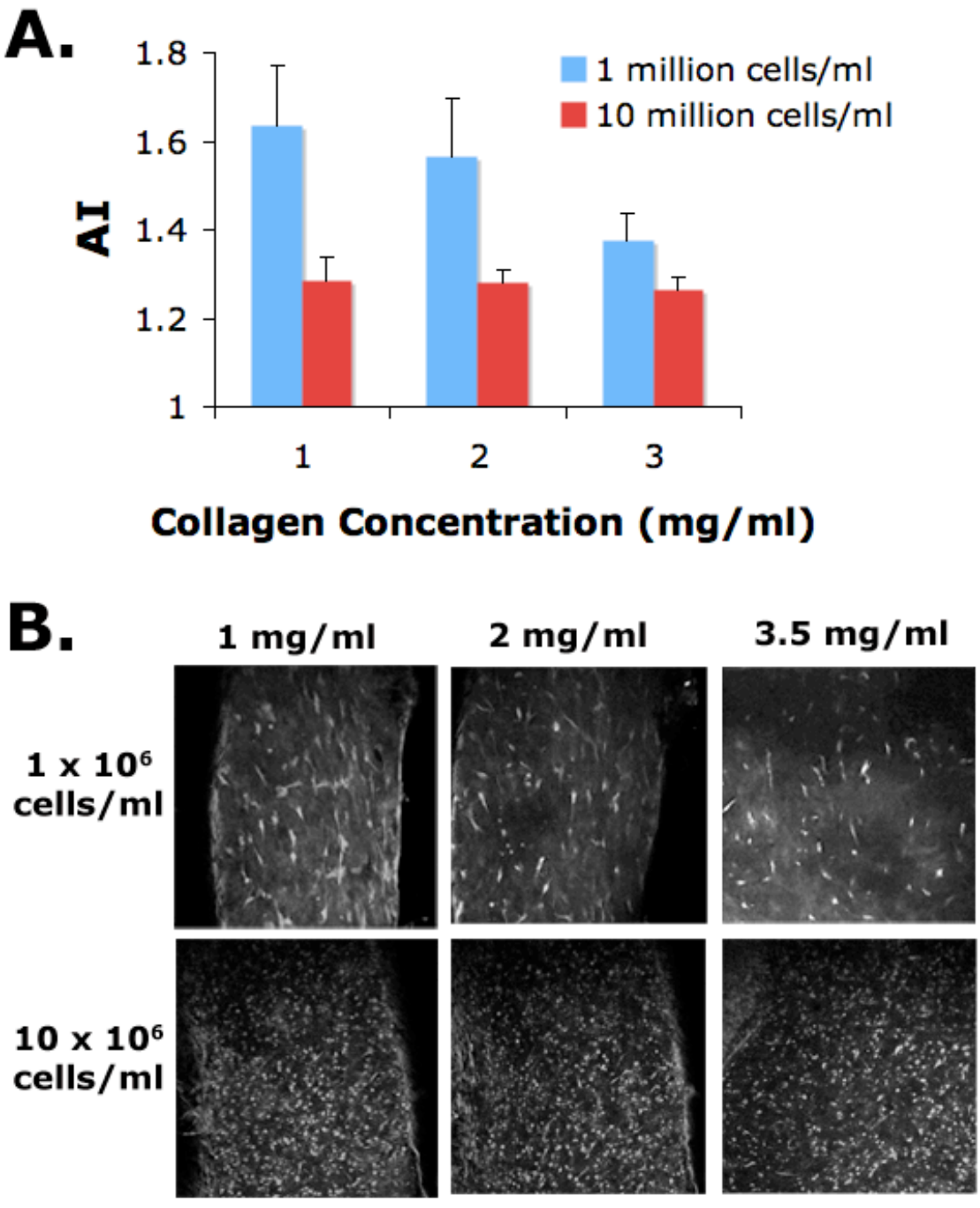

Figure 5.3 – (A.) Alignment index of the AF for the 6 groups after 2 weeks of culture. (B.) SHG images of collagen in the AF of the 6 groups after 2 weeks of culture. Note that after 2 weeks of culture, a dense pericellular collagen matrix has formed allowing the visualization of the cells in the SHG images. Data presented as mean ± standard deviation, n =6

5.3b), while in the $10x10^6$ cells/ml group, cells were round in morphology with no alignment preference (Fig. 5.3b), and had a much higher final resulting density as expected. Overall, varying the collagen concentration and cellular density led to significant changes in the AF in terms of both collagen network and cellular distribution.

Variations in collagen concentration and cellular density not only lead to structural changes in the AF, but resulted in altered composite engineered IVD mechanics as well. Equilibrium stress strain curves showed no significant difference in composite properties over full range of strain for all six groups (Fig. 5.4a, b). However, instantaneous stress strain curves demonstrate significant differences between groups at strains of 60% and above (Fig. 5.4a, b). These high strains would be experienced in the oversized-implanted tissue engineered IVD. At 60% strain, the 2 mg/ml groups show a significant ~4 fold increase in instantaneous modulus compared to the 1 mg/ml groups, and a 6-10 fold increase over the equilibrium modulus, indicating a significant time dependant mechanical property response in the engineered composite IVD similar to native IVD (Fig. 5.4b). In addition to the modulus, the effective hydraulic permeability was also significantly affected by varying the AF composition (Fig. 5.4c). The 2 mg/ml groups showed a significant drop in permeability compared to the 1 mg/ml groups, and the effective hydraulic permeability was highly negatively correlated ($r^2 = .92$) with instantaneous modulus, suggesting a change in AF permeability is playing a strong role in the altered mechanical properties between groups. No other significant correlations were observed between AF properties and the instantaneous modulus.

In vivo

The 1 mg/ml and 2 mg/ml collagen concentration groups containing $1x10^6$ cells/ml were implanted into the caudal spine of the athymic rat. These two groups

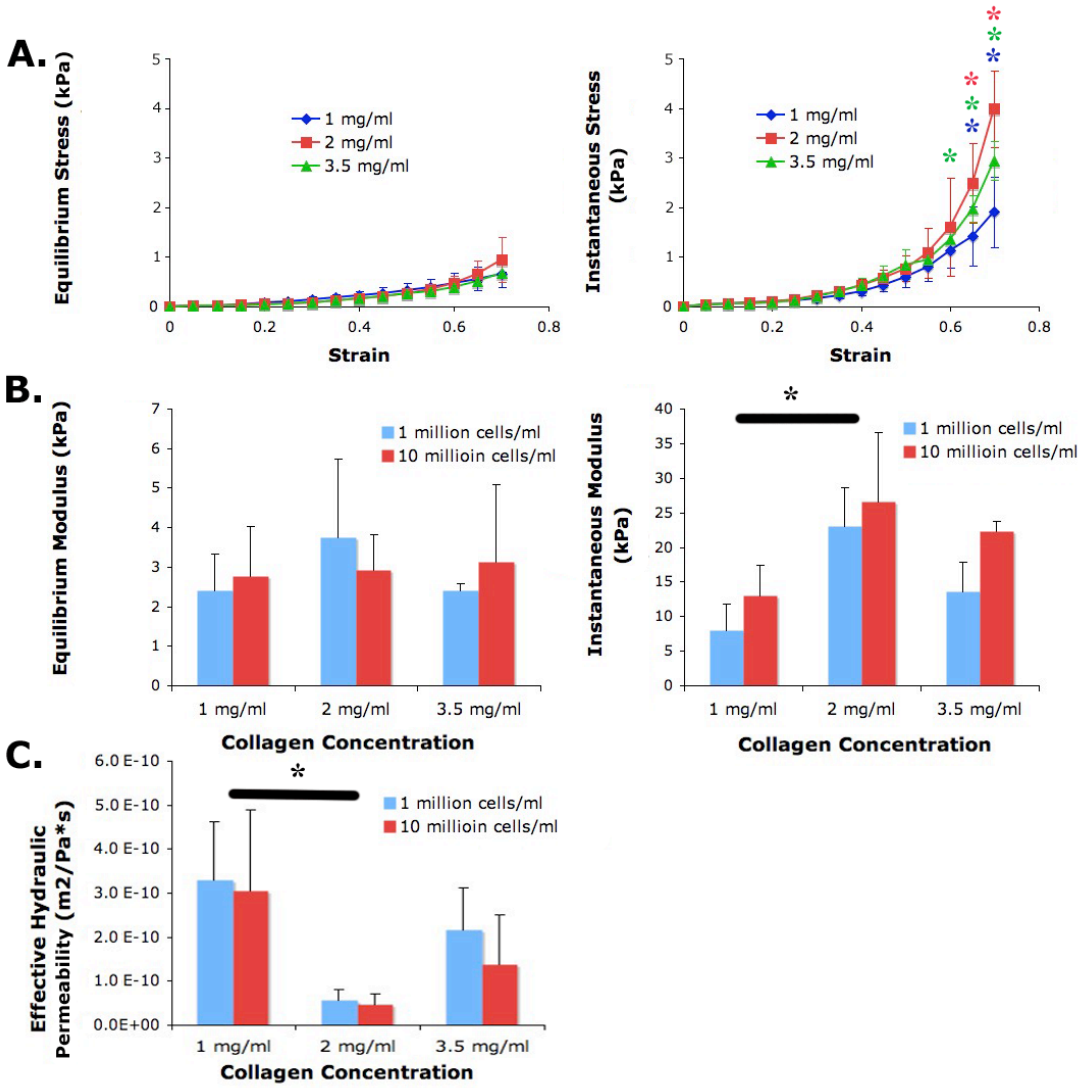

Figure 5.4 – *In vitro* mechanical testing. (A.) Mean equilibrium and instantaneous stress strain curves for the $1x10^6$ cells/ml groups. (B.) Equilibrium and instantaneous modulus for all 6 groups at 60% strain. (C.) Effective hydraulic permeability for all 6 groups at 60% strain. (Data presented as means and standard deviations, * = $p<0.05$)

were selected because they were properly sized, contained circumferentially aligned collagen fibrils in the AF, but had significantly different mechanical properties. After 6 months of implantation, both groups produced cartilaginous tissue within the disc space (Fig. 5.5); however, the regional composition of ECM in the AF and NP was significantly ($p<0.05$) different between groups. The 1 mg/ml group produced a cartilaginous tissue that was homogenous across the AF and NP. GAG levels in the 1 mg/ml group fell within the native IVD range for GAG, but failed to show a significant difference between the AF and NP, despite histology demonstrating that some preference may exist for increased GAG in the NP. In addition, GAG levels were significantly lower ($p<0.05$) in the NP in the engineered 1 mg/ml group when compared to the native NP. Collagen levels in the 1 mg/ml group showed no significant difference between the AF and NP, and the engineered NP was significantly higher ($P<0.05$) in collagen compared to the native NP. Finally, both the AF and NP showed a significantly increased ($p<0.05$) cell density compared to the native IVD. The AF region had a water content of 73 ± 9 % of wet weight compared to the native AF water content of 61 ± 11% of wet weight. The 1 mg/ml group successfully produced robust and near native levels of collagen and proteoglycans, but the distribution of ECM failed to capture the regional variation observed in the native IVD.

The 2 mg/ml implantation group produced a tissue that showed regional ECM deposition similar to the native IVD. Distinct regions could be observed macroscopically between the AF and NP (Fig. 5.5b). GAG levels were not significantly different from the native IVD in the AF or NP, demonstrating proper regional distribution with significantly higher ($p<0.05$) GAG in the NP compared to the AF. Collagen levels were, also, not significantly different from the native IVD in the AF or NP, demonstrating proper regional distribution with significantly higher

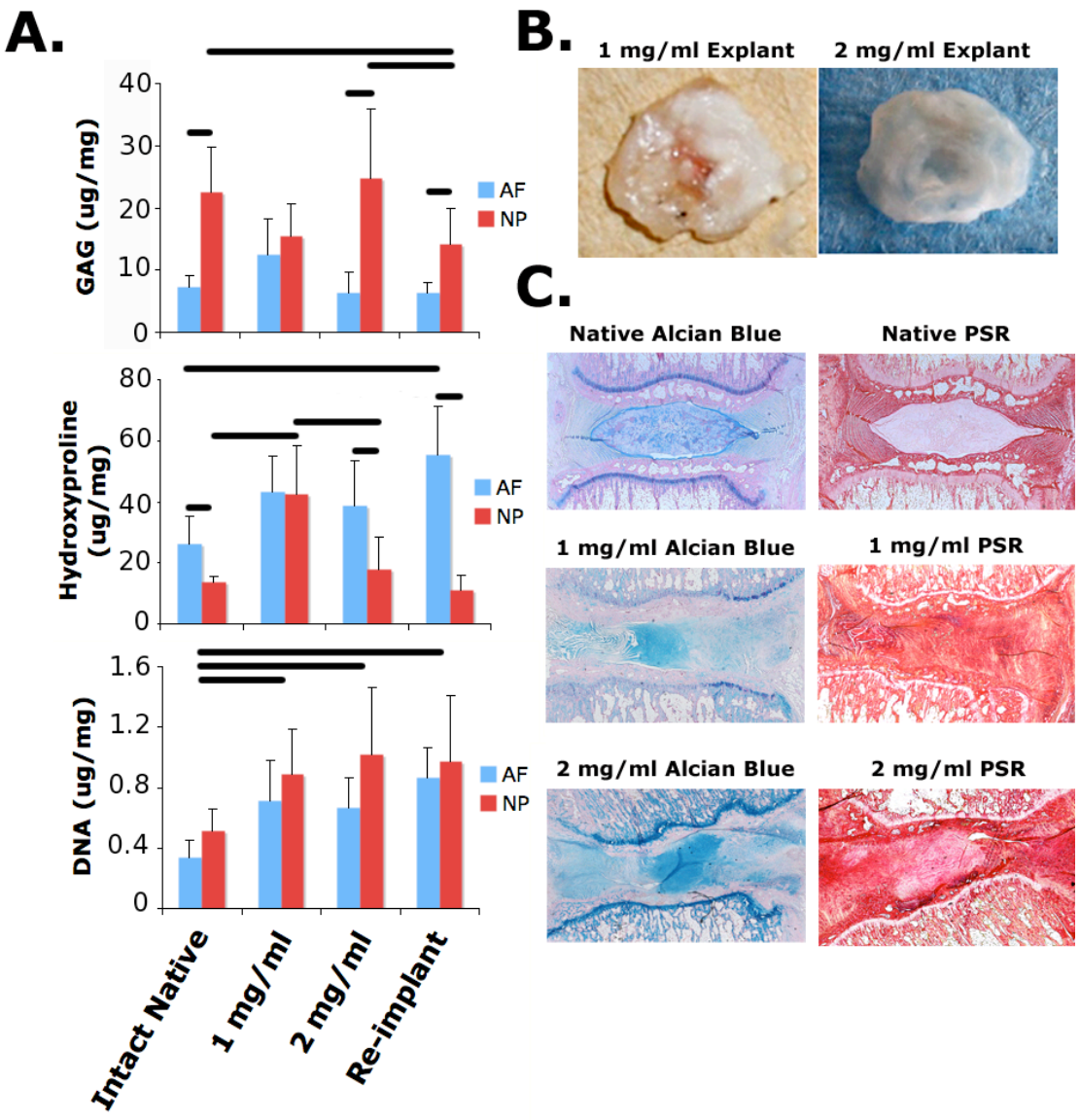

Figure 5.5 – *In vivo* tissue development. (A.) GAG, hydroxyproline, and DNA data for the native IVD, 1mg/ml TE-IVD, and 2 mg/ml TE-IVD broken down by region. (B.) Images of explanted 1 mg/ml and 2 mg/ml TE-IVDs after 6 months of implantation. (C.) Alcian blue and picrosirius red histology for the native IVD, 1mg/ml TE-IVD, and 2 mg/ml TE-IVD. (Data presented as means and standard deviations, Black Bars = $p<0.05$)

($p<0.05$) collagen in the AF compared to the NP. The AF region had a water content of 71 ± 13 % of wet weight compared to the native AF water content of 61 ± 11% of wet weight. Similar to the 1 mg/ml group, the cell content was significantly higher ($p<0.05$) in the 2 mg/ml group compared to the native IVD. Overall, the 2 mg/ml group produced an ECM with striking similarity to the native IVD after 6 months of implantation.

Both groups produced axial mechanical properties similar to the native intact motion segment after 6 months (Fig. 5.6). The 1 mg/ml group had an equilibrium modulus that was slightly, but not significantly, lower than the native intact motion segment, while the 2 mg/ml group produced an almost identical equilibrium modulus that was not significantly different than the native. The hydraulic permeability of the 1 mg/ml group was similar but significantly higher ($p<0.05$) than the native intact motion segment while the 2 mg/ml group more accurately reproduced the hydraulic permeability of the intact native motion segment, which was not significantly different. During sinusoidal dynamic mechanical testing, both the 1 mg/ml and 2 mg/ml groups produced an apparent modulus ~30% higher ($p<0.05$) than the intact native motion segment over the full range of frequencies tested.

Discussion

This work demonstrates that careful selection of AF composition of a composite engineered IVD leads to proper ECM development when implanted into the native disc space. To date a number of strategies have been investigated for use in creating a composite tissue-engineered IVD replacement. Early efforts focused on the creation of the composite structure of the IVD (58, 59), and later efforts have focused on introducing aligned and organized collagen fibril architecture into the AF region (87, 93, 119, 168). These advancements are likely integral to the success of a tissue-

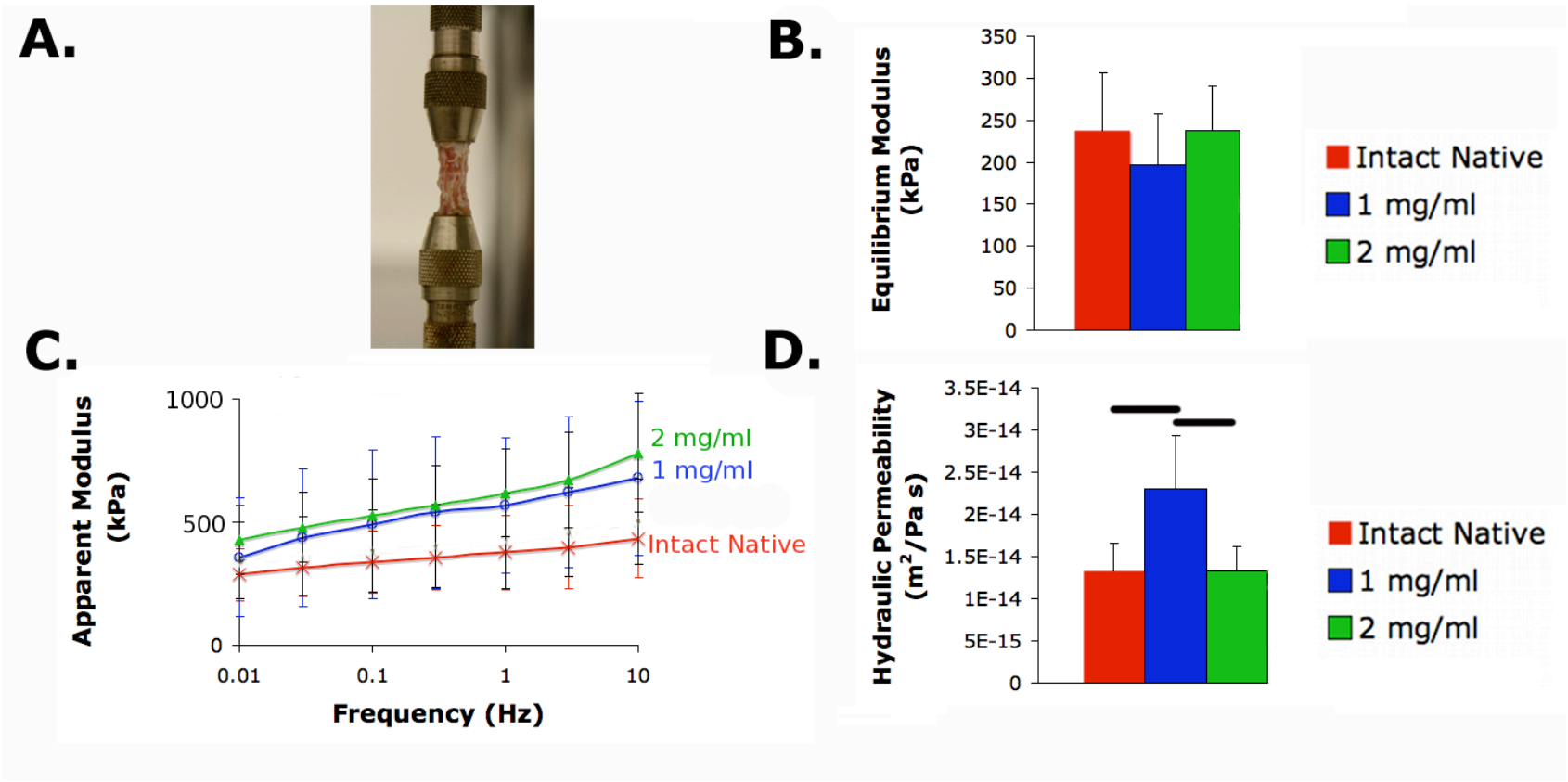

Figure 5.6 – *In vivo* mechanical testing. (A.) TE-IVD containing motion segment loaded into mechanical testing frame. (B.) Equilibrium modulus and (C.) apparent modulus (.01-10 Hz) for the native IVD, 1mg/ml TE-IVD, and 2 mg/ml TE-IVD. (D.) Effective hydraulic permeability for the native IVD, 1mg/ml TE-IVD, and 2 mg/ml TE-IVD. . (Data presented as means and standard deviations, Black Bars = $p<0.05$)

engineered total disc replacement treatment of spinal disorders; however, these studies have largely focused on *in vitro* work with little characterization of how altering the TE-IVD composition affects the composite disc mechanics, and how this relates to the success of the disc once implanted into the native disc space.

Recently, in order to address the lack of *in vivo* work in the field, we reported that composite tissue-engineered IVD could be implanted into the native disc space and restore function in the rat caudal (Chapter 4) and lumbar disc space (Chapter 3) by producing, well integrated and mechanically functional, cartilaginous tissue. In this study, we use our previously developed collagen gel (AF)/ alginate gel (NP) TE-IVD to investigate the effects of altering the AF region on *in vitro* and *in vivo* tissue development (Chapter 2) (93). By altering the original cell seeding density and collagen concentration in the AF region at fabrication, we created 6 groups of composite engineered IVDs with similar NP regions but variable AF composition. In each group, significant contraction was observed over the 2 weeks of culture (Fig. 5.2). Lower concentrations of collagen at day 0 led to significantly increased ($p<.05$) contraction over the culture period, while increasing the cell concentration at day 0 only led to increased contraction in the 3.5 mg/ml gels. The resulting difference in TE-IVD size is important because proper sizing has proven critical for successful cadeveric IVD allograft transplantation (37). In addition to changes in the final size of the implants, altering the collagen concentrations and cell seeding densities altered the collagen architecture and cellular morphology after contraction (Fig. 5.3). The $1x10^6$ cells/ml groups developed a gradient of circumferential collagen fibril and cellular alignment consistent with previous work (Chapter 2) (93), while the 10×10^6 cells/ml groups produced no collagen alignment and an unaligned-rounded cellular morphology (Fig. 5.3). As a result, we can control the AF size, final collagen density, collagen alignment, and cellular morphology in the TE-IVD by altering the original

collagen concentration and cell density. Ultimately, this tunable TE-IVD provides a framework to study the effects of AF composition on *in vitro* and *in vivo* development.

In vitro mechanical testing of the 6 groups demonstrated distinct time dependent mechanical properties between groups (Fig. 5.4). While mechanical differences were not seen between the groups in the equilibrium properties, at high strains ($\geq$ 60%) significant differences were observed in the instantaneous modulus between the varying collagen concentrations, with the 2 mg/ml groups producing the highest instantaneous modulus. These mechanical differences are due to changes in the AF composition, as the NP regions of the discs were the same between groups. One difference in AF composition that could have resulted in the mechanical property variation was the observed difference in circumferential alignment between groups; however, no significant correlations were observed between the mechanical properties being measured and alignment index. This indicates that the circumferential alignment was not playing a significant role in the compressive mechanical properties of the composite engineered IVDs and is consistent with evidence that collagen alignment does not explain the mechanical differences in contracted collagen gels (186). The mechanical property that varied most dramatically was the hydraulic permeability. In fact, the hydraulic permeability was highly correlated (r^2 =.92) to the instantaneous modulus. This likely indicates the AF's ability to resist water movement out of the engineered disc and promote pressurization was the main function of the AF in contributing to the time dependant mechanical properties. This is consistent with Native IVD, in which AF hydraulic permeabilities change with age (187) and play a significant role in the mechanical properties (188). And, as a result, the engineered IVDs were behaving in a similar manner to the native IVD by relying on the AF to resist water movement out of the disc and promote pressurization in the IVD to oppose compressive loads.

While the tunable TE-IVD provided a number of AF properties to investigate in the native disc space, the *in vitro* characterization led to the selection of two groups to be implanted and compared in the rat caudal spine. The 1 mg/ml and 2 mg/ml groups with 1 x 10^6 cells/ml were selected for implantation. These groups provided constructs with significantly different abilities to pressurize (i.e. instantaneous modulus and hydraulic permeability) while maintaining circumferentially aligned collagen fibrils and cells. As a result, these groups allow the study of how tissue development of an engineered IVD in the native disc space is affected by its ability to pressurize under compressive load and how tuning of the AF plays a role in this phenomenon.

After 6 months of implantation in the native disc space, both groups produced proteogylcan and collagen rich tissues in the disc space, but with a few key differences (Fig. 5.5). Both groups contained collagen and proteoglycans at similar levels to the native IVD; however, the 1 mg/ml group produced tissue that was distinctly homogenous across the AF and NP regions of the tissue, while the 2 mg/ml group produced a tissue with easily identifiable AF and NP regions. This resulted in the 2 mg/ml TE-IVD producing a tissue that was strikingly similar to the native IVD regional ECM composition. This reproduction of ECM amounts is key because it plays a crucial role in native IVD properties (189, 190) and its reproduction will be necessary to reproduce the function of the native disc. By altering the composition of the AF, the 2 mg/ml group resulted in a tissue that more accurately mimicked the native NP ECM composition after 6 months of implantation in the native disc space.

This demonstrates the importance of the composite structure in *in vivo* development. The reason for the altered tissue development in the NP of the 2 mg/ml AF group compared to the 1 mg/ml AF group may lie in their differing hydraulic permeability and subsequent ability to pressurize. It has been shown that NP cell

collagen and proteoglycan metabolism is sensitive to hydrostatic pressure (179) and the magnitude of that pressure (191). Regardless of the mechanism, changing the composition of the AF not only played a role in AF development, but also had the most dramatic effect on the NP development. For this reason, TE-IVD design must focus on the TE-IVD as a whole, and not simply as two independent design problems in the AF and NP.

Both groups produced well-integrated, mechanically functional motion segments after 6 months of implantation (Fig. 5.6). Both groups produced an equilibrium modulus that was not significantly different from the native IVD. This is due to the similar concentrations of collagen and proteoglycans that each group had to the native IVD. The only significant axial mechanical difference between the two groups was in the hydraulic permeability, with the 1 mg/ml AF group producing a significantly higher hydraulic permeability than the native and 2 mg/ml group motion segments. This is further indication that the 2 mg/ml implantation group was able to better reproduce the properties of the native disc after implantation. The dynamic axial mechanical properties indicate that both the 1 mg/ml and 2 mg/ml groups produced similar, but significantly stiffer (~30%) apparent moduli than the native motion segments. The increased dynamic stiffness of the 1 mg/ml and 2 mg/ml groups in comparison to the native may be indicative of the lack of lamellar and ± 30º collagen alignment observed in the native disc. This organization is likely to play a greater role in the dynamic properties than the quasi-static equilibrium modulus, where the ECM content will largely determine the properties.

Overall, this data continues to build on the evidence that a tissue engineered IVD replacement can successfully replace the native IVD in the disc space. By tuning the composition of the AF in the engineered IVD replacement, one can promote the proper ECM development in both the AF and NP regions once implanted into the

native disc space. Additional properties, such as hydraulic permeability, will need to be key design parameters in tissue-engineered AF, in addition to the creation of the complex collagen organization. In order for the field to continue to advance towards the ultimate goal of replacing a diseased or injured human IVD, further *in vivo* animal studies will be necessary along with the development of more complex and relevant animal models.

CHAPTER 6

Model-Based Inquiry of Ionic Bonding, Alginate Hydrogels, and Tissue Engineering*

Abstract

Due to cost and time, it is difficult to relate to students how fundamental chemical principles are involved in cutting edge biomedical breakthroughs being reported in the national media. The laboratory exercise presented here uses alginate hydrogels, a common material used in tissue engineering, to help students explore the relationship between chemical bonding and material properties while relating it to the field of tissue engineering. In addition, this lab is designed as a model based inquiry exercise to provide a better understanding of how contemporary science is practiced. The lab is intended to be used as part of a 4 day curriculum on tissue engineering but can be done together with the supporting curriculum or separately. The cost of this exercise is quite inexpensive, approximately $6.00 per group, and can be performed in low resource laboratories, as it requires no elaborate equipment.

*This chapter will soon be submitted for publication: Bowles, R.D., Saroka, J.M., Archer, S.D., and Bonassar, L.J. Model-Based Inquiry of Ionic Bonding, Alginate Hydrogels, and Tissue Engineering. Journal of Chemical Education. In Preparation

Preface

I had the privilege to participate in the National Science Foundation (NSF) GK-12 program. The program paired graduate students with local area high school teachers. I was paired with Jamie Saroka, a Lansing High School Chemistry teacher. During the summer of 2010, Jamie spent 6 weeks as a visiting researcher in our lab. It was my job to mentor his progress on a research project. In addition, we developed curriculum that would be taught in his Chemistry classes in the Fall of 2010. The program provided a great opportunity for both the graduate student and high school teacher to develop new skills while simultaneously contributing to science and science education.

During the summer portion of the program, Jamie worked on the lab's collagen riboflavin crosslinking project. He spent his time learning how to obtain collagen from rat tails, fabricating and photocrosslinking collagen gels, mechanically testing collagen gels, and analyzing the data using various statistical tests. Jamie's summer efforts resulted in his coauthoring of an Orthopaedic Research Society abstract. By the end, Jamie had experienced the full spectrum of the contemporary science process all the way to presenting his findings in writing. This experience will provide Jamie with a better understanding of in lab science practices that he will be able to relate to his students.

The curriculum development portion of the program provided a great collaborative opportunity for Jamie and myself. I was able to use my tissue engineering perspective to help develop new ways to teach chemistry to students, while Jamie was able to use his experience as a teacher to help mold my ideas into feasible classroom activities. In the end, we developed an inquiry based curriculum that taught ionic bonding to students through the exciting field of tissue engineering. This curriculum meets 11 of the national science standards and can be done for a

relatively low cost with very few resources. The low cost and low resource aspect of the curriculum allows it to be widely applicable and provides the opportunity for cutting edge biotechnology to be brought into low resource classrooms.

The curriculum was taught to 4 high school chemistry classes in the fall of 2010. Overall, the students responded favorably to the curriculum and were actively engaged in the activities. The students all showed an increase in comprehension of the scientific material (bonding) while also demonstrating a better grasp of the scientific process. After teaching the curriculum, both Jamie and I felt this curriculum was worthy of sharing with other classrooms and it was written up for publication in the Journal of Chemical Education.

While the students learned a great deal, both Jamie and I learned from the experience as well. Specifically, we both learned the value of a truly inquiry based approach to teaching. The students responded uncomfortably at first to the lack of directions in the labs. However, once the students began working, they were immediately engaged. Many of the students even worked through the bell as they attempted to tackle the challenge of planning and carrying out an experiment to answer their scientific question. In surveys following the curriculum, students commented on the need to actually think about the labs instead of just following directions. In addition, an essay question designed to assess the students knowledge and understanding of the content indicated that the inquiry based activities allowed them to make better connections between technology and basic chemistry principles following the activity. In the end, the students were able to obtain a deeper understanding of the material than just facts. This will certainly be a teaching technique that I will continue to utilize as I continue my career in post-secondary education.

Furthermore, teaching science content to high school level students pushed me to develop simple and effective ways to communicate my points. In everyday interactions in my lab, I can communicate in a way that requires a high level of indoctrination in tissue engineering and biomedical engineering. Unfortunately, this mode of communication will not work in communicating the principles of my field to the average person. Everyday, I see more and more a need for scientists to convey their findings and the importance of their findings to society. However, I often see these efforts fail. I think this is both a problem of the poor general science background of the average person and the inability of the scientist to communicate in a simple, clear, and effective manner. Through the GK-12 program I believe we have been working on addressing both of these shortcomings. We have developed new curriculum that will hopefully engage and more effectively teach science to society while also teaching me, as a scientist, to communicate my points more simply and effectively. This will hopefully help to make a very small dent in the dilemma of poor science literacy.

In the end, this program was a fantastic program that introduced me to a much greater passion for education than I knew I had while also revitalizing Jamie's passion for science. It is my hope that others will find the curriculum that we developed as a useful resource.

Introduction

Due to cost and time, it is difficult to relate to students how fundamental chemical principles are involved in cutting edge technological breakthroughs being reported in the national media. This ability to relate science to technology is directly addressed in the national science education standards, content standard E (192). One of the fields that students often find exciting and is frequently discussed in the national

media is tissue engineering. This field aims to treat human disease by growing new tissues and organs to replace those that are diseased or injured (193). In order for this to be accomplished, scientists and engineers from a broad range of disciplines come together to research material, cell, and signaling combinations to produce new organs and tissue. Chemistry is heavily involved in all aspects of the field, but the chemical bonding present in the material scaffolds can be harnessed to teach students about bonding while relating it to a high profile technological field.

Alginate is a common material used as a scaffold in tissue engineering and is appropriate for use in the classroom due to its safety and low cost (194, 195). Alginate, a structural component of cell walls, is a polysaccharide obtained from seaweed. This material can be maintained in solution form until mixed with a divalent cation (e.g. Ca++), at which point it will produce a hydrogel by forming ionic crosslinks (Figure 6.1a). A monovalent cation (e.g. Na+) will associate with the alginate but fail to form crosslinks between the alginate chains (Figure 6.1b). The ability to produce crosslinked gels from solution is useful in tissue engineering because cells can be entrapped within this biocompatible material as it gels. The encapsulated cells can then produce new tissue within the scaffold. As the scaffold degrades, a new healthy tissue will grow in place of the diseased or injured tissue.

Alginate has been used for classroom demonstrations due to the ease and safety with which bonding reactions can be demonstrated (194, 195). This laboratory experiment continues along the lines of these demonstrations but is designed to fit into a 4-day curriculum on tissue engineering (see appendix) while providing the student with a physical representation of ionic bond formation addressing National Science Education Standards, content standard B (192). However, this experiment can also be a stand-alone lab highlighting bonding principles. In addition, the laboratory experiment is designed as a model-based inquiry laboratory experiment to engage

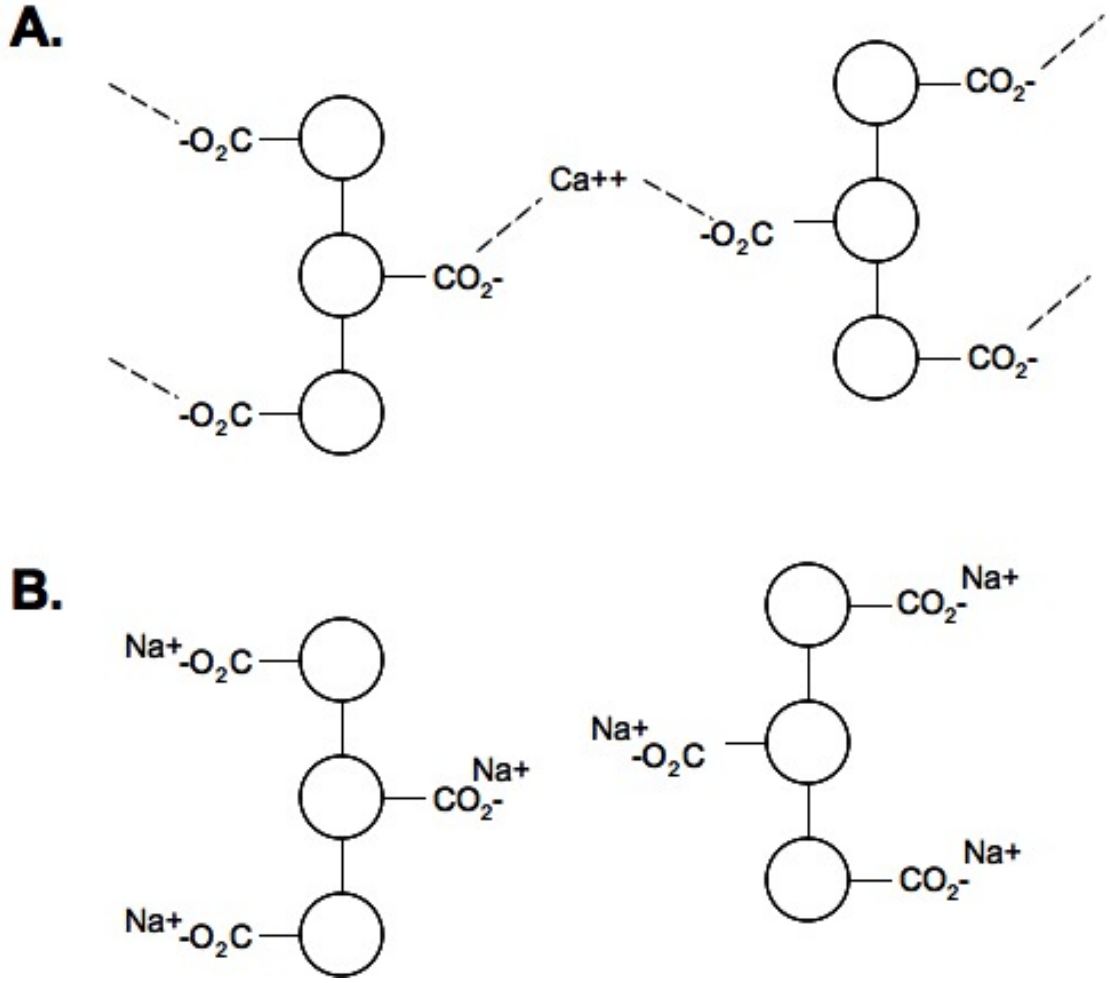

Figure 6.1 – (A.) Alginate chains crosslinked by Ca++. (B.) Alginate chains associated with Na+ but not crosslinked.

students in a deeper understanding of the content of tissue engineering and introduce a greater comprehension of the processes of contemporary science practices (196). This laboratory was originally performed in three New York State High School Regents Chemistry classes and can be carried out as a part of the developed tissue-engineering curriculum or as a stand-alone exercise.

Experimental Section

Materials. Per group (Figure 2): 30 ml of 2% (20 mg/ml) alginate solution colored with blue food dye, 30 ml of 2% (20 mg/ml) $CaCl_2$ solution colored with yellow food dye, 30 ml of 2% (20 mg/ml) NaCl solution colored with red food dye, eight 30 ml freestanding conical tubes, and 3 transfer pipettes. Total cost per group (2 to 4 students): ~$6.00, materials are available from most K-12 science suppliers.

Procedure. Students are provided with the information that the red solution contains a monovalent cation, the yellow solution contains a divalent cation, and the blue solution is alginate. In addition, they are provided with the generalized structure of alginate (similar to Fig 6.1a.) with an "x" in place of the carboxyl - group. The students are told that they are going to be using the information and supplies provided to run an experiment to determine properties of the "x" group. They are informed it is their job to develop a model of how the alginate strands will interact with the other solutions using the alginate structure provided above. They must design an experiment to test their model, collect the data from their experiment, analyze the data, make adjustments to their model based on the findings, and finally determine what the next steps would be necessary to further test their refined model. The entire exercise can be performed in two class periods totaling 84 minutes. The laboratory portion can take approximately one 42-minute class period and the analysis, model adjustments, and

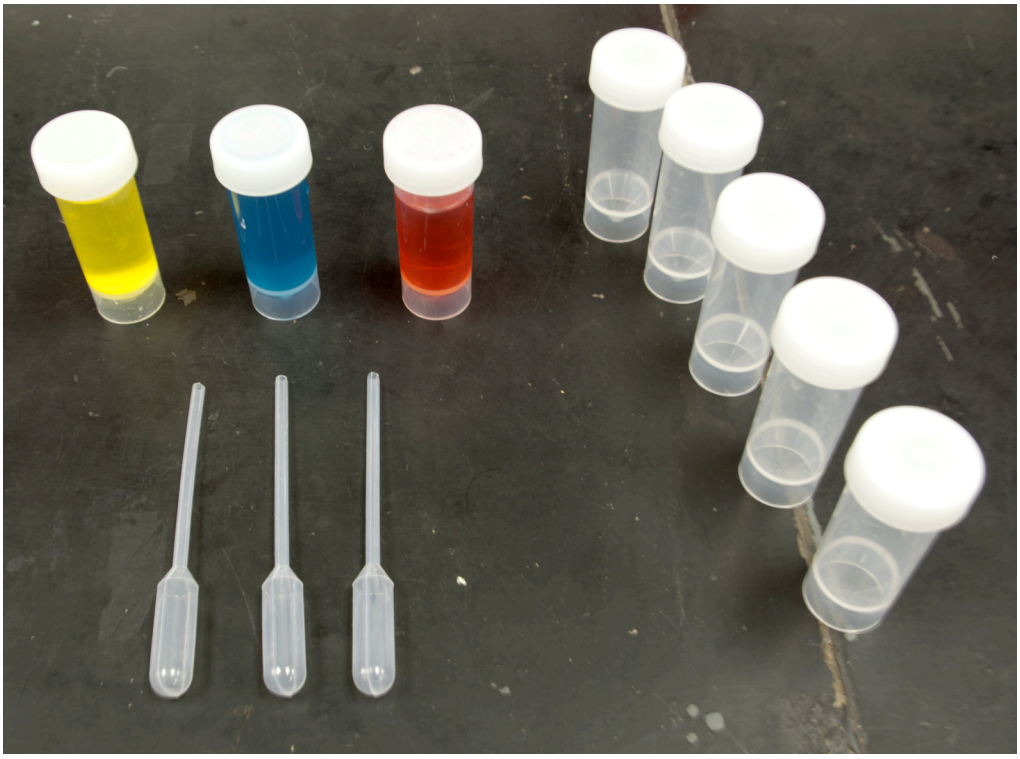

Figure 6.2 – Supplies necessary for each group

future directions another class period. However, if time limited, the analysis, model adjustments, and discussion could be assigned as homework.

Results and Discussion

Most students decide to mix each possible combination of solutions to see what happens. It is advantageous to the students if they develop a specific model before doing this experiment. The provided alginate chain structure will help in the development of this model. It is important to note that students will be hesitant that their model is incorrect. This provides a great opportunity to explain to the students that scientific models are often wrong, and that is why the experiments are carried out to test each model. The students will observe during their experimentation that the blue and yellow solutions form a gel when mixed, the blue and red do nothing observable, as do the yellow and red. The students often note a color change, but may have to be redirected back to the model. "Does a color change support or disprove your model?"

There are two main conclusions we hope the students reach and can be lightly guided if need be (the less guidance the better). The first conclusion is that the alginate "x" group is negatively charged. The negative charge is why the yellow and blue solutions gel when mixed by forming ionic bonds between the alginate chains. This conclusion provides a visual and tactile representation of how the formation of bonds can affect material properties. Most students come to this conclusion from their experimentation and analysis.

The second conclusion, based on the negative charge of alginate, is more advanced, but students are able to come to it if forced to think about it. Alginate forms a gel with the divalent cation solution because the divalent cation provides a plus two charge that can form ionic bonds with two minus one charges of the "x" groups of

alginate and form bridges (crosslinks) between these chains of alginate (Figure 6.1a). On the other hand, the monovalent cation only has a plus one charge and therefore can't bridge two chains of alginate (Figure 6.1b). The question you hope they ask is, "why does it gel with the divalent cation but not the monovalent cation?" Asking this question will start the students down the right path. If deemed appropriate, the teacher can provide this information to them after they struggle with it. Another hint that the teacher can provide late in this exercise is to draw the Lewis dot diagram for a divalent cation. This can help them to see that there are two positive charges available to form a bridge between 2 strands of alginate that have negative charges.

These two conclusions are the most useful in relating the scaffold formation of tissue engineering to ionic bonding. The student's final model will ideally resemble Figure 1. Most students will naturally move in this direction, however, this is not the only direction the students can go. The important aspect is that the students develop a model, test it through experimentation, analyze it, adjust their model, and plan for future experiments. This allows them to experience science as it is carried out every day in the laboratory. It is important that the students fill out their handouts (see supplementary material) as they carry out their experiments. The teacher can explain to them the handout is like their "lab notebook" and discuss how these notebooks are used in the lab to write down everything they do so they have a record of their experiments and thinking.

The laboratory exercise was extremely well received by the students after completing the exercise. An anonymous survey of the students indicated that 88% of the students rated the exercise positively, another 8% rated it neutrally, and only 4% rated it negatively. In addition, students indicated that the model-based inquiry approach "gave us more freedom and made us actually think instead of telling us what to do." In addition, the model-based inquiry showed them that "the step where people

change the model/hypothesis is overlooked so much in school", thus demonstrating how this form of laboratory can promote a better understanding of contemporary science practices.

The students were assessed by providing them with an essay question after a traditional lecture on tissue engineering, but before the inquiry exercise. Then the same essay question, presented as a follow up, was given to the students after the inquiry exercise (essay questions provided in supporting material). The essays were scored for discussion of key tissue engineering principles, discussion of ionic bonding, and making connections between tissue engineering and chemical bonding. The students showed no significant improvement in demonstrating a grasp of the tissue engineering principles measured; however, students demonstrated a significant improvement in understanding the relationship between chemical bonding and material properties with a 419% increase in class mean for this score. In fact, 64% of students after the laboratory, compared to 30% beforehand, were able to make a connection between chemical bonding and tissue engineering in their essay. The laboratory exercise did not promote any additional understanding of the basic tissue engineering principles after the lecture, but was extremely effective at helping students understand relationships between bonding, scaffolding materials, and the tissue engineering process.

Conclusion

Overall, this laboratory experiment provides the student with a tactile representation of bond formation and a connection between fundamental chemical principles and current technologies being developed in the cutting edge field of tissue engineering. In addition, this lab is designed as a model based inquiry exercise to provide a better understanding of how contemporary science is practiced. The exercise can be done

for a very low cost, $6.00 per group, and can be performed in low resource laboratories, as it requires no elaborate equipment.

Hazards

Alginate, $CaCl_2$, and NaCl pose little risk to the students; however, students should be expected to follow general safety guidelines and wear protective lab equipment when carrying out the laboratory exercise.

CHAPTER 7

Conclusions

This dissertation developed a novel TE-IVD and investigated the feasibility of using this technology for TE-TDR in an *in vivo* animal model. A novel TE-IVD with tunable AF composition and architecture was developed to study *in vivo* TE-TDR and investigate the relationship of AF composition on TE-IVD development (Chapter 2). Using MRI and μCT, a method that is easily translatable to the clinic was developed to produce geometrically accurate TE-IVDs (Chapter 3). These anatomically shaped TE-IVD composites were implanted into the native disc space for 6 months to study the tissue development and efficacy of TE-TDR (Chapter 4). Finally, the effects of AF composition on the *in vitro* and subsequent *in vivo* tissue development was investigated by implanting TE-IVD with altered AF composition in the native disc space for 6 months (Chapter 5). This chapter discusses the main findings of this dissertation and proposes future studies that can build on this body of work.

In chapter 2 we proposed and demonstrated the creation of a TE-IVD with circumferentially aligned collagen fibrils that mimicked the predominate organization seen in the IVD. In addition, altering the original collagen concentration and cell seeding density before AF contraction allowed the architecture and composition of the AF to be controlled. This ability to control the composition and architecture would later (Chapter 5) allow us to investigate the AF relationship to *in vitro* TE-IVD properties and development in the native disc space. The general trend in tissue engineering of a composite IVD has been to increase the complexity of the AF to more closely mimic the architecture of the native IVD. At the time of publication of this work, a TE-IVD had not been produced with any alignment in the AF region of the disc (58, 59, 87). This work was the first to introduce the predominant native

circumferential collagen fibril alignment into a TE-IVD (93). Since this paper was published, the field has continued in the direction of more closely mimicking the native AF architecture by producing TE-IVD with the ±30º collagen alignment pattern seen between adjacent lamellae in the native IVD (168). Because of the structure function relationship between the AF organization and AF mechanical properties (41, 111), it is hypothesized that introducing the AF collagen organization into the TE-IVD will allow the engineered tissue to more closely mimic the native mechanical function. While a sound hypothesis, to date it is unproven how much of this organization needs to be introduced to effectively restore mechanical function in the native disc space.

It was our belief that the field was making good progress in producing TE-IVD that increasingly mimicked the architecture of the native IVD. However, the target design principles were theoretical. There was no *in vivo* data that explored how TE-IVD would develop in the native disc space. It was unclear whether a TE-IVD would survive in the native disc space, integrate with the native endplate and vertebral bodies, or be able to withstand the complex mechanical loading of the disc space environment. In addition, as previously mentioned, it was unknown how much of the native architecture was needed to restore mechanical function to the motion segment despite the field continuing to produce TE-IVD with increasingly complex AF. For these reasons, we wanted to begin pursuing answers to these questions and moved towards implanting TE-IVD into the native disc space.

In chapter 3 we used MRI and μCT to obtain geometric data from the IVD and disc space of our intended implantation site and used this data to guide our fabrication of a anatomically shaped TE-IVD. In addition, we carried out our first pilot study of *in vivo* TE-IVD implantation into the lumbar L4/L5 disc space. The ability to create anatomically shaped IVD was the first step in moving towards understanding how a TE-IVD responds to the native disc space environment. This technique allowed us to

make discs that were properly sized and shaped for the disc space we wanted to implant into. In the future, patients could receive an MRI and CT scan that would allow the TE-IVD to be designed specifically for their anatomy and disease state. This is highly advantageous, as it has been shown that proper size matching is critical to cadaveric IVD allograft transplantation success (37) and will likely play a key role in TE-TDR success. The anatomically shaped TE-IVD was implanted into the L4/5 disc space of 5 athymic rats for 4 months and demonstrated promising results. The TE-IVD was able to maintain the disc space fully or partially in 3 of 5 animals and produced integrated cartilaginous ECM in these three animals. In the 2 animals in which the disc space collapsed, it was apparent that the posterior longitudinal ligament and supporting tissue had been cut during surgery. The disc space collapse in these animals demonstrated the importance of the supporting ligament structure to the success of TE-IVD transplantation. This was the first study that implanted TE-IVD into the native disc space and demonstrated that the TE-IVD could maintain disc space height and produce an integrated cartilaginous tissue in the disc space.

As a result of the pilot study success, a more thorough study of TE-IVD implantation into the native disc space was carried out in Chapter 4. TE-IVD was implanted into the caudal 3/4 disc space for 6 months and histology, quantitative biochemistry, MRI, dynamic mechanical testing, and quasi-static mechanical testing were used to study the tissue development in the disc space. The caudal model was chosen due to the reasonable loading observed in the disc space (169, 170) and the repeatability of the surgery. The analysis demonstrated that a mechanically functional and well-integrated IVD like ECM developed in the disc space over 6 months. This was the first study to demonstrate that TE-IVD implantation could reproduce key function in the native disc space. In fact, this study directly addressed the 3 main concerns that had been raised in relation to TE-TDR. (1.) The TE-IVD was able to

survive and produce a *de novo* mechanically functional tissue in the native disc space. (2.) The TE-IVD was able to withstand the complex mechanical loading and maintain the disc space. And (3.) the TE-IVD was able to integrate with the native endplate and vertebral body. Until this study, the idea of replacing a native disc with a TE-IVD was theoretical, but this study demonstrated that TE-TDR was viable in the native disc space. This study represents a benchmark in the field and will hopefully establish *in vivo* TE-IVD studies as the standard for determining the success of TE-IVD design.

Upon establishing that TE-IVD could produce mechanically functional tissue in the disc space, it was our goal in Chapter 5 to use our tunable TE-IVD scaffold and *in vivo* animal model to elucidate essential design principles for successful TE-TDR transplantation. Since much of the work in TE-IVD has been focused on the AF, we wanted to study the effects of altered AF composition on development of the TE-IVD in the native disc space. During the *in vitro* phase of this chapter, it was determined that by altering the original collagen concentration and cell seeding density of the AF region that we could control the collagen alignment and hydraulic permeability of the AF. In addition, we discovered that the change in AF hydraulic permeability was likely leading to the change in instantaneous modulus that we were observing between the TE-IVD groups. As a result, we hypothesized that the altered mechanical function that we observed by changing the AF permeability, would lead to altered ECM deposition when implanted into the loaded environment of the disc space.

To test this hypothesis, it was determined that we would implant the two TE-IVD groups (1 mg/ml and 2 mg/ml AF collagen concentration and 1 x 10^6 cells/ml) that had similar AF collagen alignment, but varying AF hydraulic permeability and ability to pressurize under load. After 6 months of implantation, we observed that the group with a lower hydraulic permeability and greater ability to pressurize (2 mg/ml AF) produced an ECM that better represented the AF and NP ECM phenotype

differences, with increased GAG in the NP and increased collagen in the AF. In fact, this group was able to produce an ECM that was not significantly different than the native AF and NP. The group with a higher hydraulic permeability and decreased ability to pressurize (1 mg/ml AF) produced a more homogenous tissue across the AF and NP, although it still produced near native levels of ECM. As a result, we see that the hydraulic permeability of the AF plays a key role in the tissue development of TE-IVD when implanted into the native disc space. This is likely due to the ability of AF hydraulic permeability to regulate TE-IVD mechanical properties. Unfortunately, to date hydraulic permeability of the AF has received little attention when AF design has been discussed. However, our study demonstrates that AF hydraulic permeability is a key design parameter in developing TE-IVD for TE-TDR and should be considered alongside of collagen architecture.

Overall, this dissertation presents a body of work that makes significant advances in the field of TE-TDR. The key advances presented here are the development of the first TE-IVD with a tunable AF, the development of the first image guided technique to produce anatomically shaped IVD, the first implantation of a TE-IVD into the native disc space the first evidence that TE-IVD can restore function to the motion segment, and finally, the first *in vivo* data the indicates AF hydraulic permeability is a key design parameter in TE-IVD. Each of these advances pushes the field of TE-TDR closer to providing a clinical treatment for disc related spinal disorders.

Future Work

The work presented within this dissertation lays the foundation for a number of future directions. These include further advancements in TE-IVD design, further study of

TE-IVD design parameters utilizing the tunable TE-IVD presented here, and the development of increasingly complex and clinically relevant animal models.

The TE-IVD presented here was the first to introduce circumferentially aligned collagen fibrils into the AF. However, the complexity of the native AF collagen architecture includes the alternating ±30º collagen alignment in each successive lamella. As a result, while it has not been determined that introducing this level of organization is necessary for TE-TDR, it is likely advantageous to do so. A number of ideas have been discussed to accomplish this goal. First, the creation of multiple lamellae is quite simple using the current fabrication technique and can be accomplished by successively contracting collagen gel around the previously contracted lamella in the TE-IVD. The more difficult part will be introducing the ±30º collagen alignment. Three of the ideas discussed have been to use cell patterning within the gels to guide the alignment, introduce additional internal boundaries into the collagen while it is contracting, or introduce torsional mechanical stimulation to constructs during *in vitro* development. Any of these ideas may be able to help produce the complex collagen architecture.

The current animal model and tunable TE-IVD provide a number of directions for future work. In this dissertation, the effect of AF hydraulic permeability on TE-IVD development was investigated. However, we also demonstrated that we could control collagen alignment within the AF region of the TE-IVD, as well. With all the attention on collagen alignment in the field, it would be advantageous to study how introducing this alignment into the TE-IVD, or lack thereof, will affect the development in the native disc space. Furthermore, additional variations to the TE-IVD could be studied in the native disc space, such as multi-lamellae AF TE-IVD or using alternate cell sources. Due to the lack of viable autologous AF and NP cells located in the degenerated disc, stem cells are likely necessary for clinical treatment.

It would be advantageous to investigate how using MSCs would affect the TE-IVD development in the native disc space in comparison to the AF and NP cells used within this dissertation. Overall, each of these suggested experiments would be utilizing the current model system to elucidate the design parameters that are important for TE-TDR. This type of experimentation is needed within the field so that TE-IVD design is evidence based and targeted to the native disc space.

Finally, with the success of the current work, it opens the door to testing TE-TDR in more complex and clinically relevant animal models in hopes of moving towards a human TE-TDR implantation. The current model provided a great framework for answering the key integration and development questions necessary for moving TE-TDR forward. However, the model does have limitations. The current model is in a healthy disc space, has smaller diffusion lengths, and may provide lower loading than the human IVD space. Each of these may contribute to a greater chance of success in the current athymic rat-tail model than would be seen in the human disc space. A degenerated disc space is likely to have inflammatory cytokines (3) and a less permeable endplate (176). Both of these factors would likely be detrimental to tissue development. The next step in addressing TE-TDR in a degenerated disc space can be done in the current athymic rat-tail. A common model for degenerated disc disease is to induce the disease with an annular puncture (197), which could easily be done prior to carrying out the TE-TDR surgeries. Utilizing this type of model would allow TE-TDR to be tested in a disc space that more closely mimics the disc space that would be observed in human patients.

The smaller diffusion lengths and possible decreased loading experienced in the rat tail model will need to be addressed in a larger animal model. The smaller diffusion lengths allow for nutrients to reach the interior regions of the developing tissue more easily than would be possible in the human disc space (176), while lower

loading may allow low stiffness TE-IVDs to succeed in situations that would not be possible in human TE-TDR. It is unclear whether the nutrient transport will be an issue; and techniques are available, including temporary instrumentation, which would allow low stiffness TE-IVD to withstand larger loads while developing. However, it is necessary to carry out these experiments in larger animal models so these questions can be addressed and answered before moving to human TE-TDR.

The ultimate goal of this research is to move toward implanting a TE-IVD into a human patient to treat disc related spinal disorders. And as can be seen, this body of work was both successful at moving the field towards this goal and opening up doors to new research questions. It is my hope that this work will serve as a benchmark to the field and drive TE-IVD research towards design principles obtained from *in vivo* experimentation.

APPENDICES

Appendix A: Human IVD Cells Obtained from Partial Discectomy as a Source for IVD Tissue Engineering

Introduction

This dissertation has presented a method for producing a composite TE-IVD that is capable of forming mechanically functional and well integrated cartilaginous tissue in the native disc space using an NP and AF ovine cell source. In order for this to be translated into the clinic, an appropriate cell source needs to be selected that can be used in the TE-IVD construct. There are 3 cell sources that are likely to be used in human TE-TDR. These cell sources are human AF and NP cells (93, 185, 198, 199), human MSCs (168), or iPSC cells. Human AF and NP cells have the advantage of already being differentiated into the AF and NP phenotypes. However, these cell types are likely coming from degenerated IVD and may have incurred changes in phenotype that make them unfit for TE-TDR. It is unclear whether an adequate number of cells can be obtained from the patient or whether these cells can be expanded to adequate numbers for use in TE-TDR. It was the goal of this work to access whether human AF and NP cells could be obtained in adequate numbers from partial discectomy procedures and expanded *in vitro* for use in TE-TDR.

Methods

IVD tissue was obtained from the lumbar region of human patients (Age 31 – 59) during partial discectomy procedures and separated into annulus fibrosus (AF) and nucleus pulposus (NP) tissue (n=5). Procedures were performed under the guidelines

of Weill Cornell Medical College (IRB # 0705009162). Tissue was weighed and a sample was removed to analyze cell content of tissue. Cell content was determined using Hoechst DNA assay while the remaining tissue was digested in 0.3% w/v collagenase in Ham's F12 media for 6 hours (AF) and 4 hours (NP). Digested tissue was filtered through 100 μm nylon mesh and centrifuged at 936 x g for 7 minutes to pellet cells. Cells were counted and the viability assessed using a hemacytometer. Cells were then plated at 2500 cells/cm^2 on T150 culture flasks and cultured for 2 weeks. Pictures were taken of culture flasks every 3 days and the cells counted to access the doubling time of the NP and AF cells. The same procedure was followed for healthy ovine AF and NP cells for comparison.

Results

Human IVD cells were successfully obtained from partial discectomy procedures. Cell viability was 93.49% ± 2.34 for IVD cells obtained from surgery. The mass of tissue obtained per procedure had large variations and ranged from 0.51 – 1.56 g for AF and 0.66 – 4.17 g for the NP (Figure A.1a). Cell density of tissues obtained through partial discectomy also showed relatively large variations between samples in both the AF and NP (Figure A.1b). The cellular yield was similar between NP and AF and once again showed large variations between samples (Figure A.1c). The total number of cells obtained ranged from 0.75 – 3.5 million for AF and 1.75 – 7.1 million for NP from the partial discectomy procedure (Figure A.1d). Doubling times were 3.5 ± 0.7 days and 3.2 ± 0.5 days for the degenerated human AF and NP cells, respectively, compared to 1.38 days and 3.51 days for the healthy ovine AF and NP cells, respectively (Figure A.2).

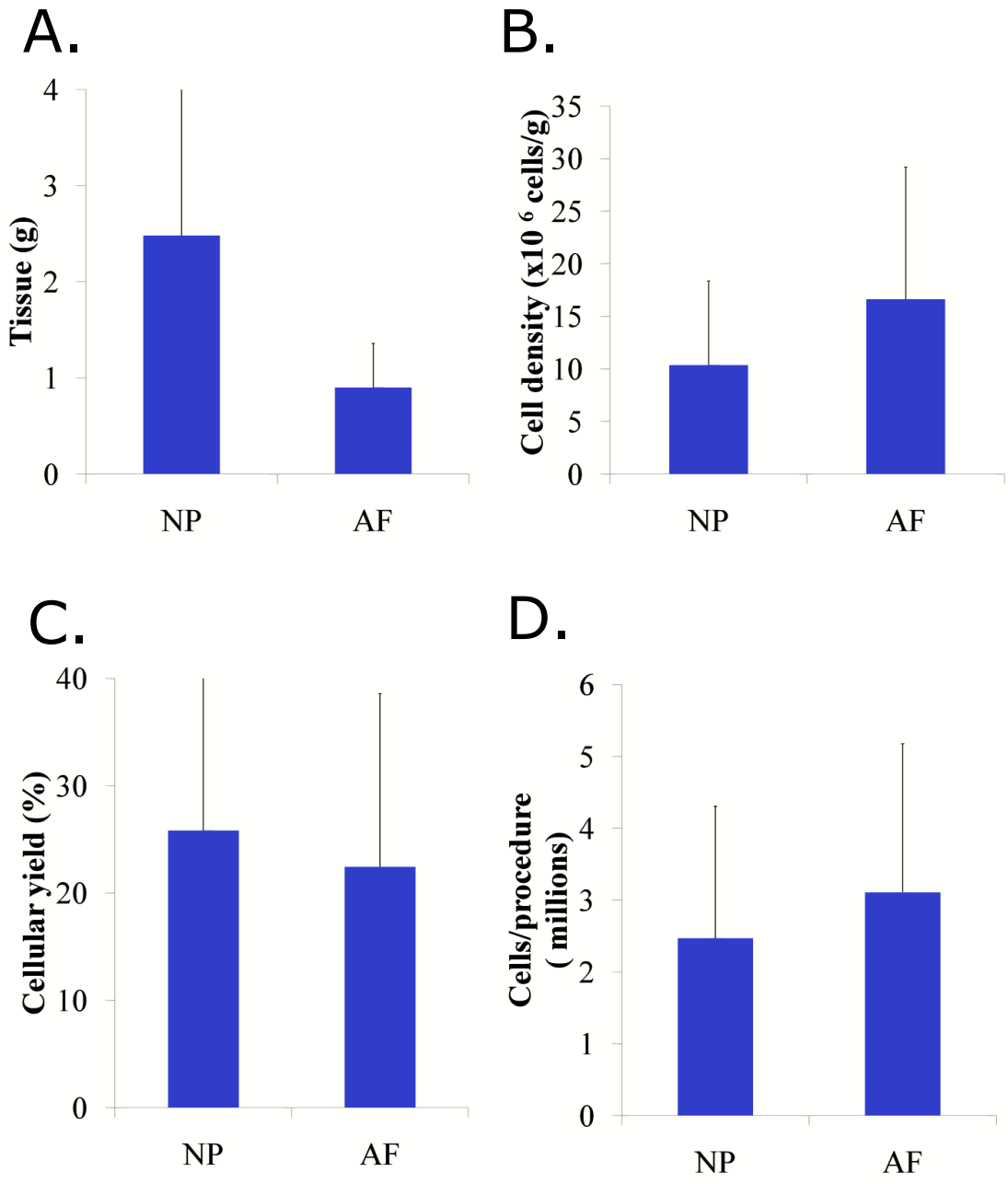

Figure A.1. (A.) Wet mass of tissue obtained from partial discectomy for the AF and NP. (B.) Cell density of the AF and NP tissue obtained from partial discectomy. (C.) Cellular yield of the AF and NP tissue obtained from partial discectomy. (D.) Total number of cells obtained from the AF and NP per PD procedure. (Data represented as mean ± standard deviation, n =12)

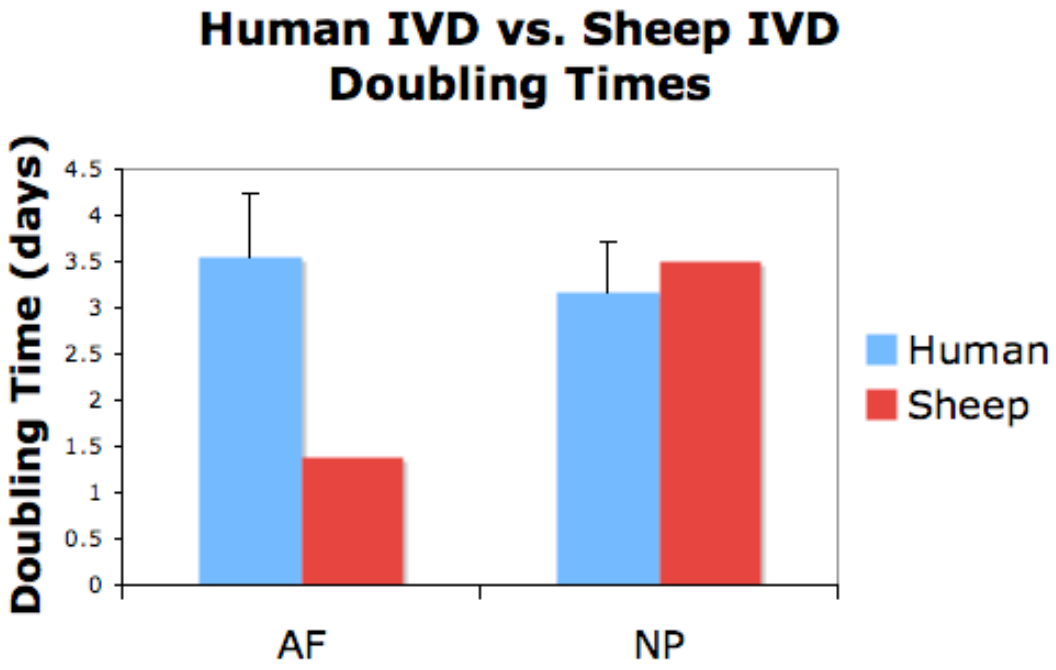

Figure A.2. Doubling times of human AF and NP cells obtained from partial discectomy surgery compared to healthy ovine AF and NP cells. (Data represented as mean ± standard deviation) (Human, n = 12; Sheep, n =1)

Discussion

Partial discectomy is shown here to be a source for expandable human IVD cells. However, the relatively low number of cells harvested indicates cell culture expansion is likely necessary to obtain a clinically relevant number of cells from partial discectomy procedures. In addition, the doubling times indicate that degenerated AF cells have an increased doubling time compared to the healthy ovine AF cells used in this dissertation. This makes expansion more difficult and may indicate fundamental differences between the healthy ovine AF cells and the degenerated human AF cells that may affect their performance in TE-IVD. Furthermore, the large standard deviations may make planning a TE-IVD procedure from partial discectomy a difficult task. While this work indicates that cells can be obtained and expanded *in vitro*, it does not investigate the phenotype of the cells and their suitability for *de novo* tissue development in the TE-IVD. In addition, it has been shown that degenerate IVD cells suffer from cellular senescence (200). While this pilot data does not eliminate the possibility of using human AF and NP cells for TE-TDR, the variability, low-cell yield, and the known issue with cellular senescence may indicate that partial discectomy is not a suitable cell source for human TE-IVD. Further work should be done to ascertain the ECM production capabilities of the degenerate human NP and AF cells in TE-IVD.

Appendix B: Mechanical Properties of Disectomized Motion Segments

Introduction

In this dissertation we have shown that we can produce mechanically functional tissue in the native disc space after 6 months. However, we have not shown the mechanical properties of the discectomized motion segments after 6 months. This is necessary to act as a negative control for our mechanical testing setup, as well as demonstrate that the motion segment loses function without a TE-IVD re-implanted after discectomy.

Methods

Discectomized motion segments were mechanically tested 6 months post-surgery (n = 6). Motion segments were explanted and were cleaned of surrounding tissue to result in bone-(remnant tissue)-bone motion segments after sacrificing the animals at 6 months. Prepared motion segments were mounted on ELF 3200 mechanical testing frame (EnduraTech; Minnetonka, MN) using modified microvices (McMaster-Carr, Atlanta, Ga) (169). Unconfined stress-relaxation tests were performed at 5% strain incremental steps to a total of 20% strain based on collapsed disc space measurements (~.3 mm). Equilibrium modulus and permeability were calculated by fitting resulting stresses to a poroelastic model (181). In addition, immediately following the previous testing protocol the motion segments were subjected to a second stress-relaxation test, in which the segments were subjected to .04 mm displacement incremental steps to a total of .2 mm displacement. The equilibrium stiffness of the motion segments was calculated from this second test at .16 mm of displacement. Values were also calculated for intact native motion segments and TE-IVD implanted motion segments for comparison.

Results

Mechanical properties indicated that discectomy remnant tissue and motion segments were mechanically dysfunctional compared to the intact native and tissue-engineered implanted motion segments (Figure B.1). The discectomy motion segment equilibrium modulus at 15% strain was ~33% of the intact native and TE-IVD implanted motion segment values (Figure B.1a). The discectomy motion segment hydraulic permeability at 15% strain was ~330% of the intact native and TE-IVD implanted motion segment values (Figure B.1b). Finally, the discectomy motion segment equilibrium stiffness was ~500% of the intact native and TE-IVD implanted motion segment values at .16 mm of displacement (Figure B.1c).

Discussion

This dissertation demonstrated the production of mechanically functional tissue in the disc space following TE-TDR. However, small remnants of tissue remained in the discectomy group (Figure 4.2c, d). It was our goal with these mechanical tests to investigate the mechanical properties of that remnant tissue, as well as determine the overall function of the motion segment in the discectomy groups. These tests would allow us to verify that it was the TE-TDR that was responsible for restoring mechanical function to the disc space and not intrinsic regenerative properties of the disc space.

The two testing protocols were selected to elucidate the mechanical properties of the remnant tissue, as well as assess the overall motion segment mechanical function. The first test was strain matched at 15% strain in the disc space between the discectomy, intact native, and TE-TDR groups. As a result, equilibrium modulus and hydraulic permeability were calculated at .045 mm of displacement, which represented

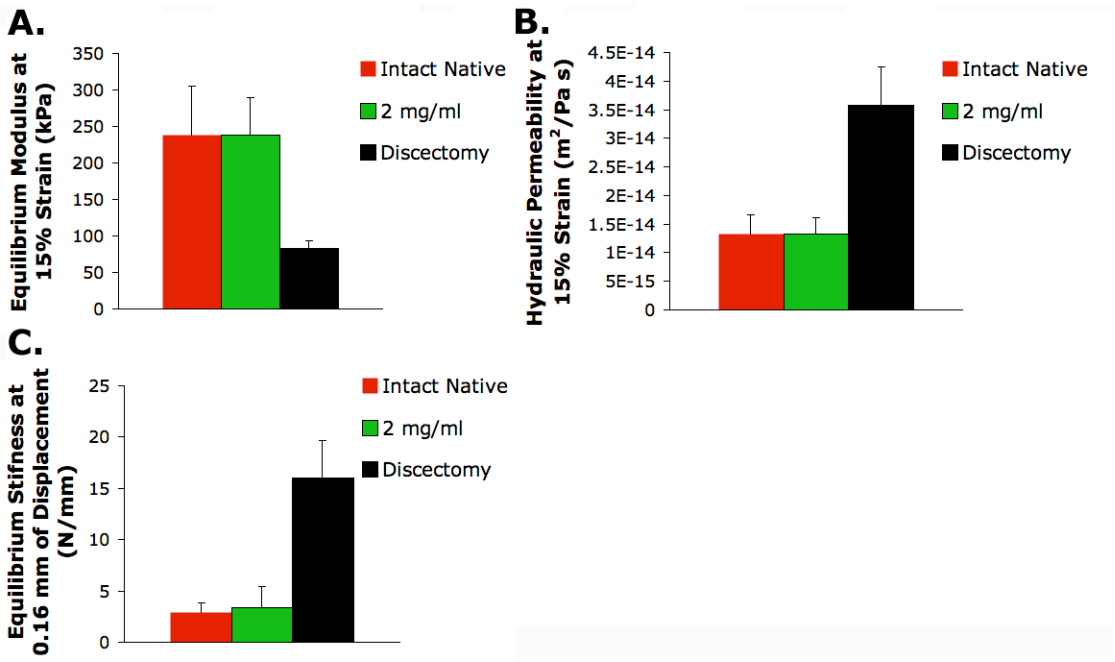

Figure B.1. (A.) Equilibrium modulus and (B.) hydraulic permeability at 15% strain. (C.) Equilibrium stiffness at .16 mm of displacement. (n = 6)

15% strain in the collapsed disc space (~.3 mm) of the discectomy motion segments. These values were calculated at .15 mm of displacement in the intact native and TE-TDR motion segments, which represented 15% strain in the un-collapsed disc spaces (~1 mm). At these displacements and strains, the measured modulus and permeability are predominantly from the tissue in the disc space, due to the modulus differences between bone and cartilaginous tissue (169). The second mechanical testing protocol was chosen to be displacement matched at .16 mm of displacement instead of strain matched between the three groups. This was selected to demonstrate the effects of the collapsed disc space on the mechanical function of the motion segment. In the uncollapsed disc space the strains would be relatively low (~16%), but in the collapsed disc space the strains would be reaching ~50% and should affect the stiffness of the motion segment.

Using these mechanical tests, it was demonstrated that discectomy motion segments were mechanically dysfunctional (Figure B.1). At 15% strain, the modulus of the discectomy group was only ~33% of the native and engineered values while the discectomy permeability was ~3x higher than the native and engineered values. As a result, this data indicates that the small amount of remnant tissue left in the disc space has substantially decreased mechanical integrity compared to native IVD and TE-IVD tissue. In addition, the increased permeability is likely due to the lack of integration observed in the remnant tissue compared to native and engineered IVD (Figure 4.2c, d). Furthermore, the 5 fold increase in equilibrium stiffness of the discectomy group compared to native and TE-TDR groups demonstrated that the loss of disc space resulted in dramatic changes in motion segment mechanical function.

This data demonstrates that the remnant tissue in the disc space has substantially decreased mechanical integrity compared to the native and TE-TDR tissue, but that the loss of disc space ultimately results in a dramatic increase in

stiffness in the motion segment at relatively moderate displacements. Overall, this exhibits that mechanically functional tissue does not form in the disc space by 6 months post discectomy surgery, and the integrated and mechanically functional tissue observed in the TE-TDR experiments are the result of TE-IVD implantation.

Appendix C: MATLAB Code for Determining Alignment in Images

The following code was written in MATLAB to analyze alignment in SHG images using an FFT. However, the code is not limited to SHG images and can be used to analyze alignment in any 512 x 512 image. The code contains the programs, Matrix.m, sumangle.m, and allindex.m Matrix.m is the main program and will call sumangle.m and allindex.m when run. Program currently reads in the image and can handle a stack of images and calculate the alignment index and mode angle for each image. Theory of the technique is covered in Chapter 2 of this dissertation.

Matrix.M

```
clear all


for p=1:1:1
A = imread('Gao.tif',p);
name1 = 'Gao.tif';



%Create Magnitude image(matrix) of FFT

F=fft2(A);
```

```
for i=1:512
   for j=1:512
      M(i,j)=sqrt(real(F(i,j))^2 + imag(F(i,j))^2); %magnitude of FFT
   end
end

rM =M*.01;



for i = 1:256
   for j =1:256
      sM(i+256,j+256)=rM(i,j);
   end
end
for i = 1:256
   for j =257:512
      sM(i+256,j-256)=rM(i,j);
   end
end
for i = 257:512
   for j =1:256
      sM(i-256,j+256)=rM(i,j);
   end
end
for i = 257:512
   for j =257:512
```

```
        sM(i-256,j-256)=rM(i,j);
    end
end

image(sM)

%Contrast Image

for i = 1:512
    for j =1:512
if (sM(i,j)<350)
    sM(i,j) = 0;
end
    end
end

for i = 1:512
    for j =1:512
if (sM(i,j)> 350)
    sM(i,j) = 1000;
end
    end
end

image(sM)
```

```
sumangle; %calls sumangle program

allindex;  % calls allignment index program

W(p,1) = I;
W(p,2) = AI;



name2= strcat(name1,'.csv');



end


csvwrite(name2,W);
%            end
%        end
%    end
```

sumangle.m

```
clear H
clear S

%0 degrees

clear Q
clear a
clear ps1
clear n
clear i
clear j

a = 1;
try
  for n = 1:256
      j = 256;
         for i = 256:1:512


                Q(i,j)=sM(i,j);


      end
```

```
  end
end

ps1 = sum(Q);
H(a) = sum(ps1);

%5 degrees

clear Q
clear a
clear ps1
clear n
clear i
clear j

a = 5;
try
  for n = 1:256
      j = (256 + (1-n));
         for i = (256-((16-a)*(1-n))):1:(266+((16-a)*(n-1)))


                Q(i,j)=sM(i,j);
```

```
        end


    end
end

ps1 = sum(Q);
H(a) = sum(ps1);

%10 degrees
clear Q
clear a
clear ps1
clear n
clear i
clear j


a = 10;
try
    for n = 1:256
        j = (256 + (1-n));
            for i = (256-((16-a)*(1-n))):1:(261+((16-a)*(n-1)))
```

```
                Q(i,j)=sM(i,j);


        end


   end
end

ps1 = sum(Q);
H(a) = sum(ps1);

%15 degrees

clear Q
clear a
clear ps1
clear n
clear i
clear j


a = 15;
try
   for n = 1:256
       j = (256 + (1-n));
```

```
        for i = (256-((19-a)*(1-n))):1:(259+((19-a)*(n-1)))


                Q(i,j)=sM(i,j);


      end


  end
end

ps1 = sum(Q);
H(a) = sum(ps1);

%20 degrees

clear Q
clear a
clear ps1
clear n
clear i
clear j

a = 20;
try
```

```
  for n = 1:256
      j = (256 + (1-n));
          for i = (256-((23-a)*(1-n))):1:(258+((23-a)*(n-1)))


                  Q(i,j)=sM(i,j);


      end


  end
end

ps1 = sum(Q);
H(a) = sum(ps1);

%25 degrees

clear Q
clear a
clear ps1
clear n
clear i
clear j
```

```
a = 25;
try
  for n = 1:256
      j = (256 + (1-n));
         for i = (256-((27-a)*(1-n))):1:(257+((27-a)*(n-1)))


                Q(i,j)=sM(i,j);


      end


  end
end

ps1 = sum(Q);
H(a) = sum(ps1);

%30 degrees

clear Q
clear a
clear ps1
clear n
clear i
```

```
clear j

a = 30;
try
  for n = 1:2:256
      j = (256 + (1-n));
         for i = (256+((34-a)*(((n+1)/2)-1))):1:(259+((34-a)*(((n+1)/2)-1)))


                Q(i,j)=sM(i,j);


      end


  end
end



ps1 = sum(Q);
H(a) = sum(ps1);

%35 degrees

clear Q
```

```
clear a
clear ps1
clear n
clear i
clear j

a = 35;
try
  for n = 1:2:256
      j = (256 + (1-n));
        for i = (256+((38-a)*(((n+1)/2)-1))):1:(258+((38-a)*(((n+1)/2)-1)))


                Q(i,j)=sM(i,j);


      end


  end
end



ps1 = sum(Q);
H(a) = sum(ps1);
```

```
%40 degrees

clear Q
clear a
clear ps1
clear n
clear i
clear j

a = 40;
try
  for n = 1:3:256
      j = (256 + (1-n));
         for i = (256+((44-a)*(((n+2)/3)-1))):1:(259+((44-a)*(((n+2)/3)-1)))


                Q(i,j)=sM(i,j);


      end


  end
end
```

```
ps1 = sum(Q);
H(a) = sum(ps1);

%45 degrees

clear Q
clear a
clear ps1
clear n
clear i
clear j

a = 45;
try
  for n = 1:256
      i = (256 - (1-n));
      j = (256 + (1-n));



                Q(i,j)=sM(i,j);









  end
```

```
end



ps1 = sum(Q);
H(a) = sum(ps1);

%50 degrees

clear Q
clear a
clear ps1
clear n
clear i
clear j

a = 50;
try
  for n = 1:3:256
      i = (256 - (1-n));
         for j = (256-((54-a)*(((n+2)/3)-1))):-1:(253-((54-a)*(((n+2)/3)-1)))



                Q(i,j)=sM(i,j);
```

```
        end


    end
end



ps1 = sum(Q);
H(a) = sum(ps1);

%55 degrees

clear Q
clear a
clear ps1
clear n
clear i
clear j

a = 55;
try
    for n = 1:2:256
        i = (256 - (1-n));
            for j = (256-((58-a)*(((n+1)/2)-1))):-1:(254-((58-a)*(((n+1)/2)-1)))
```

```
                Q(i,j)=sM(i,j);


        end


    end
end



ps1 = sum(Q);
H(a) = sum(ps1);

%60 degrees

clear Q
clear a
clear ps1
clear n
clear i
clear j

a = 60;
```

```
try
  for n = 1:2:256
      i = (256 - (1-n));
        for j = (256-((64-a)*(((n+1)/2)-1))):-1:(253-((64-a)*(((n+1)/2)-1)))


                Q(i,j)=sM(i,j);


      end


  end
end



ps1 = sum(Q);
H(a) = sum(ps1);

%65 degrees

clear Q
clear a
clear ps1
clear n
```

```
clear i
clear j

a = 65;
try
  for n = 1:256
      i = (256 - (1-n));
         for j = (256+((67-a)*(1-n))):-1:(255-((67-a)*(n-1)))



                Q(i,j)=sM(i,j);



      end


  end
end

ps1 = sum(Q);
H(a) = sum(ps1);

%70 degrees

clear Q
clear a
```

```
clear ps1
clear n
clear i
clear j

a = 70;
try
  for n = 1:256
      i = (256 - (1-n));
         for j = (256+((73-a)*(1-n))):-1:(254-((73-a)*(n-1)))


                Q(i,j)=sM(i,j);


      end


  end
end

ps1 = sum(Q);
H(a) = sum(ps1);

%75 degrees
```

```
clear Q
clear a
clear ps1
clear n
clear i
clear j


a = 75;
try
  for n = 1:256
      i = (256 - (1-n));
         for j = (256+((79-a)*(1-n))):-1:(253-((79-a)*(n-1)))


                Q(i,j)=sM(i,j);


      end


  end
end

ps1 = sum(Q);
H(a) = sum(ps1);
```

```
%80 degrees
clear Q
clear a
clear ps1
clear n
clear i
clear j



a = 80;
try
  for n = 1:256
      i = (256 - (1-n));
         for j = (256+((86-a)*(1-n))):-1:(251-((86-a)*(n-1)))



                Q(i,j)=sM(i,j);



      end


  end
end
```

```
ps1 = sum(Q);
H(a) = sum(ps1);



%85 degrees

clear Q
clear a
clear ps1
clear n
clear i
clear j

a = 85;
try
  for n = 1:256
      i = (256 - (1-n));
         for j = (256+((96-a)*(1-n))):-1:(246-((96-a)*(n-1)))



                Q(i,j)=sM(i,j);



      end
```

```
  end
end

ps1 = sum(Q);
H(a) = sum(ps1);




%90 degrees

clear Q
clear a
clear ps1
clear n
clear i
clear j

a = 90;
try
  for n = 1:256
      i = 256;
         for j = 256:-1:1
```

```
                Q(i,j)=sM(i,j);


        end


    end
end

ps1 = sum(Q);
H(a) = sum(ps1)

%95 degrees

clear Q
clear a
clear ps1
clear n
clear i
clear j

a = 95;
try
    for n = 1:256
        i = (256 + (1-n));
            for j = (256+((106-a)*(1-n))):-1:(246-((106-a)*(n-1)))
```

```
                Q(i,j)=sM(i,j);


        end


   end
end

ps1 = sum(Q);
H(a) = sum(ps1);

%100 degrees
clear Q
clear a
clear ps1
clear n
clear i
clear j


a = 100;
try
   for n = 1:256
```

```
        i = (256 + (1-n));
            for j = (256+((106-a)*(1-n))):-1:(251-((106-a)*(n-1)))


                    Q(i,j)=sM(i,j);


        end


    end
end

ps1 = sum(Q);
H(a) = sum(ps1);

%105 degrees

clear Q
clear a
clear ps1
clear n
clear i
clear j
```

```
a = 105;
try
  for n = 1:256
      i = (256 + (1-n));
         for j = (256+((109-a)*(1-n))):-1:(253-((109-a)*(n-1)))


                Q(i,j)=sM(i,j);


      end


  end
end

ps1 = sum(Q);
H(a) = sum(ps1);

%110 degrees

clear Q
```

```
clear a
clear ps1
clear n
clear i
clear j

a = 110;
try
  for n = 1:256
      i = (256 + (1-n));
        for j = (256+((113-a)*(1-n))):-1:(254-((113-a)*(n-1)))


              Q(i,j)=sM(i,j);


      end


  end
end

ps1 = sum(Q);
H(a) = sum(ps1);

%115 degrees
```

```
clear Q
clear a
clear ps1
clear n
clear i
clear j

a = 115;
try
  for n = 1:256
      i = (256 + (1-n));
         for j = (256+((117-a)*(1-n))):-1:(255-((117-a)*(n-1)))


                Q(i,j)=sM(i,j);


      end


  end
end

ps1 = sum(Q);
H(a) = sum(ps1);
```

```
%120 degrees

clear Q
clear a
clear ps1
clear n
clear i
clear j

a = 120;
try
  for n = 1:2:256
      i = (256 + (1-n));
        for j = (256-((124-a)*(((n+1)/2)-1))):-1:(253-((124-a)*(((n+1)/2)-1)))


                Q(i,j)=sM(i,j);


      end
```

```
  end
end



ps1 = sum(Q);
H(a) = sum(ps1);

%125 degrees

clear Q
clear a
clear ps1
clear n
clear i
clear j

a = 125;
try
  for n = 1:2:256
      i = (256 + (1-n));
        for j = (256-((128-a)*(((n+1)/2)-1))):-1:(254-((128-a)*(((n+1)/2)-1)))


                Q(i,j)=sM(i,j);
```

```
        end


    end
end



ps1 = sum(Q);
H(a) = sum(ps1);

%130 degrees

clear Q
clear a
clear ps1
clear n
clear i
clear j

a = 130;
try
    for n = 1:3:256
        i = (256 + (1-n));
            for j = (256-((134-a)*(((n+2)/3)-1))):-1:(253-((134-a)*(((n+2)/3)-1)))
```

```
                Q(i,j)=sM(i,j);


        end


    end
end



ps1 = sum(Q);
H(a) = sum(ps1);

%135 degrees

clear Q
clear a
clear ps1
clear n
clear i
clear j

a = 135;
```

```
try
  for n = 1:256
      i = (256 + (1-n));
      j = (256 + (1-n));


                Q(i,j)=sM(i,j);




  end
end



ps1 = sum(Q);
H(a) = sum(ps1)

%140 degrees

clear Q
clear a
clear ps1
```

```
clear n
clear i
clear j

a = 140;
try
  for n = 1:3:256
      j = (256 + (1-n));
         for i = (256-((144-a)*(((n+2)/3)-1))):-1:(253-((144-a)*(((n+2)/3)-1)))


                Q(i,j)=sM(i,j);


      end


  end
end

ps1 = sum(Q);
H(a) = sum(ps1);

%145 degrees

clear Q
```

```
clear a
clear ps1
clear n
clear i
clear j

a = 145;
try
  for n = 1:2:256
      j = (256 + (1-n));
         for i = (256-((148-a)*(((n+1)/2)-1))):-1:(254-((148-a)*(((n+1)/2)-1)))


                Q(i,j)=sM(i,j);


      end


  end
end



ps1 = sum(Q);
H(a) = sum(ps1);
```

```
%150 degrees

clear Q
clear a
clear ps1
clear n
clear i
clear j

a = 150;
try
  for n = 1:2:256
      j = (256 + (1-n));
         for i = (256-((154-a)*(((n+1)/2)-1))):-1:(253-((154-a)*(((n+1)/2)-1)))


                Q(i,j)=sM(i,j);


      end


  end
end
```

```
ps1 = sum(Q);
H(a) = sum(ps1);

%155 degrees

clear Q
clear a
clear ps1
clear n
clear i
clear j

a = 155;
try
  for n = 1:256
      j = (256 + (1-n));
         for i = (256+((157-a)*(1-n))):-1:(255-((157-a)*(n-1)))


                Q(i,j)=sM(i,j);


      end
```

```
  end
end

ps1 = sum(Q);
H(a) = sum(ps1);

%160 degrees

clear Q
clear a
clear ps1
clear n
clear i
clear j

a = 160;
try
  for n = 1:256
      j = (256 + (1-n));
         for i = (256+((163-a)*(1-n))):-1:(254-((163-a)*(n-1)))



                Q(i,j)=sM(i,j);
```

```
        end



    end
end

ps1 = sum(Q);
H(a) = sum(ps1);

%165 degrees

clear Q
clear a
clear ps1
clear n
clear i
clear j



a = 165;
try
    for n = 1:256
        j = (256 + (1-n));
            for i = (256+((169-a)*(1-n))):-1:(253-((169-a)*(n-1)))
```

```
                Q(i,j)=sM(i,j);


        end


    end
end

ps1 = sum(Q);
H(a) = sum(ps1);

%170 degrees
clear Q
clear a
clear ps1
clear n
clear i
clear j


a = 170;
try
    for n = 1:256
        j = (256 + (1-n));
            for i = (256+((176-a)*(1-n))):-1:(251-((176-a)*(n-1)))
```

```
                Q(i,j)=sM(i,j);


        end


   end
end

ps1 = sum(Q);
H(a) = sum(ps1);

%175 degrees

clear Q
clear a
clear ps1
clear n
clear i
clear j

a = 175;
try
   for n = 1:256
```

```
        j = (256 + (1-n));
            for i = (256+((186-a)*(1-n))):-1:(246-((186-a)*(n-1)))


                    Q(i,j)=sM(i,j);


        end


    end
end

ps1 = sum(Q);
H(a) = sum(ps1);

[Z,L] =
min([H(1),H(5),H(10),H(15),H(20),H(25),H(30),H(35),H(40),H(45),H(50),H(55),H(6
0),H(70),H(75),H(80),H(85),H(90),H(95),H(100),H(105),H(110),H(115),H(120),H(12
5),H(130),H(135),H(140),H(145),H(150),H(155),H(160),H(165),H(170),H(175)]);;

for a = 1:1:175
S(a) = H(a) - 0;
end

% for a = 1:1:1
```

```
%     S(a) = H(a) - Z;
% end

plot(S);
```

allindex.m

```
[C,I] = max(S);



%summing within 20 degrees in both directions of maximum alligned fiber

if ((I>20) && (I<160))
   sr = sum([S(I),S(I+5),S(I+10),S(I+15),S(I+20),S(I-5),S(I-10),S(I-15),S(I-20)]);

elseif (I == 20)
   sr = sum([S(10),S(15),S(20),S(25),S(30),S(5),S(1),S(35),S(40)]);
elseif (I == 15)
   sr = sum([S(10),S(15),S(20),S(25),S(30),S(35),S(5),S(1),S(175),]);
elseif (I == 10)
   sr = sum([S(10),S(15),S(20),S(25),S(30),S(5),S(1),S(175),S(170)]);
elseif (I==5)
   sr = sum([S(5),S(10),S(15),S(20),S(25),S(1),S(175),S(170),S(165)]);
elseif (I==1)
   sr = sum([S(1),S(5),S(10),S(15),S(20),S(175),S(170),S(165),S(160)]);
```

```
elseif (I==175)
   sr = sum([S(175),S(1),S(5),S(10),S(15),S(170),S(165),S(160),S(155)]);
elseif (I==170)
   sr = sum([S(170),S(175),S(1),S(5),S(10),S(165),S(160),S(155),S(150)]);
elseif (I==165)
   sr = sum([S(170),S(175),S(1),S(5),S(145),S(165),S(160),S(155),S(150)]);
elseif (I==160)
   sr = sum([S(170),S(175),S(1),S(145),S(140),S(165),S(160),S(155),S(150)]);
end

sall = sum(S);

fracall = (sr/sall);

AI = (fracall/.22)
```

Appendix D: Curriculum Developed for GK-12 Program on Tissue Engineering and Ionic Bonding

This curriculum was developed for the GK-12 program and accompanies Chapter 6 of this dissertation.

Tissue Engineering and Ionic Bonding

Authors: Robby Bowles and Jamie Saroka

Date Created: 12/4/10

Subject: Chemistry (Bonding, Tissue Engineering)

Level: High School

Standards

Teaching Standards

A. Standard A - Teachers of science plan an **inquiry-based** science program for their students

B. Standard B - Encourage and model the skills of scientific inquiry, as well as the curiosity, openness to new ideas and data, and skepticism that characterize science

C. Standard C – Teachers of science engage in ongoing assessment of their teaching and of student learning

D. Standard D – Teachers of science design and manage learning environments that provide students with the time, space, and resources needed for learning science.

E. Standard E – Teachers of science develop communities of science learners that reflect the intellectual rigor of scientific inquiry and the attitudes and social values conducive to science learning

Content Standards

A. Standard A – Abilities necessary to do and understand scientific inquiry
B. Standard B – As a result of their activities in grades 9-12, all students should develop an understanding of structure and properties of matter and chemical reactions (specifically bonding)
C. Standard C - As a result of their activities in grades 9-12, all students should develop an understanding of the cell.
D. Standard E - As a result of their activities in grades 9-12, all students should develop an understanding of abilities of technological design and understandings about science and technology
E. Standard G - As a result of their activities in grades 9-12, all students should develop an understanding of science as a human endeavor.

Objectives

Curriculum will teach students about ionic bonding by relating it to key tissue engineering principles and allowing them to experience ionic bonding through an inquiry based laboratory using alginate gel, a common tissue-engineering scaffold.

Students Will

Be able to state the three main components used in Tissue Engineering
Be able to state the advantages of tissue engineering over traditional treatments
Be able to state why Tissue engineering is needed
Be able to carry on an everyday conversation about tissue engineering
Be able to define ionic bonding

Be able to state that ionic bond formation causes gelation of alginate

Be able to describe how model based inquiry is carried out in laboratories

Vocabulary

Ionic Bond

Tissue Engineering

Cell

Scaffold

Cell Signaling

Biomedical Engineering

Alginate

Gel

Cation

Monovalent

Divalent

Extracellular matrix (ECM)

Materials

For Each Group:

Dry Activity

-12 toothpicks

-8 water soluble packing peanuts

-Bucket filled with water

-Styrofoam ball

-modeling clay

Inquiry Activity

- 30 ml 2% $CaCl_2$
- 30 ml 2% NaCl
- 30 ml 2% alginate
- red food coloring
- yellow food coloring
- blue food coloring
- 8 30 ml free standing conical tubes
- 3 transfer pipettes

Safety

Safety concerns are minimal within this lab exercise; however, students should be required to wear eye protection to promote proper lab safety protocol.

<u>Science Content for the Teacher</u>:

Tissue Engineering Content:

Tissue engineering is the production of novel living tissue using three main essential components: cells, scaffolding, and cell signaling. By producing these engineered tissues, one can implant and replace diseased or injured tissues. The act of creating novel engineered tissues is advantageous for three main reasons. First, traditional transplantation surgeries (e.g. kidney and heart transplants) can often have

dramatic effects on saving and improving the quality of life of those receiving the transplants. Unfortunately, there simply are not enough transplants to go around and waiting lists for life saving organs are incredibly long. In fact, every 30 seconds someone dies from a condition that could have been treated by tissue engineering. By creating and growing new tissues, the supply problem can be solved.

Furthermore, often those receiving transplantations have to go on immune suppressing drugs that have some very undesirable side effects. Tissue engineering provides an avenue in which the tissues can be grown with the patient's own cells, and thus, will not trigger an immune response. This eliminates the need for the patient to go on immunosuppressant drugs. Finally, tissue engineering provides an advantage over traditional polymer/metal implants (e.g. hip and knee replacements) by producing living and biocompatible tissues. Metal and polymer implants suffer from poor biocompatibility and mechanical failure. Tissue engineered tissues are made up of materials (cells, proteins, lipids, and carbohydrates) the body is familiar with and thus are quite biocompatible. The cellular component provides the advantage of having a self-repair mechanism that is not present in polymer/metal implants. Thus, tissue engineered tissues will last longer than traditional implant materials. Overall, it is for these main reasons that tissue engineering has become an active field of investigation in the scientific and engineering worlds.

The students will learn the three main tools/concepts of tissue engineering and what their role is in tissue engineering. The three main components of tissue engineering are the cells, the scaffold, and the cell signals. Tissue engineering is the combination of those three components in order to create tissue to replace damaged tissue caused by trauma or disease. Each of these components has a specific role in the artificial construct.

The central dogma behind tissue engineering is that cells are placed on a biodegradable "scaffold". This scaffold is usually in the shape of the tissue to be created. Over time the cell will produce proteins, lipids, and carbohydrates that will make up the "extracellular matrix". This is simply the material that is surrounding the cells. As the cells produce the extracellular matrix, the biodegradable scaffold will be degraded and the cell produced extracellular matrix will take its place resulting in a completely cell produced tissue with no synthetic aspects.

The cells are what provide the tissue with the "living" component. This allows the tissue to respond to trauma experienced during normal wear and tear that tissues undergo. Current synthetic implants made of plastics and metals are subject to wear and fatigue leading to failure of the implants. When these implants are damaged they cannot repair themselves. So by creating a living implant, these tissues can respond to these traumas and self-repair, giving it the possibility to last longer than synthetic implants. Cells also provide the tissue with their function. For example, in cartilage the proteins and proteoglycans the cells produce provide the tissue with their mechanical properties. In other tissue such as the pancreas, the cells produce the protein insulin providing the pancreas with its function. As can be seen, the cell plays a vital role in the development of tissue-engineered tissues with the desired properties.

The scaffold provides the support and shape of the tissue. The scaffold provides a place for the cells to attach and develop on. One analogy that can be used: the scaffold is the framework of a house. You put up the framework for the shape of the house you want and then build upon that framework. This is essentially how the cells utilize this framework. A very important aspect of most scaffolds used in tissue engineering is that they are biodegradable. They will be broken down inside the body. This is important because the main goal of tissue engineering is to create a tissue with non-synthetic materials but with a composition of proteins, lipids and carbohydrates

mimicking the natural tissue. So this original scaffold must be broken down for the extracellular matrix to take its place.

The signals provide the instructions to the cells. Once the cells are seeded in a scaffold they must produce the proteins that are appropriate to form the tissue desired. As a result, tissue engineering attempts to use signals that the cell sees in its natural environment. These signals can include hormones, growth factors, and mechanical signals. Tissue engineers attempt to harness these signals to control the growth and development of the new tissue.

Chemistry Content:

We will use one of the main tools of tissue engineering, scaffolds, to both teach the student about tissue engineering while also teaching them about ionic bonding. Alginate is a common scaffold used in cartilage tissue engineering. Alginate is an anionic polysaccharide obtained from brown algae with some very favorable properties for tissue engineering. (On a side note, alginate is used in a very prominent fast food restaurant's shakes as a thickener. The reason they do not call them milkshakes is because they do not contain milk, but contain alginate instead. The students usually enjoy this anecdote.) Often you hope to be able to trap cells within your scaffold. Alginate makes this process very easy. First off, alginate is non-cytotoxic (i.e. does not kill cells) and cells can be encapsulated into the alginate without deleteriously affecting the cells. The property of alginate that is most useful to the tissue engineer is its ability to gel. A solution of alginate can be mixed with a Ca++ solution and a gel will be formed. In addition, you can mix in cells before adding the Ca++ in order to encapsulate the cells within the scaffold.

The key to alginate gel formation is the anionic nature of the alginate. By adding a divalent cation, ionic crosslinks are formed between the chains of alginate. As a

result, the solution forms a gel after crosslinking. Of importance is the divalent nature of the cation. This divalent state allows ionic bonds to form between 2 chains of alginate to form the crosslinks, while a monovalent cation will only form an ionic bond with a single chain and fail to form crosslinks (Figure D.1). Thus, divalent cations produce gels when mixed with alginate and monovalent cations do not.

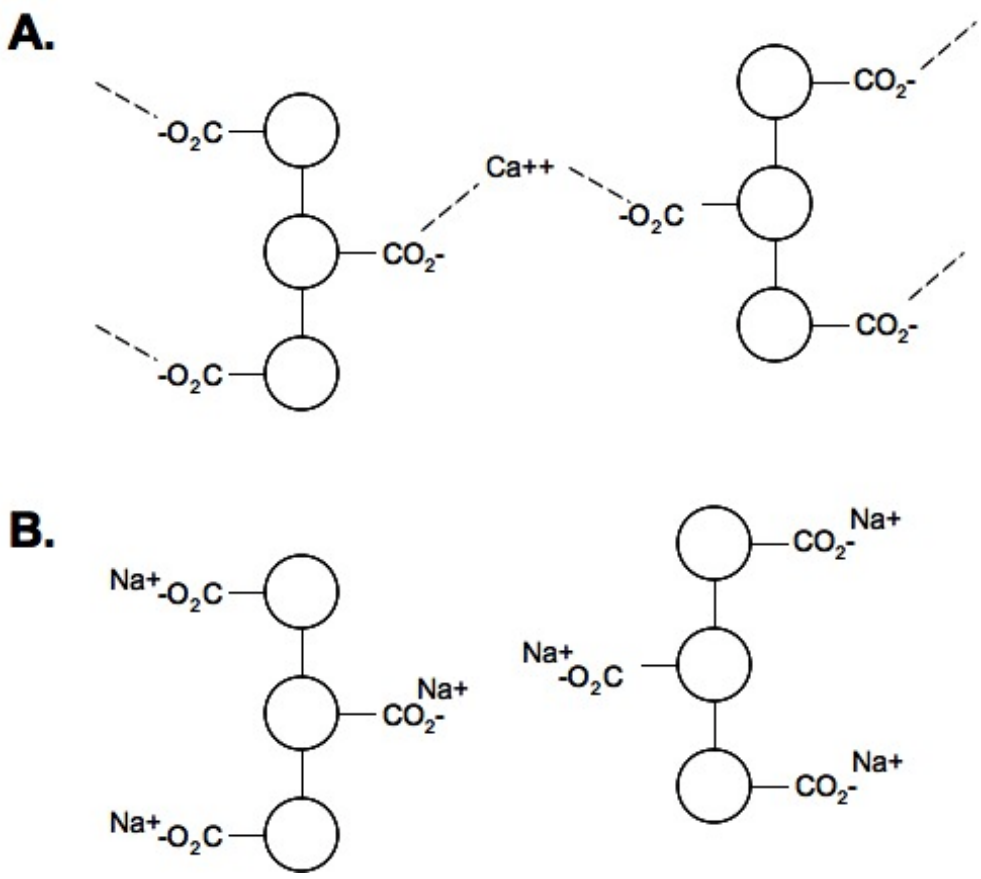

Figure D.1. (A.) Alginate chains crosslinked by Ca++. (B.) Alginate chains with Na+ but not crosslinked.

We will take advantage of alginate's ability to form gels and the different way alginate reacts with monovalent and divalent cations to teach students how bonding affects material properties and how the valence state affects this bonding. The

advantage of using alginate for this activity is that it gives students a visual and tactile representation of bond (ionic) formation when the solution turns into a solid. Secondly, it allows them to begin to understand the difference between monovalent and divalent ions and how that affects bond formation.

Preparation:

Dry Activity: A list of materials was provided on page 2 of this document (Figure D.2). The teacher will need to distribute the materials at the appropriate number of workstations as well as provide the students with handout #1. The students will be working through the handout during the activity.

Figure D.2 Dry Activity Supplies

Inquiry Activity: A list of materials was provided on page 2 of this document (Figure D.3). The teacher will need to mix 30 ml of alginate for each group at 2% (w/v) (20 mg/ml) in distilled water. This is best done with a stir bar and magnetic stirring plate. You will want to mix in the alginate slowly to avoid clumping. Mixing will often take over 2 hours and is usually best done overnight to ensure mixing before class. After mixing, add blue food dye to alginate solution. The teacher will also need to mix 30 ml of $CaCl_2$ (2% w/v) (20 mg/ml) in distilled water. The solution will be oversaturated so you will see particles in the solution. This is expected, students will just want to shake solution before using to evenly mix. After making solution, add yellow food dye to $CaCl_2$ solution. Finally, teacher will need to mix 2% w/v (20 mg/ml) NaCl solution in distilled water. After mixing add red food dye to NaCl solution.

30 ml of each solution should be distributed in 30 ml freestanding conical tubes. In addition, each group should have 5 additional freestanding 30 ml conical tubes. Also, distribute 3 transfer pipettes per group. Finally, provide students with Handout #2 and #3. The students will be working through the handout during the activity.

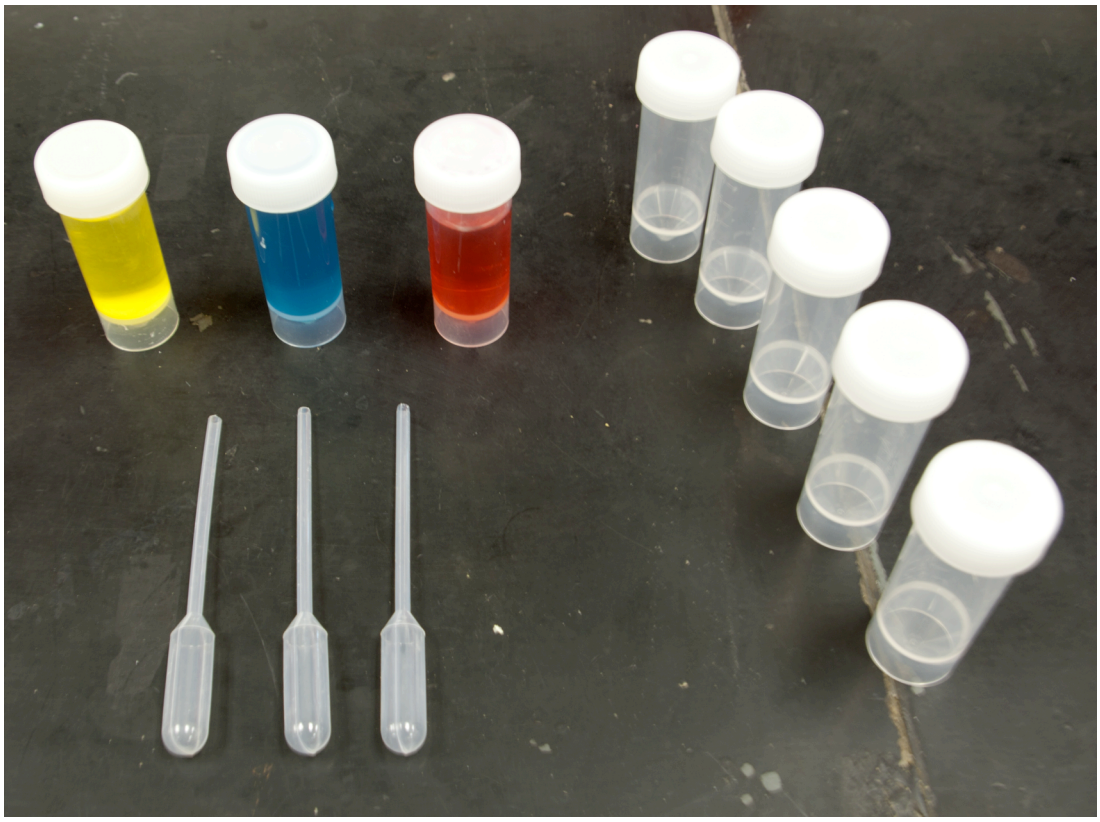

Figure D.3. Inquiry activity supplies

Handout #1 (answers in red)

Tissue Engineering Model

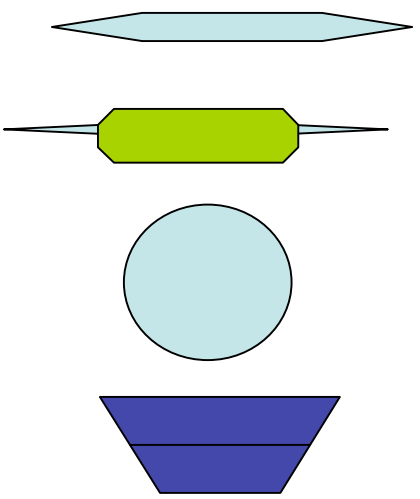

= ECM (structural protein)

= Scaffold

= Cell

= Body Environment (enzymes, signaling molecules, H20)

1. What three components were needed to produce the Tissue Engineered tissue?

   a. _____Cells

   b. _____Scaffold

   c.._____Cell signaling or signaling molecules is acceptable

2. What happened to the scaffold? What implication does that have on the body it is implanted into? Scaffold degraded. Scaffolding needs to be biocompatible so that it doesn't cause damage to the body once degraded and free inside the body.

3. What is the scaffold replaced by? What importance do you think the cell has in this role? Scaffold is replaced by ECM. The cell produces the ECM.

4. What would be the advantage of having an implant made of living tissue produced by cells rather than a man-made material? Answers including self-repair and biocompatibility are acceptable.

5. When would such an implant be required. What types of concerns would need to be considered in developing such an implant? Answers including tissue disease or injury when suitable replacement not available is acceptable. Any answer that demonstrates that the student is thinking that the scaffold properties, type of cell, and type of signaling molecules are important would be acceptable.

Handout #2

What We know…

Alginate (blue)

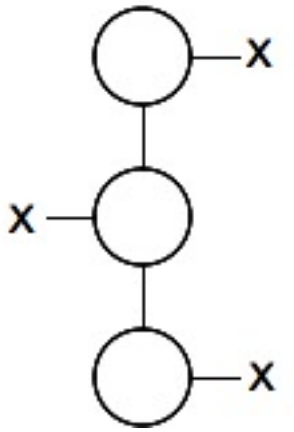

Monovalent Solution (red)

+M

Divalent Solution (yellow)

+D+

Handout #3

Investigation… (Tissue Engineering)! Name: _____

What do you know…

Develop a model for what you think will happen when mixed…

Plan an experiment to test the model…

Data:

Interpret the data…

Does your initial model need to be modified? Do you need more testing?

Classroom Procedure:

DAY 1

Teacher should cover powerpoint slides 1-8 through the "toothpicks and tissue engineering" slide. After completing slides, teacher should do "Dry Activity" discussed below.

Dry Activity: Teacher should briefly go over the key diagram at the top of handout #1. Explaining that the toothpick alone represents extracellular matrix, the toothpick with packing peanut on it represents the scaffold, the Styrofoam ball represents the cell, and the bucket full of water represents the body environment. The teacher will want to demonstrate the construction of the scaffold with cell as illustrated below in Figure D.4. The students should be instructed to place the construct into the water and observe what happens and answer the questions on the handout accordingly. (What should happen is the packing peanuts will dissolve off of the toothpicks leaving only the toothpicks. This represents the scaffold degrading and being replaced by ECM.) At the completion of the class, if you have time, go over the handout with the students. (Answers are provided in red on the handout).

Figure D.3. Constructed dry activity construct with cell.

DAY 2

Teacher should cover powerpoint slides 9-16. These slides focus on scaffolds and their properties. The final slide asks "what properties do we want in a scaffold", use this slide and time to engage in a discussion on what the students think would be important in the design of a scaffold. Try to encourage the students to engage with each other on the topic. *This day is the most boring for the students since it involves only lecturing. Attempt to engage the class as much as possible and feel free to adjust the lecture to make it as interactive as possible.

DAY 3

Inquiry Activity: This activity is inquiry based and limited instruction should be given to the students. Students are provided with the information that the red solution contains a monovalent cation, the yellow solution contains a divalent cation, and the blue solution is alginate. In addition, they are provided with the generalized structure of alginate with an "x" in place of the carboxyl - group. The students are told that they are going to be using the information and supplies provided to determine the properties of the "x" group by mixing the solutions.

The teacher should then cover the steps of model-based inquiry to the students that they are too follow in their experiments. (1.) Those steps first involve making observations about the solutions, which includes both visual observations and thinking about the information provided to them. (2.) Then the students should develop a model/hypothesis for what will happen when they mix the solutions. Force the students to be as specific as possible. (3.) Once a model is developed they should develop an experiment to test their model and (4.) The students then carry out their experiment while collecting whatever data they deem appropriate. (5.) Next they should interpret their data in terms of their model. (Is it correct, wrong, need adjustments?) (6.) Have them make those changes to the model and think about what would be next to test in their model. The important concept here is to emphasize the model-based and iterative nature of science. We make models, we test them, we adjust the models, we continue.

Most students decide to mix each possible combination of solutions to see what happens. It is advantageous to the students if they develop a specific model before doing this experiment. The provided alginate chain structure will help in the

development of this model. It is important to note that students will be hesitant that their model is incorrect. This provides a great opportunity to explain to the students that scientific models are often wrong, and that is why the experiments are carried out to test each model. The students will observe during their experimentation that the blue and yellow solutions form a gel when mixed, the blue and red do nothing observable, as do the yellow and red. The students often note a color change, but may have to be redirected back to the model. "Does a color change support or disprove your model?"

There are two main conclusions we hope the students reach and can be lightly guided if need be (the less guidance the better). The first conclusion is that the alginate "x" group is negatively charged. The negative charge is why the yellow and blue solutions gel when mixed by forming ionic bonds between the alginate chains. This conclusion provides a visual and tactile representation of how the formation of bonds can affect material properties. Most students come to this conclusion from their experimentation and analysis.

The second conclusion, based on the negative charge of alginate, is more advanced, but students are able to come to it if forced to think about it. Alginate forms a gel with the divalent cation solution because the divalent cation provides a plus two charge that can form ionic bonds with two minus one charges of the "x" groups of alginate and form bridges (crosslinks) between these chains of alginate (Figure D.1a). On the other hand, the monovalent cation only has a plus one charge and therefore can't bridge two chains of alginate (Figure D.1b). The question you hope they ask is, "why does it gel with the divalent cation but not the monovalent cation?" Asking this question will start the students down the right path. If deemed appropriate, the teacher can provide this information to them after they struggle with it. Another hint that the teacher can provide late in this exercise is to draw the Lewis dot diagram for a divalent

cation. This can help them to see that there are two positive charges available to form a bridge between 2 strands of alginate that have negative charges.

These two conclusions are the most useful in relating the scaffold formation and tissue engineering to ionic bonding. The student's final model will ideally resemble figure D.1. Most students will naturally move in this direction and the teacher will naturally nudge them in this direction; however, these are not the only directions the students can go. The important aspect is that the students develop a model, test it through experimentation, analyze it, adjust their model, and plan for future experiments. This allows them to experience science as it is carried out every day in the laboratory. It is important that the students fill out their handouts as they carry out their experiments. The teacher can explain to them the handout is like their "lab notebook" and discuss how these notebooks are used in the lab to write down everything they do so they have a record of their experiments and thinking.

DAY 4

The students should be asked to prepare and present their findings as a group to the class. Explain that this is an important aspect of science in order to educate others of your findings.

Assessment:

The following rubric can be used to assess students for each part of the inquiry activity. The term "expectations" here refers to the content, process and attitudinal goals for this activity. Evidence for understanding may be in the form of oral as well as written communication, both with the teacher as well as observed communication with other students. Specifics are listed in the table below.

1= exceeds expectations

2= meets expectations consistently

3= meets expectations occasionally

4= not meeting expectations

	Model	Experiment	Analyze and adjust model	Future Directions
1				
2				
3				
4				

In addition, the following 2 essay assignments can be assigned to the students. The first distributed after Day 1 and the second after the completion of Day 4. When distributing the second essay, ask them to expand on their answer from the original essay in context of what they have learned.

Essay #1

Name: _____ Class: ____ Date:_____

Using a **minimum** of 5 sentences, write about what you could do. Include how chemistry is involved, specifically bonding and tissue engineering…

You live in a small development in a small rural school district. Your neighbor, a real close friend of yours, was riding her bike without a helmet. She crashed and tore off most of her ear. In the mêlée of emergency crews, the pieces were lost or so badly shredded that they could not be reattached. She will have minimal scarring on the side of her face, thanks to the way she hit the pavement. However, that is nothing compared to the embarrassment of not having an ear. Her parents know you are a scientist, and the family is pleading with you to help her any way you can…

Essay #2

Name: _____ Class: ____ Date: _____

Using a **minimum** of 5 sentences, respond to your neighbor informing them about what you have developed in your lab. You will be able to help their daughter! Include how chemistry is involved, specifically bonding and tissue engineering…

(***Note*** - You know much more than you did at the start of the week. Do not think you can write the same answer that you did for the first assignment and get full credit. Try to be specific in your response.)

Supplemental Information:

Please download associated powerpoint found on the website www.climb.bme.cornell.edu . The powerpoint has notes on each slide and how to present them.

Acknowledgments:

We would like to thank the Cornell BME NSF GK-12 program: DGE 0841291. I (Robby Bowles) would like to personally thank my coauthor for his invaluable input and patience in the development of this curriculum.

Appendix E: Creation of Multi-Lamellae AF Using Contracted Collagen Gels

Methods: Polyethylene cores were placed in the center of each well of a 12 well plate. Ovine AF cells were seeded at 1 x 10^6 cells/ml in a 1 mg/ml type I collagen gel that was gelled around the polyethylene core (protocol presented in Chapter 2). Constructs were cultured for 2 days in previously described media (Chapter 2). After 2 days of culture, sell seeded collagen gel was once again poured and gelled around the construct to produce second lamella. Constructs were cultured for an additional 2 days. On day 4 of culture, sell seeded collagen gel was once again poured and gelled around the construct to produce third lamella. Constructs were cultured for 2 more days before being photographed at day 6.

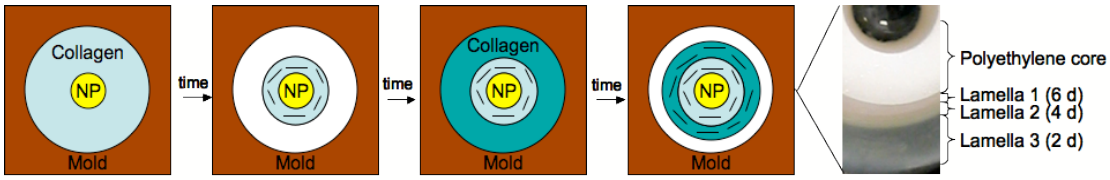

Figure E.3 – Creation of multi-lamellae AF

Results/Discussion: Technique produced annular gel with 3 distinct lamellae (figure E.1). The first and second lamellae reached equilibrium in size by day 6 after being cultured for 6 days and 4 days respectively. The third lamellae had not finished contracting since it had only been cultured for 2 days. Increasing the culture time would produce an AF with 3 equally thick lamellae. This technique of contracting multiple collagen gels around an inner core can be utilized to create TE-IVD with multi-lamellae AF.

Appendix F: Regional Shear Properties of Tissue Engineered AF

Materials and Methods: IVD tissue was harvested from the lumbar discs of a year old sheep. Annulus fibrosus cells were isolated from harvested tissues using 0.3% collagenase and grown in culture to passage 1 by established protocols (93). Collagen type I extracted from rat tail tendons was used to make 1.5 mg/ml annular gels by seeding AF cells at a final density of 1x106 cells/ml. Cell seeded gels were cultured in F12 media supplemented with 10% FBS, 100 IU/ml penicillin, 100 μg/ml streptomycin, and 25 μg/ml ascorbic acid for 0 to 3 days. 1 ml of solution was pipetted into a 6 well plate (3.5 cm OD) with inner porous polyethylene core (1 cm ID). Cells were dyed with CFDA dye prior to gel formation. Gels were contracted for 0 and 1 days. Gels were imaged using SHG microscopy across width of gel and collagen alignment was analyzed using previously described FFT technique (Chapter 2). Gels were then placed on specially designed shearing device mounted on a confocal microscope (201). 10% shear strain was applied to gels and cells were tracked using PIV software written in MATLAB. A map of the local displacements and normalized shear modulus was calculated across the width of the gel.

Results: The 3.5 cm OD annular gels showed heterogeneity in the degree of circumferential alignment across the width of the gel after 1 day of contraction (Fig. F.1). Day 0 gels showed minimal alignment across the entire width, while Day 1 gels showed enhanced alignment primarily localized to the outer boundary. Similarly the modulus of Day 0 gels did not vary across the width, while Day 1 samples were 5-10 fold higher at the inner boundary compared to the middle.

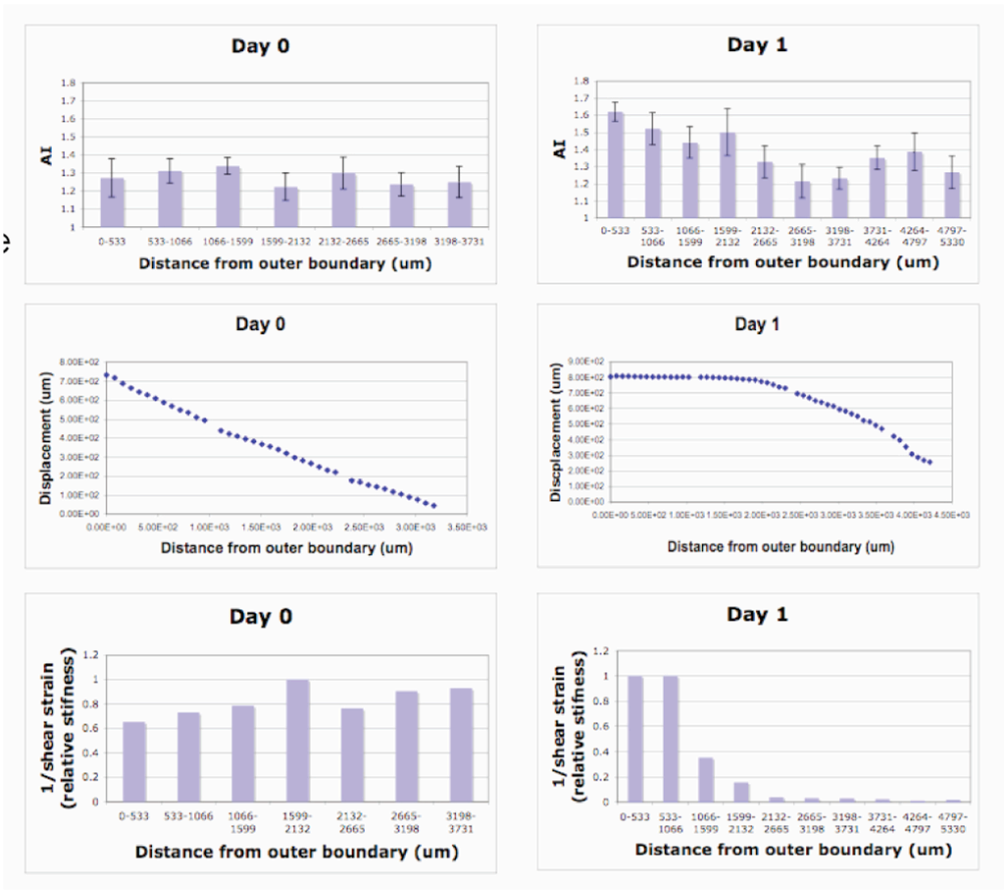

Figure F.1 - Alignment across width of contracted 3.5 cm OD gel and corresponding displacements and shear modulus across width for Day 0 and Day 1.

Discussion: This data indicates profound local structural and mechanical variations in these gels on the scale of 500 μm. Controlling these local variations of structure and properties may be critical to engineering a functional IVD replacement.

References:

1. Diwan, A.D., Parvataneni, H.K., Khan, S.N., Sandhu, H.S., Girardi, F.P., and Cammisa, F.P., Jr. Current concepts in intervertebral disc restoration. The Orthopedic clinics of North America 31, 453, 2000.

2. Aota, Y., Onari, K., An, H.S., and Yoshikawa, K. Dorsal root ganglia morphologic features in patients with herniation of the nucleus pulposus: assessment using magnetic resonance myelography and clinical correlation. Spine (Phila Pa 1976) 26, 2125, 2001.

3. Lotz, J.C., and Ulrich, J.A. Innervation, inflammation, and hypermobility may characterize pathologic disc degeneration: review of animal model data. The Journal of bone and joint surgery 88 Suppl 2, 76, 2006.

4. Shamji, M.F., Allen, K.D., So, S., Jing, L., Adams, S.B., Jr., Schuh, R., Huebner, J., Kraus, V.B., Friedman, A.H., Setton, L.A., and Richardson, W.J. Gait abnormalities and inflammatory cytokines in an autologous nucleus pulposus model of radiculopathy. Spine (Phila Pa 1976) 34, 648, 2009.

5. Nelson, M.A. A long-term review of posterior fusion of the lumbar spine. Proceedings of the Royal Society of Medicine 61, 558, 1968.

6. Ahlmann, E., Patzakis, M., Roidis, N., Shepherd, L., and Holtom, P. Comparison of anterior and posterior iliac crest bone grafts in terms of harvest-site morbidity and functional outcomes. The Journal of bone and joint surgery 84-A, 716, 2002.

7. Silber, J.S., Anderson, D.G., Daffner, S.D., Brislin, B.T., Leland, J.M., Hilibrand, A.S., Vaccaro, A.R., and Albert, T.J. Donor site morbidity after anterior iliac crest bone harvest for single-level anterior cervical discectomy and fusion. Spine (Phila Pa 1976) 28, 134, 2003.

8. Jorgenson, S.S., Lowe, T.G., France, J., and Sabin, J. A prospective analysis of autograft versus allograft in posterolateral lumbar fusion in the same patient. A minimum of 1-year follow-up in 144 patients. Spine (Phila Pa 1976) 19, 2048, 1994.

9. An, H.S., Lynch, K., and Toth, J. Prospective comparison of autograft vs. allograft for adult posterolateral lumbar spine fusion: differences among freeze-dried, frozen, and mixed grafts. Journal of spinal disorders 8, 131, 1995.

10. Zhang, Z.H., Yin, H., Yang, K., Zhang, T., Dong, F., Dang, G., Lou, S.Q., and Cai, Q. Anterior intervertebral disc excision and bone grafting in cervical spondylotic myelopathy. Spine (Phila Pa 1976) 8, 16, 1983.

11. Tsuang, Y.H., Yang, R.S., Chen, P.Q., and Liu, T.K. Experimental allograft in spinal fusion in dogs. Taiwan yi xue hui za zhi 88, 989, 1989.

12. McLain, R.F., Fleming, J.E., Boehm, C.A., and Muschler, G.F. Aspiration of osteoprogenitor cells for augmenting spinal fusion: comparison of progenitor cell concentrations from the vertebral body and iliac crest. The Journal of bone and joint surgery 87, 2655, 2005.

13. Korovessis, P., Koureas, G., Zacharatos, S., Papazisis, Z., and Lambiris, E. Correlative radiological, self-assessment and clinical analysis of evolution in instrumented dorsal and lateral fusion for degenerative lumbar spine disease. Autograft versus coralline hydroxyapatite. Eur Spine J 14, 630, 2005.

14. Ransford, A.O., Morley, T., Edgar, M.A., Webb, P., Passuti, N., Chopin, D., Morin, C., Michel, F., Garin, C., and Pries, D. Synthetic porous ceramic compared with autograft in scoliosis surgery. A prospective, randomized study of 341 patients. J Bone Joint Surg Br 80, 13, 1998.

15. Chen, W.J., Tsai, T.T., Chen, L.H., Niu, C.C., Lai, P.L., Fu, T.S., and McCarthy, K. The fusion rate of calcium sulfate with local autograft bone compared with autologous iliac bone graft for instrumented short-segment spinal fusion. Spine (Phila Pa 1976) 30, 2293, 2005.

16. Boden, S.D., Kang, J., Sandhu, H., and Heller, J.G. Use of recombinant human bone morphogenetic protein-2 to achieve posterolateral lumbar spine fusion in humans: a prospective, randomized clinical pilot trial: 2002 Volvo Award in clinical studies. Spine (Phila Pa 1976) 27, 2662, 2002.

17. Dimar, J.R., Glassman, S.D., Burkus, K.J., and Carreon, L.Y. Clinical outcomes and fusion success at 2 years of single-level instrumented posterolateral

fusions with recombinant human bone morphogenetic protein-2/compression resistant matrix versus iliac crest bone graft. Spine (Phila Pa 1976) 31, 2534, 2006.

18. Boden, S.D., Zdeblick, T.A., Sandhu, H.S., and Heim, S.E. The use of rhBMP-2 in interbody fusion cages. Definitive evidence of osteoinduction in humans: a preliminary report. Spine (Phila Pa 1976) 25, 376, 2000.

19. Johnsson, R., Stromqvist, B., and Aspenberg, P. Randomized radiostereometric study comparing osteogenic protein-1 (BMP-7) and autograft bone in human noninstrumented posterolateral lumbar fusion: 2002 Volvo Award in clinical studies. Spine (Phila Pa 1976) 27, 2654, 2002.

20. Slosar, P.J., Josey, R., and Reynolds, J. Accelerating lumbar fusions by combining rhBMP-2 with allograft bone: a prospective analysis of interbody fusion rates and clinical outcomes. Spine J 7, 301, 2007.

21. Alden, T.D., Pittman, D.D., Beres, E.J., Hankins, G.R., Kallmes, D.F., Wisotsky, B.M., Kerns, K.M., and Helm, G.A. Percutaneous spinal fusion using bone morphogenetic protein-2 gene therapy. J Neurosurg 90, 109, 1999.

22. Helm, G.A., Alden, T.D., Beres, E.J., Hudson, S.B., Das, S., Engh, J.A., Pittman, D.D., Kerns, K.M., and Kallmes, D.F. Use of bone morphogenetic protein-9 gene therapy to induce spinal arthrodesis in the rodent. J Neurosurg 92, 191, 2000.

23. Wang, J.C., Kanim, L.E., Yoo, S., Campbell, P.A., Berk, A.J., and Lieberman, J.R. Effect of regional gene therapy with bone morphogenetic protein-2-producing bone marrow cells on spinal fusion in rats. The Journal of bone and joint surgery 85-A, 905, 2003.

24. Kumar, M.N., Baklanov, A., and Chopin, D. Correlation between sagittal plane changes and adjacent segment degeneration following lumbar spine fusion. Eur Spine J 10, 314, 2001.

25. Chiu, J.C., Clifford, T., Princenthal, R., and Shaw, S. Junctional disc herniation syndrome in post spinal fusion treated with endoscopic spine surgery. Surgical technology international 14, 305, 2005.

26. Harrop, J.S., Youssef, J.A., Maltenfort, M., Vorwald, P., Jabbour, P., Bono, C.M., Goldfarb, N., Vaccaro, A.R., and Hilibrand, A.S. Lumbar adjacent segment

degeneration and disease after arthrodesis and total disc arthroplasty. Spine (Phila Pa 1976) 33, 1701, 2008.

27. Beaurain, J., Bernard, P., Dufour, T., Fuentes, J.M., Hovorka, I., Huppert, J., Steib, J.P., Vital, J.M., Aubourg, L., and Vila, T. Intermediate clinical and radiological results of cervical TDR (Mobi-C) with up to 2 years of follow-up. Eur Spine J 18, 841, 2009.

28. Kurtz, S.M., van Ooij, A., Ross, R., de Waal Malefijt, J., Peloza, J., Ciccarelli, L., and Villarraga, M.L. Polyethylene wear and rim fracture in total disc arthroplasty. Spine J 7, 12, 2007.

29. van Ooij, A., Kurtz, S.M., Stessels, F., Noten, H., and van Rhijn, L. Polyethylene wear debris and long-term clinical failure of the Charite disc prosthesis: a study of 4 patients. Spine (Phila Pa 1976) 32, 223, 2007.

30. Bozkus, H., Senoglu, M., Baek, S., Sawa, A.G., Ozer, A.F., Sonntag, V.K., and Crawford, N.R. Dynamic lumbar pedicle screw-rod stabilization: in vitro biomechanical comparison with standard rigid pedicle screw-rod stabilization. Journal of neurosurgery 12, 183.

31. Mandigo, C.E., Sampath, P., and Kaiser, M.G. Posterior dynamic stabilization of the lumbar spine: pedicle based stabilization with the AccuFlex rod system. Neurosurgical focus 22, E9, 2007.

32. Frick, S.L., Hanley, E.N., Jr., Meyer, R.A., Jr., Ramp, W.K., and Chapman, T.M. Lumbar intervertebral disc transfer. A canine study. Spine (Phila Pa 1976) 19, 1826, 1994.

33. Katsuura, A., and Hukuda, S. Experimental study of intervertebral disc allografting in the dog. Spine (Phila Pa 1976) 19, 2426, 1994.

34. Matsuzaki, H., Wakabayashi, K., Ishihara, K., Ishikawa, H., and Ohkawa, A. Allografting intervertebral discs in dogs: a possible clinical application. Spine (Phila Pa 1976) 21, 178, 1996.

35. Luk, K.D., Ruan, D.K., Chow, D.H., and Leong, J.C. Intervertebral disc autografting in a bipedal animal model. Clinical orthopaedics and related research, 13, 1997.

36. Luk, K.D., Ruan, D.K., Lu, D.S., and Fei, Z.Q. Fresh frozen intervertebral disc allografting in a bipedal animal model. Spine (Phila Pa 1976) 28, 864, 2003.

37. Ruan, D., He, Q., Ding, Y., Hou, L., Li, J., and Luk, K.D. Intervertebral disc transplantation in the treatment of degenerative spine disease: a preliminary study. Lancet 369, 993, 2007.

38. Huo, M.H., Stockton, K.G., Mont, M.A., and Parvizi, J. What's new in total hip arthroplasty. The Journal of bone and joint surgery 92, 2959.

39. Humzah, M.D., and Soames, R.W. Human intervertebral disc: structure and function. The Anatomical record 220, 337, 1988.

40. Broberg, K.B. On the mechanical behaviour of intervertebral discs. Spine 8, 151, 1983.

41. Hickey, D.S., and Hukins, D.W. Relation between the structure of the annulus fibrosus and the function and failure of the intervertebral disc. Spine (Phila Pa 1976) 5, 106, 1980.

42. Eyre, D.R., and Muir, H. Types I and II collagens in intervertebral disc. Interchanging radial distributions in annulus fibrosus. The Biochemical journal 157, 267, 1976.

43. Eyre, D.R. Biochemistry of the intervertebral disc. International review of connective tissue research 8, 227, 1979.

44. Beard, H.K., Ryvar, R., Brown, R., and Muir, H. Immunochemical localization of collagen types and proteoglycan in pig intervertebral discs. Immunology 41, 491, 1980.

45. Beard, H.K., Roberts, S., and O'Brien, J.P. Immunofluorescent staining for collagen and proteoglycan in normal and scoliotic intervertebral discs. The Journal of bone and joint surgery 63B, 529, 1981.

46. Roberts, S., Beard, H.K., and O'Brien, J.P. Biochemical changes of intervertebral discs in patients with spondylolisthesis or with tears of the posterior annulus fibrosus. Annals of the rheumatic diseases 41, 78, 1982.

47. Yu, J., Winlove, P.C., Roberts, S., and Urban, J.P. Elastic fibre organization in the intervertebral discs of the bovine tail. Journal of anatomy 201, 465, 2002.

48. Melrose, J., Ghosh, P., and Taylor, T.K. A comparative analysis of the differential spatial and temporal distributions of the large (aggrecan, versican) and small (decorin, biglycan, fibromodulin) proteoglycans of the intervertebral disc. Journal of anatomy 198, 3, 2001.

49. Sztrolovics, R., Alini, M., Mort, J.S., and Roughley, P.J. Age-related changes in fibromodulin and lumican in human intervertebral discs. Spine (Phila Pa 1976) 24, 1765, 1999.

50. Cassidy, J.J., Hiltner, A., and Baer, E. Hierarchical structure of the intervertebral disc. Connective tissue research 23, 75, 1989.

51. Marchand, F., and Ahmed, A.M. Investigation of the laminate structure of lumbar disc anulus fibrosus. Spine 15, 402, 1990.

52. Goins, M.L., Wimberley, D.W., Yuan, P.S., Fitzhenry, L.N., and Vaccaro, A.R. Nucleus pulposus replacement: an emerging technology. Spine J 5, 317S, 2005.

53. Cleveland, D. The use of methylacrylic for spinal stabilization after disc operations. Marquette Med Rev 20, 62, 1955.

54. Alini, M., Eisenstein, S.M., Ito, K., Little, C., Kettler, A.A., Masuda, K., Melrose, J., Ralphs, J., Stokes, I., and Wilke, H.J. Are animal models useful for studying human disc disorders/degeneration? Eur Spine J 17, 2, 2008.

55. Gruber, H.E., Johnson, T.L., Leslie, K., Ingram, J.A., Martin, D., Hoelscher, G., Banks, D., Phieffer, L., Coldham, G., and Hanley, E.N., Jr. Autologous intervertebral disc cell implantation: a model using Psammomys obesus, the sand rat. Spine (Phila Pa 1976) 27, 1626, 2002.

56. Chiba, K., Andersson, G.B., Masuda, K., and Thonar, E.J. Metabolism of the extracellular matrix formed by intervertebral disc cells cultured in alginate. Spine (Phila Pa 1976) 22, 2885, 1997.

57. Baer, A.E., Wang, J.Y., Kraus, V.B., and Setton, L.A. Collagen gene expression and mechanical properties of intervertebral disc cell-alginate cultures. J Orthop Res 19, 2, 2001.

58. Mizuno, H., Roy, A.K., Vacanti, C.A., Kojima, K., Ueda, M., and Bonassar, L.J. Tissue-engineered composites of anulus fibrosus and nucleus pulposus for intervertebral disc replacement. Spine 29, 1290, 2004.

59. Mizuno, H., Roy, A.K., Zaporojan, V., Vacanti, C.A., Ueda, M., and Bonassar, L.J. Biomechanical and biochemical characterization of composite tissue-engineered intervertebral discs. Biomaterials 27, 362, 2006.

60. Aguiar, D.J., Johnson, S.L., and Oegema, T.R. Notochordal cells interact with nucleus pulposus cells: regulation of proteoglycan synthesis. Experimental cell research 246, 129, 1999.

61. Sakai, D., Mochida, J., Yamamoto, Y., Toh, E., Iwashina, T., Miyazaki, T., Inokuchi, S., Ando, K., and Hotta, T. Immortalization of human nucleus pulposus cells by a recombinant SV40 adenovirus vector: establishment of a novel cell line for the study of human nucleus pulposus cells. Spine (Phila Pa 1976) 29, 1515, 2004.

62. Le Maitre, C.L., Baird, P., Freemont, A.J., and Hoyland, J.A. An in vitro study investigating the survival and phenotype of mesenchymal stem cells following injection into nucleus pulposus tissue. Arthritis research & therapy 11, R20, 2009.

63. Risbud, M.V., Albert, T.J., Guttapalli, A., Vresilovic, E.J., Hillibrand, A.S., Vaccaro, A.R., and Shapiro, I.M. Differentiation of mesenchymal stem cells towards a nucleus pulposus-like phenotype in vitro: implications for cell-based transplantation therapy. Spine (Phila Pa 1976) 29, 2627, 2004.

64. Okuma, M., Mochida, J., Nishimura, K., Sakabe, K., and Seiki, K. Reinsertion of stimulated nucleus pulposus cells retards intervertebral disc degeneration: an in vitro and in vivo experimental study. J Orthop Res 18, 988, 2000.

65. Watanabe, K., Mochida, J., Nomura, T., Okuma, M., Sakabe, K., and Seiki, K. Effect of reinsertion of activated nucleus pulposus on disc degeneration: an experimental study on various types of collagen in degenerative discs. Connective tissue research 44, 104, 2003.

66. Sakai, D., Mochida, J., Iwashina, T., Watanabe, T., Nakai, T., Ando, K., and Hotta, T. Differentiation of mesenchymal stem cells transplanted to a rabbit degenerative disc model: potential and limitations for stem cell therapy in disc regeneration. Spine (Phila Pa 1976) 30, 2379, 2005.

67. Gorensek, M., Jaksimovic, C., Kregar-Velikonja, N., Gorensek, M., Knezevic, M., Jeras, M., Pavlovcic, V., and Cor, A. Nucleus pulposus repair with cultured autologous elastic cartilage derived chondrocytes. Cellular & molecular biology letters 9, 363, 2004.

68. Kim, S., Le Visage, C., Tateno, K., Sieber, A., Kostuik, J., and Leong, K. Interaction of human mesenchymal stem cells with disc cells: changes in biosynthesis of extracellular matrix. Spine J 2, 107S, 2002.

69. Hohaus, C., Ganey, T.M., Minkus, Y., and Meisel, H.J. Cell transplantation in lumbar spine disc degeneration disease. Eur Spine J 17 Suppl 4, 492, 2008.

70. Sun, Y., Hurtig, M., Pilliar, R.M., Grynpas, M., and Kandel, R.A. Characterization of nucleus pulposus-like tissue formed in vitro. J Orthop Res 19, 1078, 2001.

71. Alini, M., Li, W., Markovic, P., Aebi, M., Spiro, R.C., and Roughley, P.J. The potential and limitations of a cell-seeded collagen/hyaluronan scaffold to engineer an intervertebral disc-like matrix. Spine (Phila Pa 1976) 28, 446, 2003.

72. Seguin, C.A., Grynpas, M.D., Pilliar, R.M., Waldman, S.D., and Kandel, R.A. Tissue engineered nucleus pulposus tissue formed on a porous calcium polyphosphate substrate. Spine (Phila Pa 1976) 29, 1299, 2004.

73. Roughley, P., Hoemann, C., DesRosiers, E., Mwale, F., Antoniou, J., and Alini, M. The potential of chitosan-based gels containing intervertebral disc cells for nucleus pulposus supplementation. Biomaterials 27, 388, 2006.

74. Ganey, T., Libera, J., Moos, V., Alasevic, O., Fritsch, K.G., Meisel, H.J., and Hutton, W.C. Disc chondrocyte transplantation in a canine model: a treatment for degenerated or damaged intervertebral disc. Spine (Phila Pa 1976) 28, 2609, 2003.

75. Meisel, H.J., Siodla, V., Ganey, T., Minkus, Y., Hutton, W.C., and Alasevic, O.J. Clinical experience in cell-based therapeutics: disc chondrocyte transplantation A

treatment for degenerated or damaged intervertebral disc. Biomolecular engineering 24, 5, 2007.

76. Atlas, S.J., Keller, R.B., Wu, Y.A., Deyo, R.A., and Singer, D.E. Long-term outcomes of surgical and nonsurgical management of lumbar spinal stenosis: 8 to 10 year results from the maine lumbar spine study. Spine (Phila Pa 1976) 30, 936, 2005.

77. Atlas, S.J., Keller, R.B., Wu, Y.A., Deyo, R.A., and Singer, D.E. Long-term outcomes of surgical and nonsurgical management of sciatica secondary to a lumbar disc herniation: 10 year results from the maine lumbar spine study. Spine (Phila Pa 1976) 30, 927, 2005.

78. Carragee, E.J., Han, M.Y., Suen, P.W., and Kim, D. Clinical outcomes after lumbar discectomy for sciatica: the effects of fragment type and anular competence. The Journal of bone and joint surgery 85-A, 102, 2003.

79. Key, J.A., and Ford, L.T. Experimental intervertebral-disc lesions. The Journal of bone and joint surgery 30A, 621, 1948.

80. Ahlgren, B.D., Lui, W., Herkowitz, H.N., Panjabi, M.M., and Guiboux, J.P. Effect of anular repair on the healing strength of the intervertebral disc: a sheep model. Spine (Phila Pa 1976) 25, 2165, 2000.

81. Bourgeault, C., Beaubien, B., and Griffith, S. Biomechanical assessment of annulus fibrosus repair with suture tethered anchors. Spine Arthroplasty Society. Berlin, 2007.

82. Bajanes, G., Perez, A., and Diaz, M. One year follow up of discectomy patients who received a mesh to repair the annulus fibrosus. Spine Arthoplasty Soceity. Berlin, 2007.

83. Taylor, W. Biologic collagen PMMA injection (Artefill) repairs mid-annular concentric defects in the ovine model. Spine J 6, 48S, 2006.

84. Gruber, H.E., Ingram, J.A., Norton, H.J., and Hanley, E.N., Jr. Senescence in cells of the aging and degenerating intervertebral disc: immunolocalization of senescence-associated beta-galactosidase in human and sand rat discs. Spine (Phila Pa 1976) 32, 321, 2007.

85. Richardson, S.M., Hughes, N., Hunt, J.A., Freemont, A.J., and Hoyland, J.A. Human mesenchymal stem cell differentiation to NP-like cells in chitosan-glycerophosphate hydrogels. Biomaterials 29, 85, 2008.

86. Nerurkar, N.L., Baker, B.M., Sen, S., Wible, E.E., Elliott, D.M., and Mauck, R.L. Nanofibrous biologic laminates replicate the form and function of the annulus fibrosus. Nature materials 8, 986, 2009.

87. Nesti, L.J., Li, W.J., Shanti, R.M., Jiang, Y.J., Jackson, W., Freedman, B.A., Kuklo, T.R., Giuliani, J.R., and Tuan, R.S. Intervertebral disc tissue engineering using a novel hyaluronic acid-nanofibrous scaffold (HANFS) amalgam. Tissue engineering 14, 1527, 2008.

88. Sato, M., Kikuchi, M., Ishihara, M., Ishihara, M., Asazuma, T., Kikuchi, T., Masuoka, K., Hattori, H., and Fujikawa, K. Tissue engineering of the intervertebral disc with cultured annulus fibrosus cells using atelocollagen honeycomb-shaped scaffold with a membrane seal (ACHMS scaffold). Medical & biological engineering & computing 41, 365, 2003.

89. Rong, Y., Sugumaran, G., Silbert, J.E., and Spector, M. Proteoglycans synthesized by canine intervertebral disc cells grown in a type I collagen-glycosaminoglycan matrix. Tissue Eng 8, 1037, 2002.

90. Gruber, H.E., Stasky, A.A., and Hanley, E.N., Jr. Characterization and phenotypic stability of human disc cells in vitro. Matrix Biol 16, 285, 1997.

91. Dang, J.M., Sun, D.D., Shin-Ya, Y., Sieber, A.N., Kostuik, J.P., and Leong, K.W. Temperature-responsive hydroxybutyl chitosan for the culture of mesenchymal stem cells and intervertebral disk cells. Biomaterials 27, 406, 2006.

92. Le Visage, C., Yang, S.H., Kadakia, L., Sieber, A.N., Kostuik, J.P., and Leong, K.W. Small intestinal submucosa as a potential bioscaffold for intervertebral disc regeneration. Spine (Phila Pa 1976) 31, 2423, 2006.

93. Bowles, R.D., Williams, R.M., Zipfel, W.R., and Bonassar, L.J. Self-assembly of aligned tissue-engineered annulus fibrosus and intervertebral disc composite via collagen gel contraction. Tissue engineering 16, 1339, 2010.

94. Ledet, E.H., Jeshuran, W., Glennon, J.C., Shaffrey, C., De Deyne, P., Belden, C., Kallakury, B., and Carl, A.L. Small intestinal submucosa for anular defect closure: long-term response in an in vivo sheep model. Spine (Phila Pa 1976) 34, 1457, 2009.

95. Feng, Z., Matsumoto, T., and Nakamura, T. Measurements of the mechanical properties of contracted collagen gels populated with rat fibroblasts or cardiomyocytes. J Artif Organs 6, 192, 2003.

96. Nirmalanandhan, V.S., Levy, M.S., Huth, A.J., and Butler, D.L. Effects of cell seeding density and collagen concentration on contraction kinetics of mesenchymal stem cell-seeded collagen constructs. Tissue engineering 12, 1865, 2006.

97. Seliktar, D., Black, R.A., Vito, R.P., and Nerem, R.M. Dynamic mechanical conditioning of collagen-gel blood vessel constructs induces remodeling in vitro. Annals of biomedical engineering 28, 351, 2000.

98. Stegemann, J.P., Dey, N.B., Lincoln, T.M., and Nerem, R.M. Genetic modification of smooth muscle cells to control phenotype and function in vascular tissue engineering. Tissue engineering 10, 189, 2004.

99. Baker, B.M., Nerurkar, N.L., Burdick, J.A., Elliott, D.M., and Mauck, R.L. Fabrication and modeling of dynamic multipolymer nanofibrous scaffolds. Journal of biomechanical engineering 131, 101012, 2009.

100. Ehrlich, G.E. Low back pain. Bulletin of the World Health Organization 81, 671, 2003.

101. Kelsey, J.L., and White, A.A., 3rd. Epidemiology and impact of low-back pain. Spine 5, 133, 1980.

102. Yasuma, T., Koh, S., Okamura, T., and Yamauchi, Y. Histological changes in aging lumbar intervertebral discs. Their role in protrusions and prolapses. The Journal of bone and joint surgery 72, 220, 1990.

103. Kuslich, S.D., Ulstrom, C.L., and Michael, C.J. The tissue origin of low back pain and sciatica: a report of pain response to tissue stimulation during operations on the lumbar spine using local anesthesia. The Orthopedic clinics of North America 22, 181, 1991.

104. O'Neill, C.W., Kurgansky, M.E., Derby, R., and Ryan, D.P. Disc stimulation and patterns of referred pain. Spine 27, 2776, 2002.

105. Bruehlmann, S.B., Rattner, J.B., Matyas, J.R., and Duncan, N.A. Regional variations in the cellular matrix of the annulus fibrosus of the intervertebral disc. Journal of anatomy 201, 159, 2002.

106. Baer, A.E., Laursen, T.A., Guilak, F., and Setton, L.A. The micromechanical environment of intervertebral disc cells determined by a finite deformation, anisotropic, and biphasic finite element model. Journal of biomechanical engineering 125, 1, 2003.

107. Maldonado, B.A., and Oegema, T.R., Jr. Initial characterization of the metabolism of intervertebral disc cells encapsulated in microspheres. J Orthop Res 10, 677, 1992.

108. Schollmeier, G., Lahr-Eigen, R., and Lewandrowski, K.U. Observations on fiber-forming collagens in the anulus fibrosus. Spine (Phila Pa 1976) 25, 2736, 2000.

109. Nerlich, A.G., Boos, N., Wiest, I., and Aebi, M. Immunolocalization of major interstitial collagen types in human lumbar intervertebral discs of various ages. Virchows Arch 432, 67, 1998.

110. Adams, P., Eyre, D.R., and Muir, H. Biochemical aspects of development and ageing of human lumbar intervertebral discs. Rheumatology and rehabilitation 16, 22, 1977.

111. Guerin, H.L., and Elliott, D.M. Quantifying the contributions of structure to annulus fibrosus mechanical function using a nonlinear, anisotropic, hyperelastic model. J Orthop Res 25, 508, 2007.

112. Huang, R.C., and Sandhu, H.S. The current status of lumbar total disc replacement. The Orthopedic clinics of North America 35, 33, 2004.

113. Guyer, R.D., McAfee, P.C., Hochschuler, S.H., Blumenthal, S.L., Fedder, I.L., Ohnmeiss, D.D., and Cunningham, B.W. Prospective randomized study of the Charite artificial disc: data from two investigational centers. Spine J 4, 252S, 2004.

114. Bertagnoli, R., Yue, J.J., Pfeiffer, F., Fenk-Mayer, A., Lawrence, J.P., Kershaw, T., and Nanieva, R. Early results after ProDisc-C cervical disc replacement. Journal of neurosurgery 2, 403, 2005.

115. Blumenthal, S., McAfee, P.C., Guyer, R.D., Hochschuler, S.H., Geisler, F.H., Holt, R.T., Garcia, R., Jr., Regan, J.J., and Ohnmeiss, D.D. A prospective, randomized, multicenter Food and Drug Administration investigational device exemptions study of lumbar total disc replacement with the CHARITE artificial disc versus lumbar fusion: part I: evaluation of clinical outcomes. Spine 30, 1565, 2005.

116. McAfee, P.C., Cunningham, B., Holsapple, G., Adams, K., Blumenthal, S., Guyer, R.D., Dmietriev, A., Maxwell, J.H., Regan, J.J., and Isaza, J. A prospective, randomized, multicenter Food and Drug Administration investigational device exemption study of lumbar total disc replacement with the CHARITE artificial disc versus lumbar fusion: part II: evaluation of radiographic outcomes and correlation of surgical technique accuracy with clinical outcomes. Spine 30, 1576, 2005.

117. Ganey, T., Libera, J., Moos, V., Alasevic, O., Fritsch, K.G., Meisel, H.J., and Hutton, W.C. Disc chondrocyte transplantation in a canine model: a treatment for degenerated or damaged intervertebral disc. Spine 28, 2609, 2003.

118. Seguin, C.A., Grynpas, M.D., Pilliar, R.M., Waldman, S.D., and Kandel, R.A. Tissue engineered nucleus pulposus tissue formed on a porous calcium polyphosphate substrate. Spine 29, 1299, 2004.

119. Chang, G., Kim, H.J., Kaplan, D., Vunjak-Novakovic, G., and Kandel, R.A. Porous silk scaffolds can be used for tissue engineering annulus fibrosus. Eur Spine J 16, 1848, 2007.

120. Shao, X., and Hunter, C.J. Developing an alginate/chitosan hybrid fiber scaffold for annulus fibrosus cells. Journal of biomedical materials research 82, 701, 2007.

121. Wan, Y., Feng, G., Shen, F.H., Laurencin, C.T., and Li, X. Biphasic scaffold for annulus fibrosus tissue regeneration. Biomaterials 29, 643, 2008.

122. Nerurkar, N.L., Elliott, D.M., and Mauck, R.L. Mechanics of oriented electrospun nanofibrous scaffolds for annulus fibrosus tissue engineering. J Orthop Res 25, 1018, 2007.

123. Nerurkar, N.L., Mauck, R.L., and Elliott, D.M. ISSLS prize winner: Integrating theoretical and experimental methods for functional tissue engineering of the annulus fibrosus. Spine 33, 2691, 2008.

124. Saad, L., and Spector, M. Effects of collagen type on the behavior of adult canine annulus fibrosus cells in collagen-glycosaminoglycan scaffolds. Journal of biomedical materials research 71, 233, 2004.

125. Barocas, V.H., Girton, T.S., and Tranquillo, R.T. Engineered alignment in media equivalents: magnetic prealignment and mandrel compaction. Journal of biomechanical engineering 120, 660, 1998.

126. Grinnell, F., and Lamke, C.R. Reorganization of hydrated collagen lattices by human skin fibroblasts. Journal of cell science 66, 51, 1984.

127. Thomopoulos, S., Fomovsky, G.M., and Holmes, J.W. The development of structural and mechanical anisotropy in fibroblast populated collagen gels. Journal of biomechanical engineering 127, 742, 2005.

128. Costa, K.D., Lee, E.J., and Holmes, J.W. Creating alignment and anisotropy in engineered heart tissue: role of boundary conditions in a model three-dimensional culture system. Tissue engineering 9, 567, 2003.

129. Zoumi, A., Yeh, A., and Tromberg, B.J. Imaging cells and extracellular matrix in vivo by using second-harmonic generation and two-photon excited fluorescence. Proceedings of the National Academy of Sciences of the United States of America 99, 11014, 2002.

130. Williams, R.M., Zipfel, W.R., and Webb, W.W. Interpreting second-harmonic generation images of collagen I fibrils. Biophysical journal 88, 1377, 2005.

131. Zipfel, W.R., Williams, R.M., Christie, R., Nikitin, A.Y., Hyman, B.T., and Webb, W.W. Live tissue intrinsic emission microscopy using multiphoton-excited native fluorescence and second harmonic generation. Proceedings of the National Academy of Sciences of the United States of America 100, 7075, 2003.

132. Elsdale, T., and Bard, J. Collagen substrata for studies on cell behavior. The Journal of cell biology 54, 626, 1972.

133. Saltzman, W.M., Parkhurst, M.R., Parsons-Wingerter, P., and Zhu, W.H. Three-dimensional cell cultures mimic tissues. Annals of the New York Academy of Sciences 665, 259, 1992.

134. Chaudhuri, S., Nguyen, H., Rangayyan, R.M., Walsh, S., and Frank, C.B. A Fourier domain directional filtering method for analysis of collagen alignment in ligaments. IEEE transactions on bio-medical engineering 34, 509, 1987.

135. Pourdeyhimi, B., Dent, R., and Davis, H. Measuring fiber orientation in nonwovens: 3. Fourier transform. Textile Res. J. 67, 143, 1997.

136. Nishimura, T., and Ansell, M.P. Fast Fourier transform and filtered image analyses of fiber orientation in OSB. Wood Sci. Technol. 36, 287, 2002.

137. van Zuijlen, P.P., de Vries, H.J., Lamme, E.N., Coppens, J.E., van Marle, J., Kreis, R.W., and Middelkoop, E. Morphometry of dermal collagen orientation by Fourier analysis is superior to multi-observer assessment. The Journal of pathology 198, 284, 2002.

138. Johnson, W.E., Wootton, A., El Haj, A., Eisenstein, S.M., Curtis, A.S., and Roberts, S. Topographical guidance of intervertebral disc cell growth in vitro: towards the development of tissue repair strategies for the anulus fibrosus. Eur Spine J 15 Suppl 3, S389, 2006.

139. Wagenseil, J.E., Elson, E.L., and Okamoto, R.J. Cell orientation influences the biaxial mechanical properties of fibroblast populated collagen vessels. Annals of biomedical engineering 32, 720, 2004.

140. Schneider, T.O., Mueller, S.M., Shortkroff, S., and Spector, M. Expression of alpha-smooth muscle actin in canine intervertebral disc cells in situ and in collagen-glycosaminoglycan matrices in vitro. J Orthop Res 17, 192, 1999.

141. Lee, C.H., Shin, H.J., Cho, I.H., Kang, Y.M., Kim, I.A., Park, K.D., and Shin, J.W. Nanofiber alignment and direction of mechanical strain affect the ECM production of human ACL fibroblast. Biomaterials 26, 1261, 2005.

142. Torkian, B.A., Yeh, A.T., Engel, R., Sun, C.H., Tromberg, B.J., and Wong, B.J. Modeling aberrant wound healing using tissue-engineered skin constructs and multiphoton microscopy. Arch Facial Plast Surg 6, 180, 2004.

143. Ohsumi, T.K., Flaherty, J.E., Evans, M.C., and Barocas, V.H. Three-dimensional simulation of anisotropic cell-driven collagen gel compaction. Biomech Model Mechanobiol, 2007.

144. Kobayashi, S., Meir, A., and Urban, J. Effect of cell density on the rate of glycosaminoglycan accumulation by disc and cartilage cells in vitro. J Orthop Res 26, 493, 2008.

145. Grunhagen, T., Wilde, G., Soukane, D.M., Shirazi-Adl, S.A., and Urban, J.P. Nutrient supply and intervertebral disc metabolism. J Bone Joint Surg Am 88 Suppl 2, 30, 2006.

146. Burden of Musculoskeletal Diseases in the United States: Prevalence, Societal and Economic Cost American Academy of Orthopaedic Surgeons, 2008.

147. Bowles, R.D., Williams, R., Zipfel, W., and Bonassar, L.J. Self-Assembly of Aligned Tissue Engineered Annulus Fibrosus and IVD Composite via Collagen Gel Contraction. Tissue engineering, 2009.

148. Ballyns, J.J., Cohen, D., Malone, E., Maher, S.A., Potter, H.G., Wright, T.M., Lipson, H., and Bonassar, L.J. An Optical Method for Evaluation of Geometric Fidelity for Anatomically Shaped Tissue Engineered Constructs. Tissue Eng Part C Methods, 2009.

149. Ballyns, J.J., Gleghorn, J.P., Niebrzydowski, V., Rawlinson, J.J., Potter, H.G., Maher, S.A., Wright, T.M., and Bonassar, L.J. Image-guided tissue engineering of anatomically shaped implants via MRI and micro-CT using injection molding. Tissue engineering 14, 1195, 2008.

150. Cheah, C.M., Chua, C.K., Leong, K.F., Cheong, C.H., and Naing, M.W. Automatic algorithm for generating complex polyhedral scaffold structures for tissue engineering. Tissue Eng 10, 595, 2004.

151. Sun, W., Starly, B., Darling, A., and Gomez, C. Computer-aided tissue engineering: application to biomimetic modelling and design of tissue scaffolds. Biotechnology and applied biochemistry 39, 49, 2004.

152. Van Cleynenbreugel, T., Van Oosterwyck, H., Vander Sloten, J., and Schrooten, J. Trabecular bone scaffolding using a biomimetic approach. Journal of materials science 13, 1245, 2002.

153. Fields, A.J., Eswaran, S.K., Jekir, M.G., and Keaveny, T.M. Role of trabecular microarchitecture in whole-vertebral body biomechanical behavior. J Bone Miner Res 24, 1523, 2009.

154. Luoma, K., Vehmas, T., Riihimaki, H., and Raininko, R. Disc height and signal intensity of the nucleus pulposus on magnetic resonance imaging as indicators of lumbar disc degeneration. Spine 26, 680, 2001.

155. Sato, K., Kikuchi, S., and Yonezawa, T. In vivo intradiscal pressure measurement in healthy individuals and in patients with ongoing back problems. Spine (Phila Pa 1976) 24, 2468, 1999.

156. Bibby, S.R., Jones, D.A., Lee, R.B., Yu, J., and Urban, J.P.G. The pathophysiology of the intervertebral disc. Joint Bone Spine 68, 537, 2001.

157. Rousseau, M.A., Bass, E.C., and Lotz, J.C. Ventral approach to the lumbar spine of the Sprague-Dawley rat. Lab animal 33, 43, 2004.

158. Hott, M.E., Megerian, C.A., Beane, R., and Bonassar, L.J. Fabrication of tissue engineered tympanic membrane patches using computer-aided design and injection molding. The Laryngoscope 114, 1290, 2004.

159. Sharma, M., Langrana, N.A., and Rodriguez, J. Role of ligaments and facets in lumbar spinal stability. Spine 20, 887, 1995.

160. Regatte, R.R., Akella, S.V., Borthakur, A., and Reddy, R. Proton spin-lock ratio imaging for quantitation of glycosaminoglycans in articular cartilage. J Magn Reson Imaging 17, 114, 2003.

161. Johannessen, W., Auerbach, J.D., Wheaton, A.J., Kurji, A., Borthakur, A., Reddy, R., and Elliott, D.M. Assessment of human disc degeneration and proteoglycan content using T1rho-weighted magnetic resonance imaging. Spine 31, 1253, 2006.

162. Gray, M.L., Burstein, D., and Xia, Y. Biochemical (and functional) imaging of articular cartilage. Seminars in musculoskeletal radiology 5, 329, 2001.

163. Zheng, S., and Xia, Y. The collagen fibril structure in the superficial zone of articular cartilage by microMRI. Osteoarthritis and cartilage / OARS, Osteoarthritis Research Society 17, 1519, 2009.

164. de Visser, S.K., Bowden, J.C., Wentrup-Byrne, E., Rintoul, L., Bostrom, T., Pope, J.M., and Momot, K.I. Anisotropy of collagen fibre alignment in bovine cartilage: comparison of polarised light microscopy and spatially resolved diffusion-tensor measurements. Osteoarthritis and cartilage / OARS, Osteoarthritis Research Society 16, 689, 2008.

165. Botelho, R.V., Moraes, O.J., Fernandes, G.A., Buscariolli Ydos, S., and Bernardo, W.M. A systematic review of randomized trials on the effect of cervical disc arthroplasty on reducing adjacent-level degeneration. Neurosurgical focus 28, E5.

166. Bartels, R.H., Donk, R., and Verbeek, A.L. No justification for cervical disk prostheses in clinical practice: a meta-analysis of randomized controlled trials. Neurosurgery 66, 1153.

167. O'Halloran, D.M., and Pandit, A.S. Tissue-engineering approach to regenerating the intervertebral disc. Tissue Eng 13, 1927, 2007.

168. Nerurkar, N.L., Sen, S., Huang, A.H., Elliott, D.M., and Mauck, R.L. Engineered disc-like angle-ply structures for intervertebral disc replacement. Spine (Phila Pa 1976) 35, 867.

169. Elliott, D.M., and Sarver, J.J. Young investigator award winner: validation of the mouse and rat disc as mechanical models of the human lumbar disc. Spine (Phila Pa 1976) 29, 713, 2004.

170. Stokes, I.A., Aronsson, D.D., Spence, H., and Iatridis, J.C. Mechanical modulation of intervertebral disc thickness in growing rat tails. Journal of spinal disorders 11, 261, 1998.

171. Espinoza Orias, A.A., Malhotra, N.R., and Elliott, D.M. Rat disc torsional mechanics: effect of lumbar and caudal levels and axial compression load. Spine J 9, 204, 2009.

172. Luk, K.D., and Ruan, D.K. Intervertebral disc transplantation: a biological approach to motion preservation. Eur Spine J 17 Suppl 4, 504, 2008.

173. Enobakhare, B.O., Bader, D.L., and Lee, D.A. Quantification of sulfated glycosaminoglycans in chondrocyte/alginate cultures, by use of 1,9-dimethylmethylene blue. Analytical biochemistry 243, 189, 1996.

174. Kim, Y.J., Sah, R.L., Doong, J.Y., and Grodzinsky, A.J. Fluorometric assay of DNA in cartilage explants using Hoechst 33258. Analytical biochemistry 174, 168, 1988.

175. Neuman, R.E., and Logan, M.A. The determination of hydroxyproline. The Journal of biological chemistry 184, 299, 1950.

176. Shirazi-Adl, A., Taheri, M., and Urban, J.P. Analysis of cell viability in intervertebral disc: Effect of endplate permeability on cell population. Journal of biomechanics 43, 1330.

177. Iatridis, J.C. Tissue engineering: Function follows form. Nature materials 8, 923, 2009.

178. Nerurkar, N.L., Elliott, D.M., and Mauck, R.L. Mechanical design criteria for intervertebral disc tissue engineering. Journal of biomechanics 43, 1017.

179. Hutton, W.C., Elmer, W.A., Boden, S.D., Hyon, S., Toribatake, Y., Tomita, K., and Hair, G.A. The effect of hydrostatic pressure on intervertebral disc metabolism. Spine 24, 1507, 1999.

180. Wang, D.L., Jiang, S.D., and Dai, L.Y. Biologic response of the intervertebral disc to static and dynamic compression in vitro. Spine 32, 2521, 2007.

181. Kim, Y.J., Bonassar, L.J., and Grodzinsky, A.J. The role of cartilage streaming potential, fluid flow and pressure in the stimulation of chondrocyte biosynthesis during dynamic compression. Journal of biomechanics 28, 1055, 1995.

182. Surgeons, A.A.o.O. Burden of Musculoskeletal Diseases in the United States: Prevalence, Societal and Economic Cost 2008.

183. Kurtz, S.M., Lau, E., Ianuzzi, A., Schmier, J., Todd, L., Isaza, J., and Albert, T.J. National Revision Burden for Lumbar Total Disc Replacement in the United States: Epidemiologic and Economic Perspectives. Spine (Phila Pa 1976).

184. McGirt, M.J., Eustacchio, S., Varga, P., Vilendecic, M., Trummer, M., Gorensek, M., Ledic, D., and Carragee, E.J. A prospective cohort study of close interval computed tomography and magnetic resonance imaging after primary lumbar discectomy: factors associated with recurrent disc herniation and disc height loss. Spine (Phila Pa 1976) 34, 2044, 2009.

185. Bowles, R.D., Gebhard, H.G., Dyke, J.P., Ballon, D.J., Tomasino, A.T., Cunningham, M.E., Hartl, R., and Bonassar, L.J. Image-Based Tissue Engineering of a Total Intervertebral Disc Replacement for Restoration of Function to the Rat Lumbar Spine. NMR in Biomedicine, 2010.

186. Thomopoulos, S., Fomovsky, G.M., Chandran, P.L., and Holmes, J.W. Collagen fiber alignment does not explain mechanical anisotropy in fibroblast populated collagen gels. Journal of biomechanical engineering 129, 642, 2007.

187. Gu, W.Y., Mao, X.G., Foster, R.J., Weidenbaum, M., Mow, V.C., and Rawlins, B.A. The anisotropic hydraulic permeability of human lumbar anulus fibrosus. Influence of age, degeneration, direction, and water content. Spine (Phila Pa 1976) 24, 2449, 1999.

188. Yao, H., Justiz, M.A., Flagler, D., and Gu, W.Y. Effects of swelling pressure and hydraulic permeability on dynamic compressive behavior of lumbar annulus fibrosus. Annals of biomedical engineering 30, 1234, 2002.

189. Barbir, A., Michalek, A.J., Abbott, R.D., and Iatridis, J.C. Effects of enzymatic digestion on compressive properties of rat intervertebral discs. Journal of biomechanics 43, 1067.

190. Perie, D.S., Maclean, J.J., Owen, J.P., and Iatridis, J.C. Correlating material properties with tissue composition in enzymatically digested bovine annulus fibrosus and nucleus pulposus tissue. Annals of biomedical engineering 34, 769, 2006.

191. Neidlinger-Wilke, C., Wurtz, K., Urban, J.P., Borm, W., Arand, M., Ignatius, A., Wilke, H.J., and Claes, L.E. Regulation of gene expression in intervertebral disc cells by low and high hydrostatic pressure. Eur Spine J 15 Suppl 3, S372, 2006.

192. National Science Education Standards. 1996.

193. Bonassar, L.J., and Vacanti, C.A. Tissue engineering: the first decade and beyond. Journal of cellular biochemistry 30-31, 297, 1998.

194. Pignolet, L.H., Waldman, A.S., Schechinger, L., Govindarajoo, G., Nowick, J.S., and Ted, L. The Alginate Demonstration: Polymers, Food Science, and Ion Exchange. Journal of Chemical Education 75, 1430, 1998.

195. Friedli, A.C., Schlager, I.R., and Stephen, W.W. Demonstrating Encapsulation and Release: A New Take on Alginate Complexation and the Nylon Rope Trick. Journal of Chemical Education 82, 1017, 2005.

196. Windschitl, M., Thompson, J., and Braaten, M. Beyond the Scientific Method: Model-Based Inquiry as a New Paradigm of Preference for School Science Investigations. Science Education., 2008.

197. Yang, F., Leung, V.Y., Luk, K.D., Chan, D., and Cheung, K.M. Mesenchymal stem cells arrest intervertebral disc degeneration through chondrocytic differentiation and stimulation of endogenous cells. Mol Ther 17, 1959, 2009.

198. Bowles, R.D., Gebhard, H.G., Hartl, R., and Bonassar, L.J. Annulus Fibrosus Composition Regulates ECM Development in Tissue Engineered Total Disc Replacement. Biomaterials.

199. Bowles, R.D., Gebhard, H.G., Hartl, R., and Bonassar, L.J. Tissue-Engineered Intervertebral Disc Implants Restore Function to the Spine In Vivo. Science Translational Medicine, 2010.

200. Le Maitre, C.L., Freemont, A.J., and Hoyland, J.A. Accelerated cellular senescence in degenerate intervertebral discs: a possible role in the pathogenesis of intervertebral disc degeneration. Arthritis research & therapy 9, R45, 2007.

201. Buckley, M.R., Gleghorn, J.P., Bonassar, L.J., and Cohen, I. Mapping the depth dependence of shear properties in articular cartilage. Journal of biomechanics 41, 2430, 2008.